NANO-MATERIAL BASED FLEXIBLE RADIO FREQUENCY SENSORS FOR WEARABLE HEALTH AND ENVIRONMENT MONITORING: DESIGNS AND PROTOTYPES UTILIZING 3D/INKJET PRINTING TECHNOLOGIES

A Dissertation
Presented to
The Academic Faculty

By

Taoran Le

In Partial Fulfillment
of the Requirements for the Degree
Doctor of Philosophy
in
Electrical and Computer Engineering

School of Electrical and Computer Engineering
Georgia Institute of Technology
August 2016

NANO-MATERIAL BASED FLEXIBLE RADIO FREQUENCY SENSORS FOR WEARABLE HEALTH AND ENVIRONMENT MONITORING: DESIGNS AND PROTOTYPES UTILIZING 3D/INKJET PRINTING TECHNOLOGIES

Approved by:

Dr. Manos M. Tentzeris, Advisor

School of Electrical and Computer Engineering
Georgia Institute of Technology

Dr. Ching Ping Wong

School of Materials Science and Engineering
Georgia Institute of Technology

Dr. Andrew Peterson

School of Electrical and Computer Engineering
Georgia Institute of Technology

Dr. Yang Wang

School of Civil and Environmental Engineering
Georgia Institute of Technology

Dr. Alenka Zajic

School of Electrical and Computer Engineering
Georgia Institute of Technology

Date Approved: [June 23rd, 2016]

To my parents,

Kesheng Wang and Qingyou Le

ACKNOWLEDGEMENTS

First and foremost, I would like to express my deepest gratefulness to my advisor, Prof. Tentzeris, for the many opportunities he so generously provided to me to expand my knowledge and experiences. It is hard to imagine who I am today and what I have achieved today without Prof. Tentzeris' constant support financially and intellectually. I deeply thank him for his guidance in many aspects of the academic life and personal life challenges. He taught me how important it is to perform research in a focused and thorough way aiming for excellence and innovation. I would also like to express my gratitude to Prof. C.P. Wong for his endless support and encouragement. I am really fortunate to have Prof. Andrew Peterson, Prof. Alenka Zajic and Prof. Yang Wang as my Ph.D. committee members and their thoughtful feedback and suggestions on my proposal and my thesis. I am indebted to Prof. Yoshihiro Kawahara and Prof. Z. L. Wang for their truly support, expert advice, enthusiasm and encouragement in the completion of my Ph.D. Also, I am thankful to Dr. Bingnan Wang at Mitsubishi Electric Research Laboratories for his guidance during my internship there.

I owe the fruitful results in my work largely to the assistance of my dear ATHENA members and friends I met in Atlanta, including Dr. Vasileios Lakafosis, Dr. Sangkil Kim, Dr. Rushi Vyas, Dr. Amin Rida, Dr. Trang Thai, Dr. Chiara Mariotti, Dr. James Cooper, Dr. Stefano Moscato, Bijan Tehrani, Yan Pan, Ryan Bahr and John Kimionis. Dear all, all your support have carried me through this roller coaster ride and brought me joy in those Ph.D. journey. I also want to thank all other ATHENA members for making our lab an enjoyable environment, and all the staff of GEDC and ECE office for their excellent assistance. I would also like to thank my collaborators from MSE in Georgia Tech, Dr.

Ziyin Lin, Dr. Zhuo Li, Dr. Wenzhuo Wu, Dr. Zhenkun Wu, Kathy Chia-Chi Tuan and Bo Song. Without your support, my research would have been difficult to complete by now.

Furthermore, I would like to acknowledge the Georgia Electronic Design Center, National Science Foundation, Defense Threat Reduction Agency, U.S. Geological Survey and Mitsubishi Electric Research Laboratories for providing the grants to support this research work and myself during all these years.

Additionally, I couldn't have better friends during my Ph.D. journey than Dr. Yacin Nadji, Robert Pienta and Casey Battagl. They have supported me more than they think. I have countless great time to enjoy interesting conversations and bike rides with them. I was so lucky to have Yiming Kong, Jacques Florence, David Stolarsky, Francesco Amato and Rob Solomon as my dear friends and roommates. They have been so generous to take care of my cat while I was traveling. Especially, I would like to express my great gratitude to Dr. Daniela Staiculescu and Dr. Octavian Stan for their invaluable support during tough times. All of you made my life in Atlanta colorful and enjoyable.

Most importantly, I am in endless debt to my beloved parents, Kesheng Wang and Qingyou Le. Both of you have made constant and tremendous sacrifices for me to have the best you can provide. I owe who I am today to both of you for my entire education, my integrity and my health. This Ph.D. is for both of you, and yet it is only a fraction of what you deserve. I was lucky enough to have Prof. Linhua Zhai as my mentor since my childhood. This Ph.D. would have not started at all without your help and encouragement. I would not be who I am today without your guidance, unconditional support and endless love.

This final paragraph is for my beloved Dr. Alex Streit. No words can express my deepest gratitude for you. It is your love, patience, support, and encouragement to keep me going.

TABLE OF CONTENTS

LIST OF TABLES

LIST OF FIGURES

LIST OF SYMBOLS AND ABBREVIATIONS

°	Degree
3D	Three Dimensional
ACA	Anisotropically conductive adhesives
ALD	Atomic layer deposition
ASK	Amplitude Shift Keying
BW	Bandwidth
CNT	Carbon Nanotube
dB	Decibels
dBi	Decibels Isotropic
DC	Direct Current
ECA	Electrically Conductive Adhesive
EM	Electromagnetics
EPC Gen2	Electronic Product Code Generation 2
ε_0	Permittivity of free space
ε_r	Dielectric constant
ε_{eff}	Effective dielectric constant

f	Frequency
FCC	Federal Communication Commission
GHz	Giga Hertz
GO	Graphene Oxide
GPS	Global Positioning System
HCI	Human-computer Interaction
HDG	Hand Data Glove
IC	Integrated circuit
ICA	Isotropically conductive adhesives
ID	Identification
IDT	Interdigitated transducer
IL	Insertion Loss
IoT	Internet of Things
λ	Wavelength (Greek lambda)
kHz	Kilo Hertz
L	Inductor
LCP	Liquid Cristal Polymer

$LiNbO_3$	Lithiumniobate
LiTaO3	Lithiumtantalate
LNA	Low Noise Amplifier
M2M	Machine-to-Machine
MHz	Mega Hertz
mm	Millimeter
NCA	Non-conducting adhesives
nm	Nanometer
με	Microstrain
μm	Micrometer
μ_0	Permeability of free space
μStrip	Microstrip
Ω	Ohm
PCB	Printed Circuit Board
PEC	Perfect Electric Conductor
PLGA	Poly(lactic-co-glycolic) acid
PLL	Phase Locked Loop

PMMA	Polymethyl methacrylate
ppm	Part Per Million
PSK	Phase Shift Keying
Q	Quality Factor
RCS or σ	Radio Cross Section
RF	Radio Frequency
RFID	Radio Frequency Identification
RGO	Reduced Graphene Oxide
SAR	Synthetic Aperture Radar
SAW	Surface Acoustic Wave
SEM	Scanning electron microscopy
SHM	Structure Health Monitoring
SiO_2	Quartz
SNR	Signal to Noise Ratio
SRR	Split Ring Resonator
STL	STereoLithography
SWS	Smart Wearable System

TDS	Time Domain Sampling
TFT	Thin Film Transistor
TGA	Thermogravimetric Analysis
TL	Transmission Line
TRL	Thru-Reflection-Line
tanδ	Loss tangent
UWB	Ultra-Wide Band
VNA	Vector Network Analyzer
WBAN	Wireless Body Area Network
WLAN	Wireless Local Area Network
WSN	Wireless Sensor Network

SUMMARY

My Ph.D. research is mainly focused on passive RF sensing, in particular on the design and development of nanomaterial based flexible sensors for high frequency applications utilizing 3D/Inkjet printing technologies. One major advantage of nanomaterial based RF sensing platforms is the easy realization of completely passive flexible remote sensors with high sensitivity in miniaturized packaging. The utilized 3D and inkjet printing technologies inherently make feasible the large-scale fabrication of flexible sensors at a very low cost. To demonstrate the potential of the proposed approach, address effectively the major challenges, and stress the achieved advances in the field of wireless sensing, my research introduces the design and development of a passive RF gas sensor and two RF strain sensors, with a 2D bow-tie antenna and a 3D dipole antenna, respectively. This work also includes the thorough discussion of the first generation of stretchable RF sensors highlighting a hand gesture RD design for wearable remote and passive sensing platform that takes full advantage of novel stretchable conductors developed as part of the reported research.

CHAPTER 1
INTRODUCTION

Over the last five years, the ubiquitous "Internet of PCs" is rapidly moving towards a much larger "Internet of Things" (IoT) in which 50 to 100 billion devices will be connected to the Internet by 2020 [1]. Sensing devices, as the essential part of IoT, typical measure some physical parameters of an object and convert them into electrical signals. Those electrical signals can be received and processed by the object itself or other objects in the Internet. Examples include a tactile sensor for a touch-sensitive elevator button or an atomic layer deposition (ALD) based metal oxide sensor for ozone detection.

For many applications, wires are impractical and a wireless device is needed. The explosive development of microwave circuits has recently allowed sensors to be easily integrated in wireless devices for remote sensing applications. The combination of the sensor and the radio frequency (RF) device creates a feasible system that is capable of wirelessly tracking and wirelessly monitoring various time-conditions of human health or ambient environment. The variations of physical parameters such as chemical absorption, pressure, and strain are transformed into detectable variations of RF parameters, such as scattering parameters or radar cross section (RCS). Through the use of Radio Frequency Identification (RFID) technology and real-time cognition approaches, the performed research presented in this thesis could create the first generation of a truly intelligent and ubiquitous network of flexible RF sensors.

1.1 Motivation

The first implementations of IoT have redefined business practices, created new industries and provided an unprecedented level of security, comfort, and convenience in our daily lives.

Wireless sensors, as the critical part of IoT, are responsible for monitoring changes of objects' properties and wirelessly communicating with the rest of Internet. The ability to monitor and sensor health and environmental conditions in real time over large areas is typically a difficult and expensive task, especially when it comes to monitoring in harsh environments. Whether it is monitoring suspension bridges that experience immerse forces from storms and earthquakes on a structural integrity point of view, detecting noxious gases in manufacturing facilities, or making sure the vegetables or other perishable materials on the supermarket shelf are still fresh and being kept at the correct temperature and humidity levels, these sensors and sensor networks have the ability to greatly improve cognitive intelligence and knowledge of the environment around us, as long as they come at the right price.

Current methods for deploying large-scale sensor networks involve miles of cabling that deliver power and collect data, or battery operated wireless sensors, which pose a serious environmental risk with the disposal of billions of batteries every year. While these methods are necessary in some situations where real-time data or harsh environments prohibit manual monitoring of critical environment parameters, the high cost, installation difficulty, and challenging maintenance rarely justify their use over manual inspections and monitoring.

Among sensor design specifications, sensitivity is the most critical one. Sensitivity indicates how much the sensor's output electrical signal changes as a function of the measured physical state changes. Generally, sensors can be divided into active sensors and passive sensors. An active sensor needs an internal or external power supply, which makes continuously non-intermittent charging a major problem. On the other side, a passive sensor can be interrogated utilizing the incident reader's energy through an attached antenna, without requiring a permanent electrical connection to the interrogation system or power supply. Flexible sensors can wrap

around complex curvilinear shapes or biological tissues, and allow for an easy tuning of the resonant frequency and/or scattering parameters caused by mechanical deformation. In order to create a completely ubiquitous network, the sensors need to be inexpensive. Therefore, modern industry has a strong demand for highly sensitive, power efficient, flexible, low-cost and rugged methods to remotely sense the condition of objects the human body and ambient environment. As this demand has been dramatically increased over the past 5-10 years, novel materials and patterning methods become crucial to delivering reliable solutions.

Especially, nanomaterial-based RF sensing is a very fast-growing field. Advanced Nanotechnology enables the implementation of novel highly sensitive, miniaturized, flexible and wireless sensing devices that can monitor body, structural health and environmental conditions and enable correlation of multimodal sensors. Flexible electronics don't have a universally agreed definition, but this term typically includes bendable, stretchable, foldable, and other non-rigid electronics [2]. Thanks to the development of advanced material science, there are many options for conductors in flexible electronics ranging from well-established copper, silver, indium, and tin oxide to various nanoparticle metallic inks. More recently there has been developed high-performance nanomaterials, such as carbon nanotubes (CNT) and graphene. Various manufacturing techniques, such as inkjet printing, have been widely used in this area due to their low cost, the lack of environmentally-detrimental processes, the quick fabrication time and the wide range of materials that can be used on flexible substrates.

Today, the most common gas sensors are solid-state and semiconducting metal oxide devices, which are inexpensive and highly sensitive [3-7]. However, these sensors usually require operation at high temperatures (200°C - 600°C), that enhance the chemical reactivity between the sensor materials and the gas molecules. Furthermore, the high-cost and time-consuming

manufacturing processes of wireless gas sensors make them unable to meet the large-scale demands of industry and personal use. In my research I have used low cost and extremely sensitive carbon nano-materials, environmentally friendly flexible substrates, and inkjet printing technology for fast material patterning to overcome these limitations.

The development of highly deformable artificial skin with strain sensing capabilities is a critical technology to the areas of wearable computing [8], tactile sensing in robotics [9] and Structure Health Monitoring (SHM). SHM means an automated method for tracking the health of a structure by combining damage detection algorithms with structural monitoring systems, based on work by J. Lynch and K. Loh [10]. One of the most widely used methods is to detect structural deformation with embedded strain sensors in an artificial skin [11]. However, the typically required wires between the strain sensors and the interrogating base-stations increase the complexity of the design and the cost of replacing damaged or degraded sensors. By implementing the strain sensors in a wireless fashion through the incorporation of energy coupling and communication functionalities, it is possible to integrate the data acquisition and signal processing system in the same sensor unit [12]. With potentially hundreds of wireless sensors installed in a single structure, the resulting wireless monitoring system can be better equipped to screen for structural damage by monitoring the behavior of critical structural components, thereby implementing localized damage detection. Due to the fact that power consumption is a major limitation of wireless sensors operating on batteries, “zero-power” wireless sensors, such as passive RFID sensors, can be a good solution. This thesis introduces a RFID-enabled strain sensor utilizing printed flexible conductors, which are silver-filled electrically conductive adhesives (ECA). The whole flexible sensor device can be wrapped around generic mounting objects. The changes in the object’s dimensions will be reflected to resulting changes in the dimensions of the

flexible strain sensor, thus leading to a shift of the resonant frequency. The acquired resonant frequency is then used to calculate the strain on the object.

Additionally, there is a pressing demand for more accurate, lower cost and more comfortable techniques to wirelessly detect human body motion in Wireless Body Area Network (WBAN) or Smart Wearable Systems (SWS) [13]. These networks join several devices worn by a human, such as navigation devices and health monitors. An example of a SWS is shown in Figure 1. SWS is important for health care and worker protection in extreme working conditions (e.g. mines or oil platforms) [14, 15]. Hand gesture sensor/recognition is a common category of SWS. Hand gesture is a very useful communication method, especially in low- or no- visibility scenarios operators with limited mobility, and in harsh environments. Examples include underwater applications, smoke filled rooms or for patients on ventilators. A hand gesture sensor for patients on ventilators can give a timely signal to nurses. In emergency situation, it can even save a patient's life. Traditionally, wired sensors are used to monitor a patient's heart rate pulse, temperature and other bio-information. These wires can restrict the mobility of a patient whereas wireless wearable sensors can bring a much higher freedom to the patient's movement.

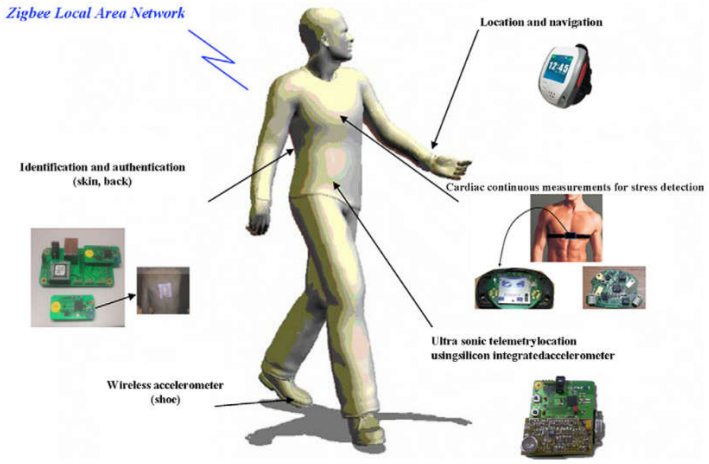

Figure 1 Example of a smart wearable system [13]

Current approaches for hand gesture sensors use vision-based hand gesture sensors or wearable Hand Data Glove (HDG). Vision-based hand gesture sensor/recognition is a popular technology, which generally includes four types camera technologies: video camera [16], depth camera [17, 18], time of flight (TOF) camera and stereoscopic camera. Depth camera which can sense directly depth images, is different from traditional video camera. Microsoft Kinect and AUSU Xtion the popular ones [19-27]. TOF cameras, such as Mesa Swiss Ranger, determine pixel depths in one of two ways: by measuring the round-trip flight-time of light projected onto the scene and reflected back to the sensor, or by measuring the phase-shift of the reflected light [28-31]. Stereoscopic camera capture two simultaneous imagines from a pair of calibrated video cameras, and use image registration methods to create a disparity map that approximates per-pixel depth [32-34]. Vision-based gesture sensor/recognition system is usually limited by the threshold of the depth/range estimation, influenced by the environment color and light and requiring effective methods for capturing and processing images. And most importantly, there cannot be objects between the cameras and the hands. Wearable Hand Data Glove (HDG) is another popular technology for hand gesture sensor/recognition, which can address these above limitations. Hand Data Glove (HDG) is an electronic device equipped with sensors which can sense the movements of hand and fingers individually, and pass those movements to computer in analog or digital signal wirily or wirelessly [35]. These sensors can be accelerometer [36, 37], bend/flex sensor [38, 39], infrared sensor [40] or force sensor [41], and so on. Following the flexible/stretchable conductor quick developments, there are more comfortable HDGs reported in the past five years. But all of these HDGs need batteries [35, 37] or wired with energy source [42, 43] to record and communicate the real-time hand gestures.

This thesis proposed a comfortable HDG technology for hand gesture sensor/recognition system using passive chipless RFID, which is easy to wear and without the battery burden. The chipless RFID technology will be discussed in Section 2.3.2. This thesis applied the same flexible conductor (ECA) to the development of the novel chipless RFID based hand gesture sensor, using 3D printing technology. The present approach relies upon the strain-dependent behavior of the propagation of electromagnetic waves in resonance/scattering based systems. Common movements of the joints in the hand produces distinguishable differences in electromagnetic signature for various hand gestures. By continuously monitoring the electromagnetic signature of the gestures using a strain sensor at each hand joint, we can uniquely code and characterize various hand gestures across a wide range of movements using a short-range reader (50cm interrogation distance). Chipless RFID technology, added on the top of in-house-made ECA materials, could provide a potentially very promising solution to lowering the total system cost of this type of wearable sensors [44].

1.2 Research Objectives

The sensors presented in this thesis have involved a multidisciplinary research effort. Therefore, the description of each sensor will include a nanomaterial study section, an electromagnetic design section, and a fabrication process section. To optimize the sensors performance in practical remote-interrogation passive sensing platforms, the introduced sensors will be investigated in real gas/strain scenarios.

The objective of the proposed research is the design and fabrication of novel, low-cost, battery-free and flexible wireless gas/strain sensors with enhanced sensitivity and miniaturized size by utilizing nanomaterials on 3D/Inkjet printers. The thesis groups the development of passive wireless sensors into three sections:

- Use of carbon nanomaterials to detect extra low concertation of gases
- Use of electrically conductive adhesives to fabricate and utilize antennas as strain sensors
- Use of electrically conductive adhesives to pattern cascaded spiral resonators as a hand gesture sensor

1.3 Significance

The significance of this work is that it is among the pioneering efforts to develop nanomaterial-based flexible RF sensors for wearable health and ambient environment monitors utilizing 3D/inkjet printing technologies.

The ability to monitor and sense environmental conditions in real time over large areas is a difficult and expensive task. First, this thesis presents the first time inkjet printed graphene based wireless gas sensor to overcome this task. The in-house-made graphene oxide ink is under a pending patent. The novel ink feathered the novel gas sensor a great sensitivity. It shows a potential low-cost way for industry standard manufacture of passive gas sensors.

Secondly, Chapter 4 introduces two flexible/stretchable strain sensor prototypes using novel flexible/stretchable conductors. The in-house-developed ECA materials have a conductivity of 1.51×10^4 S/cm and can maintain conductivity above 1.11×10^3S/cm, even at a large stain of 240%. One strain sensor is based on a 2D bow tie antenna. The other one is based on a 3D antenna. Note that not just the antenna was printed using a commercial 3D printer, but the substrate is printed on the same printer as well. The novelty of this design points out the bright future of flexible electronics.

Thirdly, a novel 3D printed wearable hand gesture sensor is a combination of chipless RFID technology and flexible/stretchable conductors fabricated by a commercial 3D printer. This

section shows the bright future of wearable flexible electronics for WBAN and SWS applications and the huge potential of 3D printing technology in this area.

1.4 Dissertation Outline

The outline of this dissertation is as follows. Chapter 2 provides a thorough literature survey of the related state-of-the-art in the areas of remote sensing, while highlighting the novelty of the research work presented in this thesis. Chapters 3 and 4 present the two main types of nanomaterial-based sensor systems: a gas sensor and two strain sensors. For the gas sensor, carbon nanomaterials were chosen to be inkjet printed on Kapton substrate for proof-of-concept demonstration purposes. The strain sensor section includes the introduction of in-house-made silver-filled ECA and its application to two strain sensors: one with a 2D bow-tie antenna and one with a 3D dipole antenna. The 2D antenna was fabricated by stencil printing on a silicone substrate. The 3D antenna was 3D printed on flexible 3D printed NinjaFlex. In Chapter 5, a hand gesture sensor is designed based on cascaded spiral resonators and implemented and tested using the same flexible ECA. Chapter 6 discussions the conclusions and some potential directions for future work.

CHAPTER 2
LITERATURE REVIEW

2.1 Sensor Background

The Internet of Things (IoT) has attracted a growing attention from both academia and industry over the past decade. The IoT is the network of physical objects or things embedded with electronics, software, sensors, and network connectivity, which enables these objects to collect and exchange data [45]. Sensors form a critical part of the IoT by providing the interface between an object's physical state and its representation communicated to the rest of the Internet. For example, the Global Positioning System (GPS) sensors in smart phones provide geo-location data, which the phone can communicate to others. Sensors can measure anything from motion to chemical environment changes, as shown in Figure 2. In other words, sensors are the eyes, ears, noses and hands of the IoT.

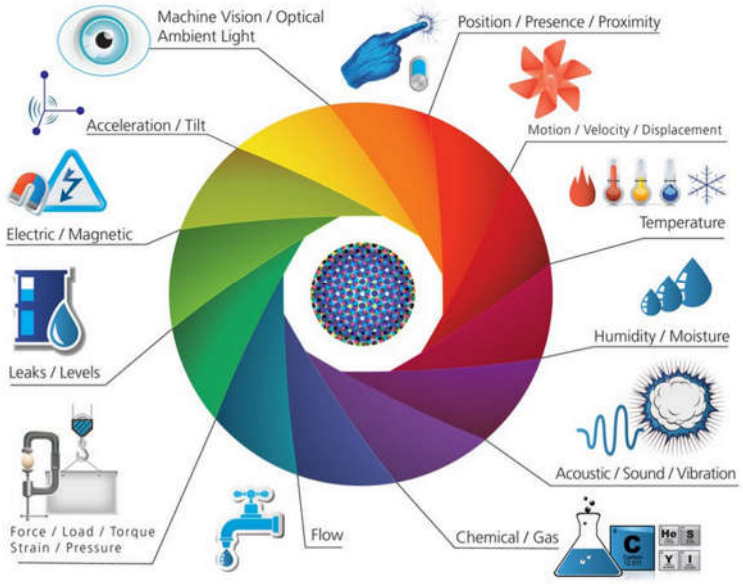

Figure 2 Sensors in the Internet of Things[46]

The term “sensor” is defined as “a device that receives a signal or stimulus and responds with an electrical signal” [47]. The “stimulus” can be any kind of an input physical property. The “electrical signal” can be channeled, amplified, and modified by electronic devices. All sensors are either passive, active, or a hybrid of the two. The passive sensors directly convert the input stimulus energy into output energy without the need for an additional power source, e.g. utilizing piezoelectric materials. Active sensors require an internal power source to produce their output signal, e.g. utilizing temperature sensitive resistors.

There are numerous sensors available in the IoT. It is necessary to classify sensors in order to study them. In considering the applications, sensors can be classified as, but not limited to:

Table 1 Types of Sensors[48]

Sensor categories	Sensing Application Examples
Acoustic	Geophone, hydrophone, seismometer,etc.
Automotive	Crank sensor, defect detector, MAP sensor, speedometer, etc.
Chemical	Breathalyzer, carbon dioxide sensor, hydrogen sensor, pellistor, etc.
Electric current, magnetic, radio	Ammeter, current sensor, magnetometer, metal detector, voltmeter, etc.
Flow	Air flow meter, gas meter, mass flow meter, etc.
Ionizing radiation, subatomic particles	Geiger counter, neutron detection, particle detector, etc.
Navigation instruments	Air speed indictor, altimeter, gyroscope, variometer, etc.
Position, angle, acceleration	Accelerometer, inclinometer, rotary encoder, etc.
Optical, light, imaging	Colorimeter, Nichols radiometer, Photodiode, etc.
Pressure, force, density	Anemometer, barograph, hydrometer, oscillating u-tube, etc.
Thermal, temperature	Bolometer, calorimeter, thermocouple, thermometer, etc.
Proximity, presence	Motion detector, occupancy sensor, reed switch, etc.

2.2 Nanomaterial Based Sensors

The term nano in SI units means 10^{-9}. Nanomaterials typically have at least one dimension smaller than 100nm. Nanomaterial science is currently in the forefront of scientific technological discussions, debates and developments as scientists, policy makers and entrepreneurs endeavor to fully harness its capabilities and unleash a broad range of novel applications, including sensors. By enhancing the interactions that occur at the nanoscale level, nanomaterial-based sensors can offer significant advantages over conventional sensors. Nanomaterials are small, lightweight and have high surface-to-volume ratio, making them the best candidates to dramatically enhance the sensitive detection of chemical and biological analytes in ambient environment [49]. At the extreme nanoscale limit, it has been reported that nanomaterials can detect a single molecule or atom [50-54]. Ultra-fast response is another benefit of nanomaterial based sensors' dynamic performance, since nanostructures minimize the time taken for a molecule to diffuse into and out of the same volume [49]. Generally, nanomaterial-based sensors can respond in a few seconds to one minute [55] enabling very effective alarm configurations capable of averting various potential disasters.

Nanomaterial-based sensors have already found applications in numerous fields, like physical sensors, electro sensors, chemical sensors, optical sensors, biosensors, etc. For instance, a large array 3D array of circuitry integrating of piezotronic transistors based on vertical zinc oxide nanowires has been reported as active pressure/force sensor matrix for tactile imaging [56]. Highly sensitive optical sensors based on fluorescent polymer nanofiber films have been also reported [57]. Multiple nanothermocouples can be circumferentially mounted on a catheter balloon to become an arterial wall temperature sensor system [58]. Polymer nanofibers have been used in developing functional sensors, as the high surface area of the nanofibers enhances their sensitivity.

Poly(lactic-co-glycolic) acid (PLGA) nanofibers have been employed as a novel sensing interface for developing chemical and biochemical sensors [58, 59].

The market for nanomaterial based sensors is constantly growing due to the dramatically decreasing cost of nanomaterials. Advances in nanotech-logy have already significantly facilitated further the nanomaterial-based sensors' integration with sophisticated electronic signal processing and communication circuits to form the critical backbone of IoT.

2.3 Radio Frequency Sensing Platforms

Most of the existing sensors require a power supply. The connection of wires for power and data transmission renders the system complex, difficult to maintain and costly. Wireless sensors are commonly needed in various remote monitoring applications in health care, environmental observation and industry. A typical wireless sensor is a device that is capable of sensing, processing data, transmitting, and communicating to other wireless devices [48].

There are two approaches in the implementation of wireless sensor systems: a completely passive system (no battery) and a sensor system with internal battery. Recharging or replacing these batteries remains a major issue of the latter and limits the operational life in the field [60-62]. Promising alternative power technologies in the sensor node level are being heavily researched, including efforts utilizing power-harvesting [63-65] and solar power [66]. While these technologies feature a large coverage range and a good sensitivity, most of them increase the complexity, the size and the cost of these active sensor systems. Therefore, passive wireless sensor technology has grown in the past decade, due to the elimination of the requirement for permanent electrical connections to an interrogation system and internal or external power supply.

RFID tags are the basic components that are bound to realize mass-scale networks with uniquely identified tagged items, obtain real time sensing data and generate a lot of new sensing applications based on the data. For RFID-enabled sensor tag, the sensor is usually integrated onto the tag antenna and the sensing-related electrical signals are communicated through common RFID technologies.

2.3.1 Passive RFID-enabled Sensor System

Passive RFID technologies have attracted a broad attention for their numerous inherent advantages: low-cost, security, long read distance, fast data transfer and low-power consumption. RFID use electromagnetic waves to identify physical objects and enable them to be connected into the ubiquitous networks of the IoT [67]. Typical passive RFID sensor systems consist of two main hardware components: a transponder/tag containing a sequence of electronic codes used for the identification of an object and a "gateway" device called an interrogator/reader for collecting information from the tags, as shown in Figure 3. Inside an RFID tag, there is an integrated circuit (IC) chip used for reading/writing and storing functionalities. The IC of the tag has an internal memory containing a unique electronic product code (EPC), which is used for identification purposes.

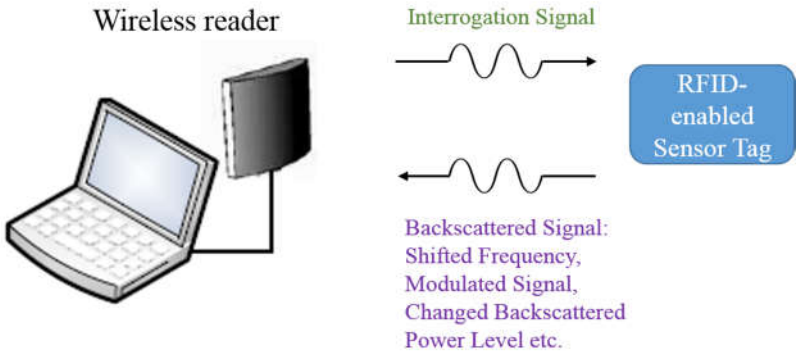

Figure 3 RFID-enabled sensor system mechanism

At the beginning of the communication process, the reader sends a continuous unmodulated carrier wave, which is received by the tag antenna. The incoming signal is routed to the tag's IC, which uses its internal rectifier to transform the weak alternating current into direct current (DC). Next, internal voltage doublers are used to charge a capacitor, which acts as a power storage device to allow short operation periods without the presence of the carrier wave. After the capacitor is charged to a sufficiently high DC voltage, the tag is ready to communicate and receive commands from the reader [68]. The reader sends commands by means of amplitude shift keying (ASK), to which the tag replies by backscattering. During backscattering, the IC switches its input impedance between two states ("load modulation"), reflecting and absorbing, according to the data contained in its internal memory, while the reader sends an unmodulated carrier wave. As the IC's input impedance is in the absorbing state, the input impedance is ideally the complex conjugate of the antenna impedance, allowing maximal power transfer between the antenna the IC. In the reflecting impedance state, the IC's input impedance is ideally short circuited, producing a complete power reflection of the carrier wave back to the reader [69]. By switching its input impedance, the IC produces either an ASK or phase shift keyed (PSK) response, depending on the modulating impedance [70].

The schematic of a typical RFID tag and its equivalent circuit is shown in Figure 4. The power reflection coefficient of the RFID antenna can be calculated to evaluate the reflected wave strength in the following formula

$$\eta = \left| \frac{Z_L - Z_A^*}{Z_L + Z_A} \right|^2 \quad (1)$$

where Z_L and Z_A represent the complex impedance of the load and the antenna terminals, respectively [71].

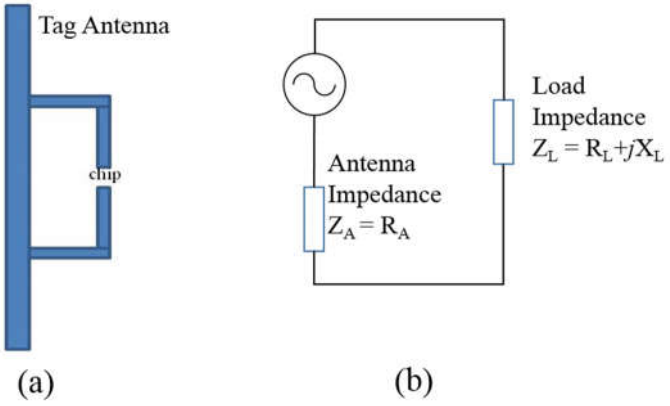

Figure 4 (a) RFID tag schematic; (b) The equivalent circuit

For RFID-based sensor systems, the load impedance is the critical part, strongly depending on the environment or other physical quantity variations, such as temperature, strain or humidity. For every variation in the tag's load impedance values, the power level of the received and reflected signals' changes. Based on the Friis free space transmission formula, the power level of the received signal at the RFID tag antenna is following

$$P_{tag} = P_T G_T G_R (\frac{\lambda}{4\pi d})^2 \quad (2)$$

where P_T is the power fed into the reader antenna, G_R and G_T is the gain of the reader antenna and the tag antenna respectively, λ is the wavelength of the carrier frequency, and d is the distance between the reader and the tag.

Due to the mismatch between the load and the tag antenna, some portion of the received power would be reflected back, called P_{ref}.

$$P_{ref} = \eta P_{tag} \quad (3)$$

For RFID-enabled sensors, η varies by the changes in the sensed quantities, therefore, the received power at the reader P_R also varies accordingly, utilizing the Friis free-space transmission formula again, assuming no polarization loss and that all other parameters remain constant during the sensing interrogation time.

$$P_R = P_{ref} G_T G_R (\frac{\lambda}{4\pi d})^2 = P_T {G_T}^2 {G_R}^2 \eta (\frac{\lambda}{4\pi d})^4 \quad (4)$$

Radar cross section (RCS) can be calculated from the reflected power as following

$$\sigma = \frac{P_{ref}}{\mathrm{S}} = \frac{P_{ref}}{P_T G_T / 4\pi d^2} = \frac{\lambda^2 {G_A}^2 {R_A}^2}{\pi |Z_A + Z_L|^2} \quad (5)$$

Since the return loss $|S_{11}|^2 \approx P_R/P_T$, the RCS can be expressed and calculated by the return loss S_{11} [72]

$$\sigma = |S_{11}|^2 \frac{(4\pi)^3 r^4}{G_t^2 \lambda^2} \quad (6)$$

When the sensor is directly integrated with a RFID tag, sensing can be based on the RCS variation of the RFID tag for an effective amplitude modulation, or on the tracking of the frequency shift of the RFID tag for an effective frequency modulation. In general, a RFID reader is considered to be fixed and associated with its respective domain. For more cost-effective and large-scale sensor system in IoT, mobile readers with location or cell ID concept can be considered [73]. This is illustrated in Figure 5 with the aid of the given example of sensor IDs. In this model, the sensor deployment field is divided into a large number of cells or locations, and each cell is assigned a unique cell ID. A reader can move from cell to cell while reading the sensor tags. The

size of a cell and the numbers or readers determine the cost and performance of the sensor system. A smaller cell size and more readers give better performance, but at higher cost.

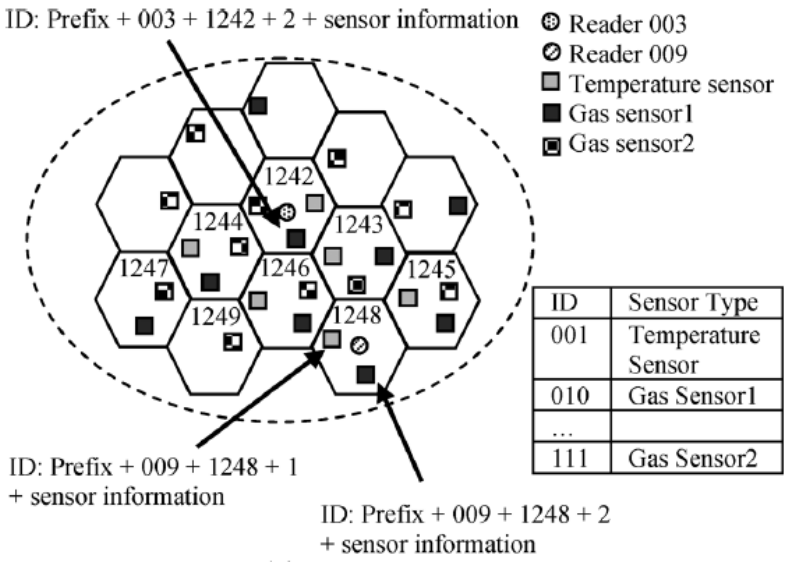

ID	Sensor Type
001	Temperature Sensor
010	Gas Sensor1
…	
111	Gas Sensor2

Figure 5 Cell RFID-enabled Sensor System Concept [73]: reader 003 located in cell 1242 and reader 009 in cell 1248

RFID tags alllow for automated tracking, as well as complex data management, reliability and non-line-of-sight reading, which make them a competitive replacement to optical barcodes[74]. The prime reason why RFID tags have not replaced optical barcodes is their relatively high cost, which is mainly due to the silicon IC chips [44, 75-79]. Additionly, the assembly process of integrating silicon chips with tag antennas and substrates is not standardized yet; thus, the production yield and efficiency is limited.

In recently years, chipless RFID technique has attracted a significant attention in the pursuing of low-cost RFID tags. Contrary to conventional chip-enabled RFID tags, passive chipless RFIDs with no IC chips can offer a more competitive price than normal silicon IC based tags [80]. The lowest attainable cost per chip-enabled tag is approximately five cents with the employment of modern, relative inexpensive chips for passive RFID tags [81, 82]. In contrast,

chipless RFID tags are expected to be less than two cents or even at a sub-cent level that would be very comparable to optical barcodes [81, 83]. However, the removal of the chip from the tag makes it inflexible for a large coding capacity.

2.3.2 Passive Chipless RFID Sensor System

Numerous investigations on chipless RFID tags have been reported. Table 2 shows a summary of recently reported chipless RFID tags based on the electromagnetic properties of metallic structures. Different chipless RFID tag solutions are compared in terms of components, scalability (increment in size with number of bits), size, coding capacity and operating frequencies in the table.

Table 2 Summary of Recently Reported Chipless RFID Tags

Classes	Components	Scalability	Size	Coding capacity [Bits]	Operating frequencies
Time domain	SAW [84]	Y	Various	>1	Various
	TL [85-88]	N	11.2×5.3 cm^2	4	UHF
	capacitor [89]	N	Length=40cm	8	1-3.5 GHz
Frequency domain	Spiral resonator [76]	N	8.8×6.5 cm^2	35	3-7 GHz
	Dual-L resonator [90]	Y	52×22.3 mm^2	6	4-7 GHz
	Single LC [91]	Y	4×4 cm^2	1	8.2 MHz
	Dipole barcode [92]	Y	N/A	5	5-6 GHz
	SRR array [93]	Y	8.6×5.4 cm^2	4	8-12 GHz
	“C”-like resonator [94]	Y	4×2 cm^2	22.9	2.5-7.5 GHz

Table 2 Summary of Recently Reported Chipless RFID Tags (cont'd)

Frequency domain	Space filling curve [95, 96]	Y	N/A	3	3-4.5 GHz
	Elliptical dipole [97, 98]	N	30.25×25 mm^2	6	0-15 GHz
	Patch antenna [99]	N	12×5.5 cm^2	3	2.17-2.51 GHz
	Dual polarized I slot [100]	N	1.65×1.65 cm^2	16	6-13 GHz
	Multi-resonant dipole antenna [101]	Y	N/A	6	3.2-5.2 GHz

Based on the adopted encoding principles for the identification, these tags are generally classified into two categories: time-domain-based RFID tags and frequency-domain-based RFID tags. Time-domain-based RFID tags usually exploit transmission lines (TLs) to propagate RF waves and utilize either microwave circulators [85, 102] to introduce propagation delays or capacitors [89] to introduce reflections, for the encryption of binary ID codes. For frequency-domain-based RFID tags, interrogation is possible only if the reflections from the environment are negligible and not mixed with the signals from other tags. In the frequency domain, ID codes are likely encoded into spectrum signatures. The ID codes can be recognized by observing the presence of either resonant frequencies [76, 81, 92, 94] or specific phases and phase differences [99, 103], or both [94]. In general, frequency-domain chipless RFID tags can feature large coding capacities and miniaturization at the same time compared to time-domain chipless RFID tags. For most frequency-domain chipless RFID tags, their size increases almost linearly with the coding capacities, because of the required extra components. It has to be stressed that there exists a bandwidth limitation to encode a large number of bits within a specific spectrum. A commonly

used solution to alleviate this issue is to place frequency-domain based signatures in ultra-wide-band (UWB) bands, typically referring to the spectrum from 3.1–10.6 GHz [104]. To utilize UWB bands, the corresponding regulations, especially the emitting power restrictions formulated by the Federal Communication Commission (FCC), have to be followed requiring power spectral density only up to −41.3 dBm/MHz [105], in order to avoid interference with other charted radio applications.

2.3.2.a Surface Acoustic Wave Based Sensor System

In the current market, the most successful commercialized chipless products are relying on surface acoustic wave (SAW) tags [106, 107]. The most attractive merits of these tags exist in their compatibility with present RFID band regulations (2.45 GHz) as well as in their large coding capacity (up to 96-bits) [84]. SAW devices are based on the piezoelectric effect and on the surface-related dispersion of elastic waves at low propagation speeds [108]. Typically device substrates are made of a single piezoelectric crystal, which generate surface charges when it is elastically deformed in certain directions, e.g. quartz (SiO_2), lithium-niobate ($LiNbO_3$), and lithiumtantalate ($LiTaO_3$).

SAW-based sensors utilize an interdigitated transducer (IDT), connected to a tag antenna, to convert the RF signal into an acoustic wave. The acoustic wave then travels across the surface of the device substrate to the interdigitated transducer, reflecting the wave back to the IDT in a series of echoes like bar code signals. These echoes are converted back into EM waves at the IDT by the piezoelectric effect and transmitted through the tag antenna. The echo pulses allow for the effective identification of the tag. Figure 6 shows the schematic of a typical passive SAW tag. Sensors can be designed to quantify many different phenomena, because the characteristics of the surface wave can be modified by the changes in the surface properties as a result of various

physical phenomena [109, 110]. Those SAW devices are the only up-to 96-bits and chipless RFID tags currently available commercially [84].

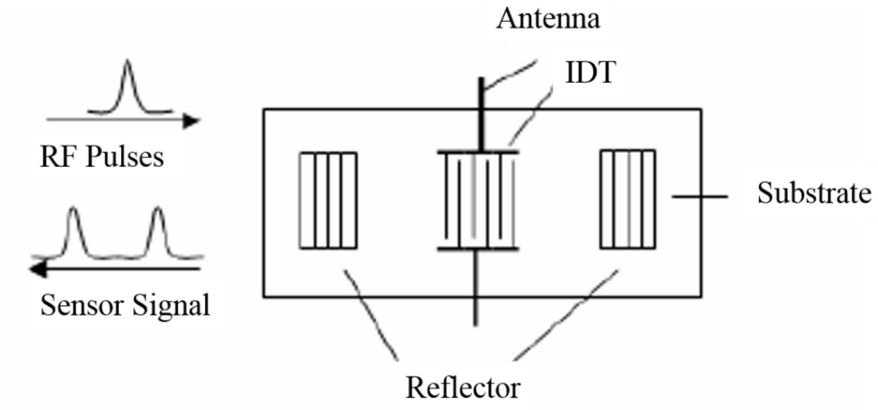

Figure 6 Diagram of a SAW based sensor tag

However, the main drawbacks of the SAW tags are that they necessitate the use of sub-micron lithographic process and expensive piezoelectric substrates [73, 78, 100] keeping the cost of SAW tags close to that of the chip-enabled RFID tags. A more aggressive approach to adress this issue is to develop printable chipless RFID tags. However, most of the reported types of time-domain chipless RFID tags lack an acceptable coding capacity or sufficient miniaturization. For this reason, more printed frequency domain chipless RFID tags have been reported than time domain tags.

2.3.2.b Frequency Domain chipless RFID Sensor System

A number of frequency domain chipless RFID tags have been reported. MEMS based strain sensors and LC/RC circuit sensors are listed in Table 3. A low-cost chipless RFID system for secure near-field data transfer is presented with a 9-bit tag [111]. It uses a frequency shifting principle by length variation of the dipoles and complex higher order mode detection techniques. Another design uses a multi-resonant dipole antenna attached to a monopole antenna to encode

bits [101]. However, it requires dual-side printing alignment and number of dipoles increases linearly with the number of bits. A chipless tag using a stub-loaded multiple patch antenna has been reported in [99], where data is encoded in the cross-polarized backscattered phase. However, if the backscattered phase is varied due to multipath, then it may cause bit-encoding errors. Two split ring resonators (SRRs) are used to encode each bit. It also is too large for many applications. Preradovic et al. successfully demonstrated a compact 35-bit chipless RFID system with a multi-frequency signal to detect the variation in the magnitude and phase of the received interrogation signal and to decode the binary information stored within the structure of the 35-bit low-cost tag, as shown in Figure 7 [76].

Table 3 Comparison of various types of wireless strain sensors [9]

Parameter	MEMS sensors	LC/RC circuit sensors	Antenna sensors
Power supply	Need battery for wireless monitoring.	LC circuits could receive power wirelessly. RC circuits need cables/wires.	Can receive power wirelessly from a transmitter antenna.
Active/Passive	Could be active and passive.	Could be active and passive	Passive.
Ability to detect strain direction	Could be designed to detect strain in any direction.	Generally unidirectional.	Could be designed to detect strain in any direction.
Wireless range	Can transmit signals over long distances.	Can transmit signals and receive power effectively only over few centimetres.	Has a small wireless range (< 1m).
Design complexity	Highly complex due to integration of various components.	Complex due to presence of inductor and capacitor integration.	Simple design due to the presence of only the antenna.
Size and weight	Large in size and heavy due to presence of battery and antenna.	Moderately large in size and less heavy compared to MEMS.	Smaller in size and much lighter compared to other sensors.

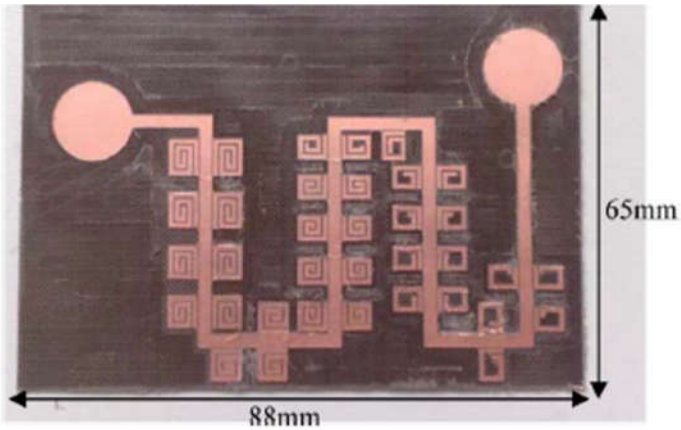

Figure 7 UWB 35-bit chipless RFID tag [76]

Most of these resonator and antenna based strain sensor systems' principle is based on the resonant frequency changing due to the dimension's change [112-119]. The detailed techniques of these resonator/antenna based strain sensor systems are listed in the Table 4 for comparison.

Table 4 Resonator/antenna Based Strain Sensor Systems' Techniques Comparison

Papers	Techniques
[114, 115]	Split rings and metamaterial based strain sensor
[116]	A dipole antenna based strain sensor
[117]	A rectangular microstrip patch antenna based strain sensor
[112, 113]	A rectangular microstrip patch antenna with a IC chip based RFID strain sensor
[119]	A circular microstrip patch antenna based strain sensor

Chipless tags could potentially possess a longer communication range –mainly depending on the reader's sensitivity - since it is unnecessary to use transistors as do silicon-based tags where a threshold voltage is a requisite to power up IC chips [80, 98]. A monolithic chip typically requires

-15 dBm at the chip terminals to start the communication [98]. The power required to read the tag significally increases while the read range increases. Meanwhile chipless RFID tags do not have such an issue. There are a number of chipless RFID sensor systems reported in the past decade. In Chapter 5, a compact strain sensor system will be presented based on a chipless RFID tag with resonators. As mentioned in Section 1.1, a wireless strain sensor system can be used for SHM, WBAN or SWS.

2.4 Nanomaterial-Based Radio Frequency Sensors

The combination of nanotechnology and RF sensing technology has enabled the development of numerous novel highly efficient, miniaturized, inexpensive and fast response wireless sensors. The first nanomaterial based RF chemical/gas sensor was introduced in 2002 [120]. This sensor used a RF resonator coated with CNT to achieve sensitivity to ammonia in quantities as low as 92.69 ppm with a resulting maximum frequency shift of 6.25 MHz. The first nanomaterial based RF strain sensor was presented in 2005 [121], using a conductive coaxial electromagnetic cavity and an antenna with a sensitivity of 2.45 kHz per micro strain (με). The relatively simple system architecture and small size of passive nanomaterial-based RFID sensing systems open up new possibilities, such as on-demand sensor systems as a smart skin for strain. In ambient conditions and biomonitoring sensing applications, they can act as Machine-to-Machine (M2M) communication nodes when integrated to Wireless Sensor Networks (WSNs). This smart skin can be embedded into clothes or directly wrapped around non-planar and biological surfaces and widely used to monitor human body motions and offer new opportunities for real-time health monitoring [122-124].The nanomaterial-based RF sensor systems could potentially be one of the most enabling factors to implement realistic large-scale topologies of IoT in the future [125]. This

new field is still in its infancy, but product requirements and technical capabilities point to a bright future for nanomaterial based RF sensors.

2.5 Flexible Electronics

The electronics of the future will be soft, conformal, and rubbery, widely known now-a-days as "flexible electronics". Devices will be flexible, stretchable, twistable, and deformable into curvilinear shapes, thereby enabling applications that would be impossible due to the rigid, brittle, and planar nature of the electronics of today [126]. Flexible electronics is a wide-open and rapidly developing field of research, development, and pilot production, especially in the past two decades [127]. However, the concept of flexible electronics has a long history. In the 1960's, the first flexible solar cell arrays were made by thinning single crystal silicon wafer cells to ~100 μm and then assembling them on a plastic substrate to provide flexibility [128]. In 1968, Brody and colleagues made the first flexible thin film transistor (TFT) of tellurium on a strip of paper and proposed using a TFT matrix for flexible displays.

Flexible can mean many qualities: bendable, conformally shaped, elastic, light weight, non-breakable, roll-to-roll manufacturable, foldable, stretchable or wearable. From an electronic engineering point of view, flexible electronics mean –among others- conformally shaped displays and sensors, electronic textiles, soft robotics and electronic skin [9, 11, 128-132].

Historically, the strategy for enabling flexibility in rigid materials has involved a simple idea of mechanics- any material can flex as long as it is sufficiently thin. For a thin film, there is a well known relationship between strain and thickness, described by

$$\varepsilon = \frac{d}{2r} \tag{7}$$

where ε is the strain, d is the thickness of the thin film and substrate, and r is the bending radius [133].

Today, two general approaches are mainly used for the fabrication of flexible electronics. The first utilizes conventional rigid materials, but employs wavy or arc-shaped structures that are capable of accommodating applied strains of 100% or more [134-136]. The second approach is to maintain the conventional circuit layout, but embed stretchable or flowable conductive materials, such as conductive polymers [137, 138], conductive polymer composites [139] or liquid metal alloys [140-142] to implement fully stretchable conductive lines. The fabrication processes of the first approach are more complex and expensive, leading to more and more attention on the second approach.

Liquid metals, mainly Gallium Indium (GaIn) Eutectic, are low cost and highly scalable flowable conductive materials. However, they are commonly toxic and have a low melting point. For example, GaIn's melting point is 10.2°C, which is well below the average operational temperature required for consumer electronics. The crucial part of embedded flexible conductors is to maintain a high conductivity during bending, stretching, or even folding. Besides liquid metal, other flexible conductive materials mainly consist of composites formed from conductive particles embedded in a polymeric resin, such as epoxy, polyimide, polyurethane or silicone. In these composites the polymer provides the properties of flexibility, toughness, physical shape and structure, while the metallic fillers, such as silver, gold, nickel, copper, or carbon, provide electrical conductivity. Previous studies have mostly focused on 1-D high aspect ratio fillers, such as CNTs and silver nanowires [136, 143-145]. However, the conductivity is maintained only if the applied stress is in the longitudinal direction of the fillers and extension in other directions causes poor conductivity. 2-D conductive flake fillers have significantly higher overall conductivity in all

directions and therefore have become a trending solution [146, 147]. Compared to metallic, mainly tin-lead (Sn-Pb) alloy, solder technology, polymer-based composites like ECAs are not just the ideal interconnect alternatives [148, 149]. They also feature numerous advantages, such as environmental friendliness (elimination of lead usage and flux cleaning), mild processing conditions (enabling the use of heat-sensitive and low-cost components and substrates), fewer processing steps (reducing processing cost), low stress on the substrates, and fine pitch interconnect capability (enabling the miniaturization of electronic devices) [149-155]. Specially, polymer-based ECAs offer the advantage that they can be processed at low temperature ($T < 150°C$), which is significantly lower than metallic solders.

ECAs have been commonly classified into three categories with respect to conductive filler loading level: isotropically conductive adhesives (ICA, with 1-10 μm sized fillers), anisotropically conductive adhesives / films (ACA / ACF, with a typical 3-5 μm sized conductive fillers, or in a film form) and non-conducting adhesives (NCA , no conductive filler particles) [148]. NCA bonding technology requires no fillers and instead uses a relatively high bonding pressure to make direct physical contact between two conductive surfaces and a permanent joint by NCA resin curing solidification [156-158]. NCA doesn't have conductivity by itself. Based on the percolation theory, the percolation threshold depends on the shape and size of the fillers, but typically in the order of 15~25% volume fraction [159, 160]. For ICA, the loading level of conductive filler exceeds the percolation threshold, as shown in Figure 8, proving electrical conductivity in all directions [161-163]. For ACA/ACF, the loading level of conductive fillers is far below the percolation threshold, which is insufficient for inter-particle contact and prevents conductivity in the XY plane of adhesive. Therefore, they provide a uni-directional electrical conductivity in the

vertical or Z-axis [164, 165]. In electronic packaging industries, ICAs have attracted more and more attention due to their uni-directional electrical conductivity.

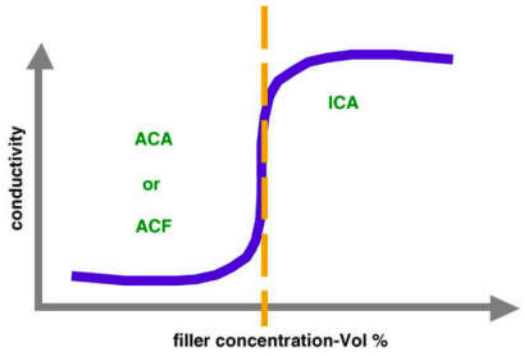

Figure 8 A typical percolation cureve showing the abrupt increase in conductivity at the percolation threshold [149]

In ICAs, the conductive fillers provide the composite with electrical conductivity through contact between the conductive particles. The possible conductive fillers include silver (Ag), gold (Au), nickel (Ni), copper (Cu) and carbon in various sizes and shapes. Silver flakes are the most popular conductive fillers. Beside their intrinsic flexibility, high conductivity, simple process and low cost, they are unique among all the cost-effective metals by nature of silver conductive oxide. Oxides of most common metals are electrical insulator. Copper powder, for instance, becomes a poor conductor after aging.

ECAs have been adapted as interconnect materials for electronic packaging industries in the past two decades. With the increased electrical and mechanical performance of ECAs, there are more and more potential applications for flexible electronics in WBAN, flexible display[166-169], flexible energy storage devices [170, 171] and SWS. In Chapter 4 and 5, we will introduce ECA based strain sensors.

2.6 Patterning Technologies for Flexible Electronics

The Patterning processes for functional materials, such as those compared in Table 5, are among the key technologies to enable flexible electronics.

Table 5 Feature Comparison of Patterning Processes [172]

	Environment	Deposition mode	Patterning type	Contact	Scaleable
Rigid Support	Vacuum	Subtractive	Indirect	Photolithography	No
Vacuum R2R	Vacuum	Subtractive	Indirect	Photolithography	Yes
Flexography	Atmospheric	Additive	Direct	Contact	Yes
Soft Lithography	Atmospheric	Additive	Direct	Contact	Partially
Gravure	Atmospheric	Additive	Direct	Contact	Yes
Imprinting	Either	Subtractive	Indirect	Contact	Yes
Offset Lithography	Atmospheric	Additive	Direct	Contact	Yes
Flatbed screen	Atmospheric	Additive	Direct	Usually contact	Yes
Rotary screen	Atmospheric	Additive	Direct	Contact	Yes
Ink jet	Atmospheric	Additive	Direct	Non contact	Partially
Aerosol jet	Atmospheric	Additive	Direct	Non contact	Partially
e-jet	Atmospheric	Additive	Direct	Non contact	No
Pen/dispensing	Atmospheric	Additive	Direct	Either	No
Thermal/laser	Atmospheric	Additive	Direct	Contact	Yes
Electophotography	Atmospheric	Additive	Direct	Contact	Yes

Additive patterning processes are more material efficient compared with subtractive patterning processes, since the patterned material is deposited only in the desired position. These processes eliminate the need for etching and material waste. Direct patterning means less intermediate material/process involved. For flexible patterning processes, contact during the process can lead several problems, such as contamination or perturbation (scratches) of the physical structure of the underlying materials. Scalability is another consideration for patterning processes, which is desirable for the translation of small scale research and prototype processes to industrial scales via roll-to-roll processing, which is well known for its use in the newsprint industry. The roll-to-roll technology shown in Figure 9, where the substrate is printed on as it comes off a reel. The printing is followed by in-line curing, where the material is cured on the substrates. This method can print conformal electronics that are kilometers long, if required, which

makes printing an optimal fabrication method [173]. For manufacturing at industrial scales, of course, cost is another consideration. This thesis focuses on two additive, non-contact, scalable and low-cost patterning processes: inkjet printing and 3D printing technologies.

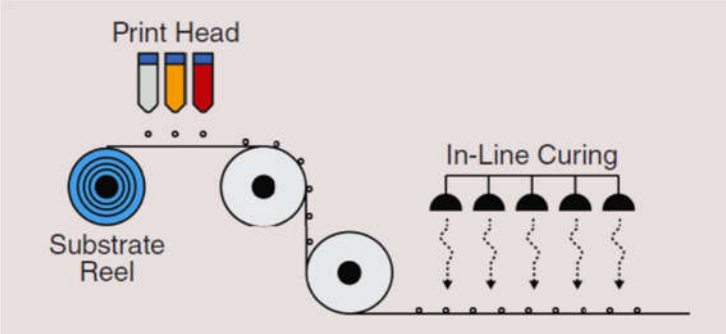

Figure 9 Roll-to-roll printing process used in an industrial environment

2.6.1 Inkjet Printing Technology

Traditional wet etching techniques, which form the backbone of the conventional PCB fabrication process, involve complete metallization of substrate laminates and subsequent selective etching of portions of the metal layer on top of the substrate. Milling machines are also used to realize circuits on metal laminated substrates. They operate like plotting machines, with milling bits that selectively remove unwanted metal from the PCB boards. Both methods suffer from a significant amount of waste during the fabrication process. Up to now, most typical fabrication processes on flexible substrates have been taking place in a clean-room environment or are subtractive processes meaning that they are expensive and have detrimental environmental effects due to the hazardous chemicals required, while being especially wasteful for circuits which do not contain large metal areas.

Printing technologies have been playing an ever increasing role in the growing field of flexible and conformal electronics. This is due to their low operation cost, ability to deal with

flexible substrates, and capacity to work at a large scale [174]. Printing processes, such as inkjet printing, are strictly additive and therefore do not waste material. For flexible electronics, piezoelectric inkjet is by far the most common technology in inkjet printing, which uses an electrostatic potential difference (normally 5 ~ 12 V) between a charged electrode attached to the ink cartridge and the base plate on which the substrate is mounted [175]. The two stages of piezoelectric inkjet printing process are presented in Figure 10. The cost effective and "green" nature of inkjet printing technology as a fabrication method on low cost organic flexible substrates, such as paper, make it ideal for large scale roll-to-roll processing with high repeatability. It is especially suitable for fabrication of large area circuits that do not contain large metal areas, such as wireless sensors and RF communication and control modules [176].

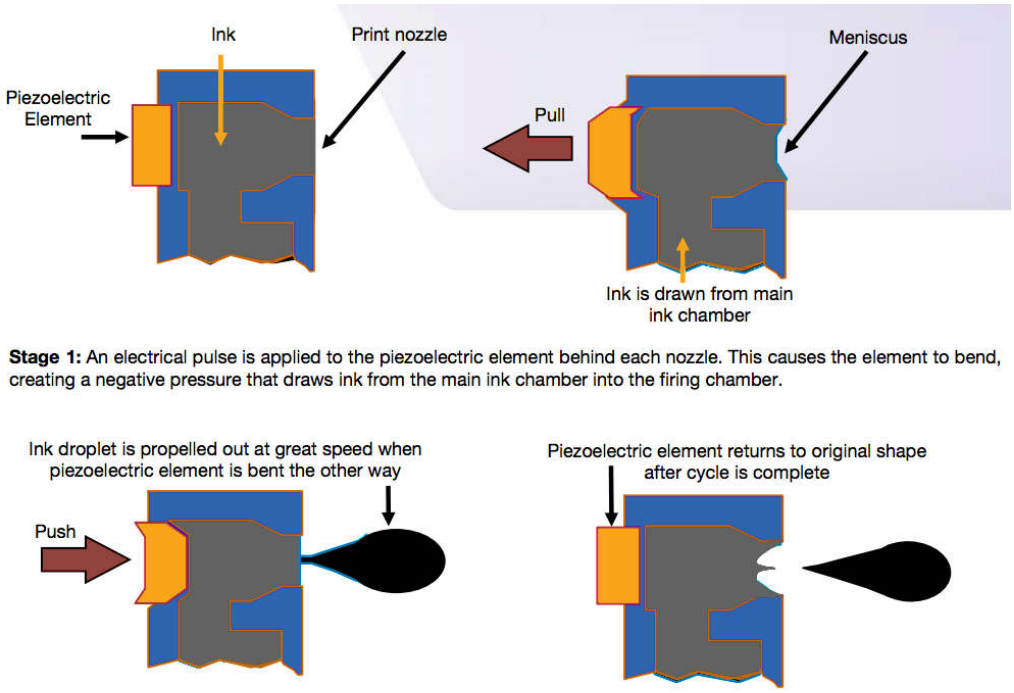

Figure 10 The piezoelectric inkjet printing process [177]

A number of manufacturers have produced print heads that are designed specifically for the printing of functional materials (such as silver nanoparticles, SU8, PMMA) through micro-sized nozzles in the past two decades [178-180]. Several nozzles can run at once to pattern multiple materials simultaneously. Once the materials are patterned onto the substrate, curing methods such as heat, laser, or atmospheric modification, melt or link the printed nanoparticles into bulk structures [178, 181, 182]. The entire process can be completed in a matter of minutes allowing for rapid production at large scale. An example of this process is shown in Figure 11. Because of the wide variety of materials, the use of nano-enabled ink has become more and more popular for flexible electronics up to the millimeter-wave frequency ranges. In Chapter 3, Inkjet printing carbon nanoparticles will be applied in the gas sensor fabrication process.

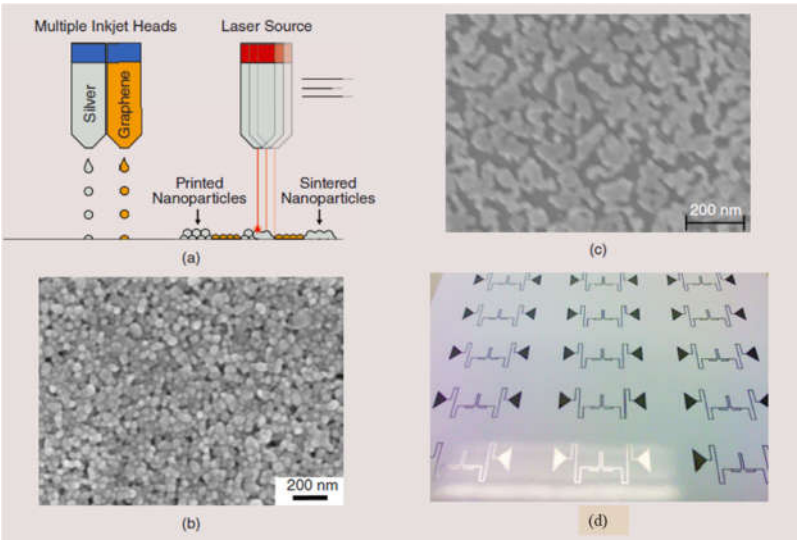

Figure 11 (a) Diagram of an in-line laser sintering process to anneal printed nanoparticles; (b) SEM of non-annealed printed silver nanoparticles; (c) SEM of sintered silver nanoparticles; (d) an inkjet printed RFID array.

2.6.2 3D Printing Technology

The enormous diversity of materials and support materials that can be used for flexible electronics requires different patterning processes in order to handle the different combinations of properties and complex structures. 3D printing is the technology of building physical objects up layer by layer, based on detailed digital blueprints [183]. Even though 3D printing has been used in some industries for three decades, freely available softwares, the falling cost of 3D printers, and increasing number of 3D printing materials are bringing 3D printing technology to the mainstream. The advantages of 3D printing technology include time saving and the capability to fabricate complex full 3D structures with multiple materials which are not possible with standard fabrication methods. The rapid growth in 3D printing technology offers unique advantages in terms of optimal non-orthogonal shapes, on-demand deposition of nanostructures and antennas, as well as multilayer stretchable hermetic RF packages for flexible RF modules.

2.6.2.a Different Types of 3D Printers

In the past decade, the growing affordability of 3D printers has brought 3D printing technology more attention. So far, there are several different types of 3D printer technologies in the market: fused deposition modeling (FDM), stereolithography (SLA), selective laser sintering (SLS), Selective laser melting (SLM), electronic beam melting (EBM), digital light processing(DLP), laminated object manufacturing (LOM) and micro dispensing.

FDM, for which the patent was first filed in 1989 by S. Scott Crump [184], is the most popular technology in the current 3D printer market. This technology begins to slice a 3D model file, usually in a STereoLithography (STL) file, into horizontal layers with a collection of paths. The FDM printer head pushes a filament through a heated extruder. The material is extruded through the printer nozzle while following the paths. The material feed rate and printing speed can

be controlled in the sliced file. After finishing one layer, the extruder will be moved up by a single layer height. New thermoplastic materials are constantly being introduced into filament form for FDM printers. Some popular ones include: acrylonitrile butadiene styrene (ABS), polylactic acid (PLA), polyethylene terephthalate (PET), polyvinyl acetate (PVA), NinjaFlex and polycarbonate (PC). In Chapter 4, the 3D antenna based strain sensor has NinjaFlex printed part.

SLA is the oldest technology in the history of 3D printing and the second most popular in the current market. SLA printers turn liquid plastic into solid object layer by layer by a laser. There are more and more SLA machines showing up in the market, like Carbon3D and 3D Systems, VisJet and Loctite. They use different liquid plastic, so the printing quality and the printing time varies in a large range.

Among all the current 3D printing technologies, micro dispensing , which belongs to direct writing additive manufacturing (DWAM), is a good option for various materials and random patterns [185, 186]. Micro dispensing machines include nScrypt, Hyrel 3D, Optomec, Nordson Asymtec, and Camelot. Micro dispensing usually pushes the material through the printer nozzle directly onto the desired area. The nScrypt 3D printer uses a patented valve near the dispensing nozzle to accurately control the start point and the end point of the material flow. Figure 12 shows the cross section of the valve assembly from nScrypt. The valve rod is driven by a moto and travels along the channel of the valve body with a resolution of 0.1 μm [187]. The shape of the pen tip is specially designed to reduce the pressure needed to push material through the nozzle with a small size, such as 50 um or 12.5 um. The assembly is capable of handling materials with an extreme viscosity range from 0.001 to 1000 P_A·s. Figure 13 shows the printing samples by SmartPump^{TM}. In Chapter 5, the hand gesture sensor is printed by nScrypt SmartPump^{TM}.

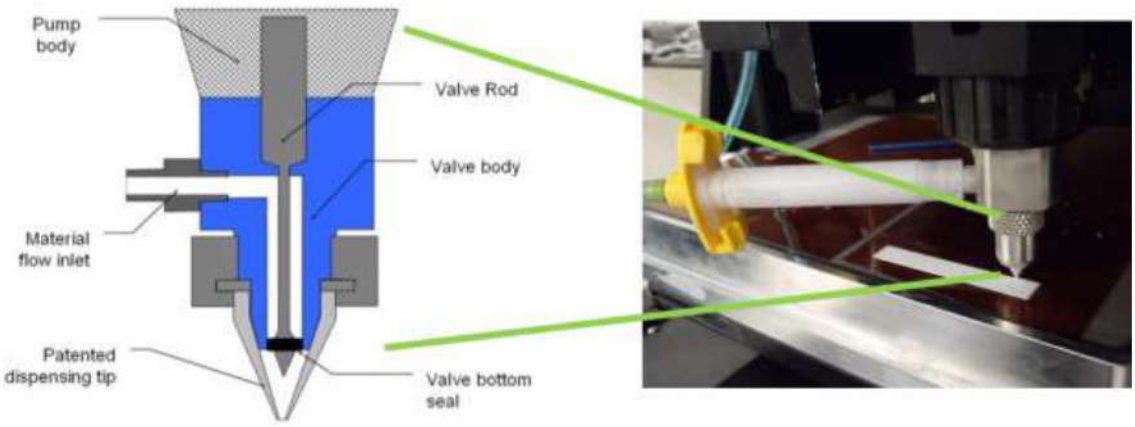

Figure 12 nScrypt Inc. SmartPump^{TM} valve assembly (by Xudong Chen in nScrypt) [188]

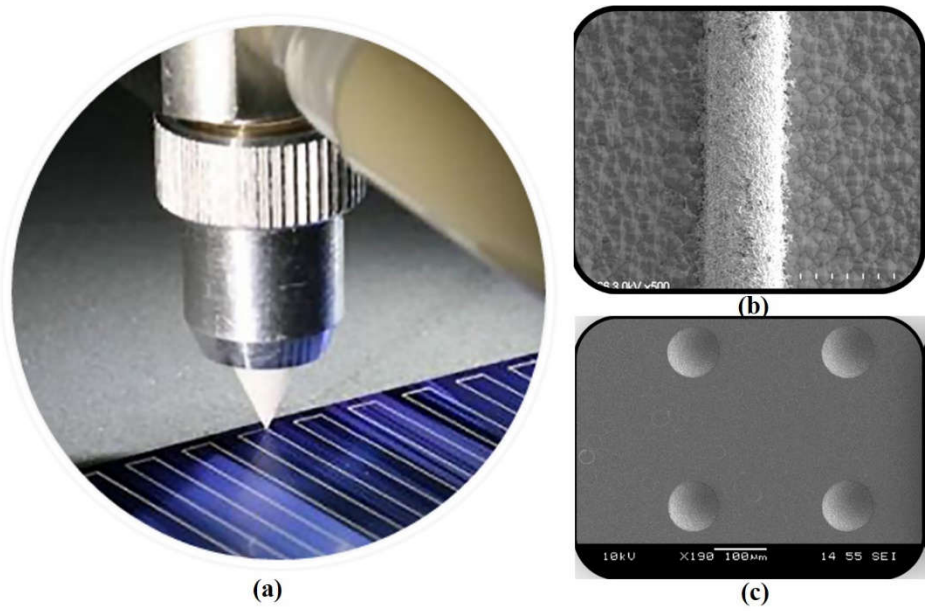

Figure 13 SmartPumpTM printing results (a) SmartPumpTM during printing process; (b) SEM of 50 µm wide conductive lines; (c) SEM of 100 µm diameter adhesive dot. [187]

2.6.2.b 3D Printing Materials for Flexible Electronics

In the past few years, a flurry of new flexible materials have emerged in the 3D printing market. NinjaFlex and FilaFlex [189] feature the best performance during the stretch tests among the new materials [190]. NinjaFlex is the most popular flexible/stretchable 3D printing material [191, 192] and it is also able to bond to PLA and ABS, which are the most common 3D printing

materials potentially enabling 3D printing to be applied to numerous new areas, such as flexible electronics. Nevertheless, it has to be stressed that most previously reported NinjaFlex projects have only been in the DC or low frequency domains. In Chapter 4, the substrate of the strain sensor is printed by NinjaFlex by FDM technology.

In the past decade, flexible/stretchable conductive materials by direct writing method has been attracting more and more attentions in wire bonding [166, 193], strain sensor [42] and RF components [194]. These technologies are still in their infant stage, not mature enough to be commercialized. In Chapter 5, the hand gesture sensor is 3D printed using an in-house produced ECA.

CHAPTER 3
NOVEL INKJET-PRINTED GRAPHENE-ENABLED WIRELESS GAS SENSORS

The early and accurate detection of hazardous chemicals is advantageous for both industrial use and for environmental cognition, and is of benefit to both the public and private sectors. Recent advances in materials science have led to the employment of novel nanomaterials, such as carbon nanotube (CNT) and graphene, for chemical sensing applications [50-55, 120]. These materials alter their properties in the presence of a given substance by absorbing the chemicals on their surface. Chemical/physical absorption produces changes in material properties such as real and imaginary impedance, DC resistance, or effective dielectric constant [112]. These changes can be exploited to determine the presence of various chemical compounds by translating the material effects into measurable electrical quantities, such as changes in voltage, current, resonant frequency, or backscattered power amplitude.

3.1 Carbon Nanomaterials

This study will consider the use of graphene as a means to enhance the sensitivity performance, and as a means to introduce selectivity into the functionality of gas sensor efforts. Graphene is a single planar layer of carbon atoms with exotic physical properties including high mobility of charge carriers (200K $cm^2V^{-1}s^{-1}$), and high thermal conductivity (~5K $Wm^{-1}K^{-1}$) [52]. Most importantly, as a zero bandgap semiconductor, graphene's high metallic conductivity and low charge carrier density enable extreme sensitivity, because small variations in charge carrier density yield notable changes in conductivity. Single gas molecule detection has been demonstrated in a prototype device [52].

Graphene was chosen in the proposed work for three reasons. Firstly, it exhibits remarkable electronic and mechanical properties [195-197], and graphene oxide materials can be easily dispersed in water for ink [54]. Previous work in our group on a CNT based wireless gas sensor found that the short lifetime and poor dispersion of CNT ink limited the obtainable material performance [112, 178]. Secondly, since graphene is an extremely low-noise material electronically, graphene offers clear advantages in terms of minimum detection levels compared to other solid-state gas sensors, such as those created from CNT [52]. Lastly, graphene's ability to be functionalized for a wide range of chemicals makes it an ideal candidate for the development of portable and wearable sensors with a broad detection spectrum. The ability to deposit graphene oxide materials via inkjet printing of aqueous solutions on low cost, flexible, and environmentally friendly substrates opens the possibility of mass producing such devices and taking advantage of economies of scale.

3.2 Reduced Graphene Oxide (RGO) Based Gas Sensor Prototype

The proposed work establishes for the first time the principles of wireless gas sensor design utilizing graphene thin films. It combines both analog and digital wireless remote transmission principles with graphene-based enhanced selectivity, featuring the first ever inkjet-printing of an aqueous graphene solution on flexible Kapton substrates. Regarding the digital transmission scenario, the coupling of gas sensing with power-efficient wireless data transmission is achieved by deploying Intel's Wireless Integrated Sensing Platform (WISP) [198]. WISP adds microcontroller functionality to traditional RFID tags, which operate as the sensor's integration platform. The WISP can be programmed to sample a variety of different responses and produce gas detection results taking advantage of additional processing, such as time-averaged stabilized or normalized difference gas-induced material changes.

The core of the wireless gas sensor is a prototype board made from graphene deposited onto Kapton substrate by inkjet printing. There are six fabrication/integration steps for this prototype.

3.2.1 Creation of Graphene Oxide Ink

The first step in the sensor development process was the creation of stable, long-life, inkjet-printable graphene-based inks. This was accomplished by first converting the graphene into graphene oxide (GO) powder. Unlike pristine graphene, which has very poor dispersion in common solvents, GO exhibits excellent solubility in water due to the existence of hydrophilic functional groups on the surface [199], rendering it an excellent candidate for development of environmental friendly water-based inks. After deposition, pure graphene was obtained by the reduction of GO, which reverts to the conjugated basal plane and restores the electrical properties of the material. The reduction of GO is one of most promising methods for low-cost, high-yield and scalable preparation of graphene materials [200].

The GO was produced by chemical oxidation of graphite, which introduces oxygen-containing functional groups to exfoliate pristine graphite into individual GO sheets. GO was prepared with Hummers' method [201]. Specifically, graphite flakes are placed into a $NaNO_3$ /concentrated H_2SO_4 solution in an ice bath. Subsequently, $KMnO_4$ is slowly added to the solution while maintaining the temperature under 20°C. The mixture is stirred in the ice bath for 2 hours, then for an additional 30 minutes in a 35°C water bath. After that, 70°C water is added slowly to the flask. The heat generated via exothermic reaction raises the solution temperature to 98°C. Additional 70°C water is added, followed by hydrogen peroxide solution to terminate the reaction. The mixture is filtrated and washed with water to remove excess acid and inorganic salts. The resulting GO is dried overnight at 55°C to produce the GO powder. For this gas sensor prototype,

dry GO powder was dispersed in a water/glycerol solution and sonicated to form a homogenous dispersion to prepare the GO ink. Figure 14 shows brown color GO ink in an inkjet printer cartridge.

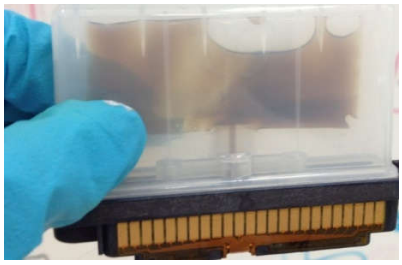

Figure 14 GO ink in an inkjet printer cartridge

3.2.2 Fabrication via Inkjet Printing

Inkjet printing of electronics has been enabled by the discovery of printable conductive nanoparticles. In [202], the silver ink has been characterized up to 12.5 GHz and the highest conductivity by inkjet printing achieved 1.1×10^7 S/m. These nanomaterial-based inks also consist of nanometer sized particles of CNTs, graphene, or a wide range of semiconducting and polymer compounds, in addition to metals, as long as the particles are small enough to be printed through the micron-sized nozzles of an inkjet printer head. Several nozzles can be run at once to pattern multiple materials simultaneously. Once the materials are patterned onto the substrate, curing process, such as heat, laser, and atmospheric modification, melts or links the printed nanoparticles into bulk structures [181, 182, 202]. The entire process can be completed in a matter of minutes allowing for the rapid production at large scale. An example of this process is shown in Figure 15. Because of the wide variety of materials this process can deposit, the use of nano-enabled ink has become popular for printing RFID-based antennas, sensors, and even CNT-based diodes and transistors [203-205]. This makes the printing process a very appropriate process to integrate monolithic integrated sensors, antennas, and RFIDs into smart skins.

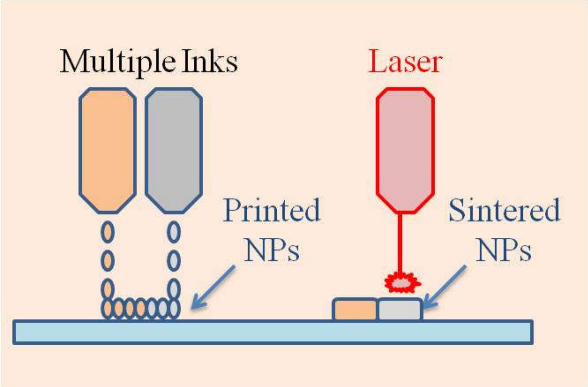

Figure 15 Diagram of an in-line laser sintering process to anneal printed nanoparticles

For this gas sensor prototype, a Dimatix Materials Printer (DMP-2800) series material deposition system was used to print both the silver and GO inks, as shown in Figure 16. The substrate is 125-um-thick Kapton 500HN polyimide film by DuPont [206]. Before printing, the Kapton substrate was treated by UV-Ozone to improve its hydrophilicity. The treated Kapton demonstrated improved performance during printing compared to the native Kapton substrate, enabling higher resolution prints and more layers to be printed during a given cycle.

Figure 16 Dimatix Materials Printer

The fabrication process involved deposition of 10 layers of conductive silver onto the kapton substrate, followed by 17 to 27 layers of graphene oxide. First, the 10 layers of silver ink

were deposited and cured at 120°C for 8 hours. Cabot's CCI-300 conductive silver nanoparticle ink was used to print here. Based on [202], 10 layers of silver ink and the curing time make sure the good electrical performance of the silver electrodes. Next, two layers of GO were deposited and cured at 80°C for four hours to serve as a foundation for further prints. These two foundational layers overlapped the silver pads by 0.5mm to ensure optimum connectivity. These two foundation layers need to be reduced as the method in Section 3.2.3. Next, the GO was deposited in five layer increments with curing in between to ensure the highest consistency between samples. After the reducion of the GO thin film, another two layers of silver ink was printed following the previous 10 layers silver traces. Figure 17 (a) illustrates the printing of GO ink. Figure 17 (b) shows the completed sensor elements prototypes prior to reduction of the GO thin films.

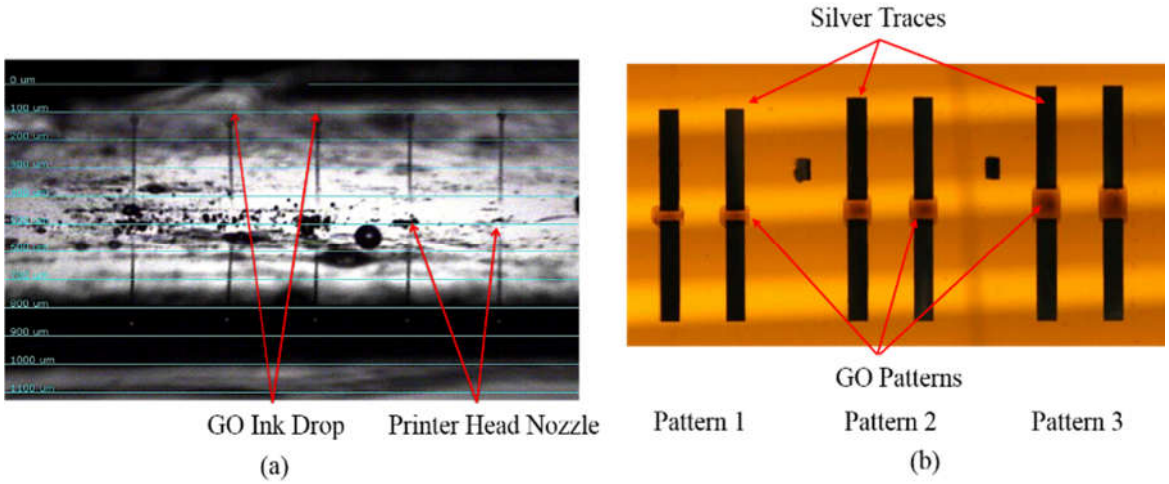

Figure 17 (a) GO ink drop ejected from printer head; (b) GO thin films inkjet printed in-between and overlapping inkjet printed silver traces on a Kapton substrate.

3.2.3 Reduction of Graphene Oxide

After printing and curing, each sample was reduced to obtain the desired graphene from the GO. Due to the requirements for the reduction process of graphene oxide, we fabricated the samples on Kapton substrates. After thermal reduction, the resistance became as low as 150Ω,

approximately 1000 times better than the performance mentioned in current literature [207]. Reduction was achieved by placing the printed GO thin films in a hydrogen and argon atmosphere under elevated temperature. The samples were reduced at 200°C for 30 min and 300°C for another 30 min. The heating rate was 5°C/min. After reduction, the samples were left to cool to room temperature. Scanning electron microscopy (SEM) was used to determine the overall quality of the graphene thin films (i.e. presence of defects in the print, etc.), and to make adjustments in processing to further prints. Figure 18 provides SEM images of both the initial GO and (reduced) RGO thin films. The wrinkles on the surface of the samples in Figure 18 are typical characteristics of GO and RGO thin films produced by chemical oxidation methods. The wrinkles are due to structural defects caused by oxygen functional groups. Oxygen bonds created in exfoliating the graphene oxide from graphite distort the carbon bonds, producing the "characteristic" wrinkles in the RGO thin films. These wrinkles are reduced, but still present after the reduction process.

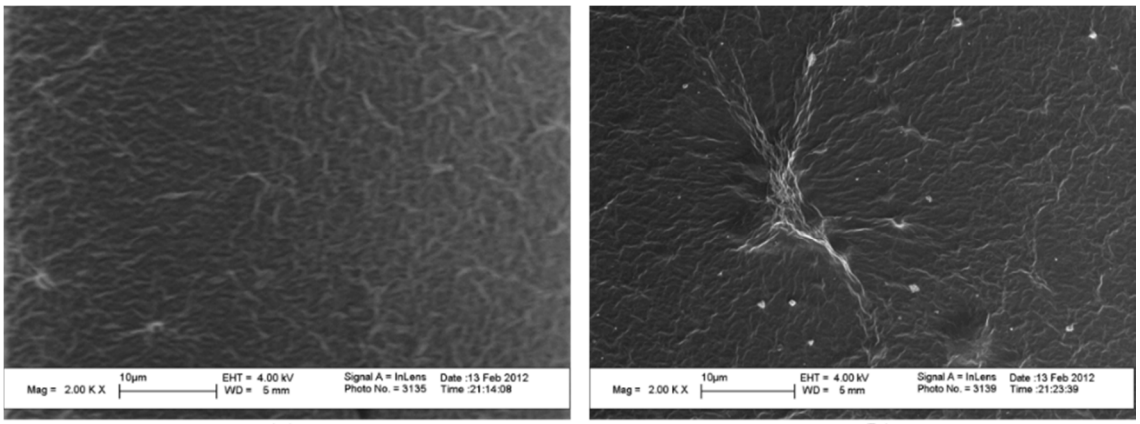

Figure 18 (a) SEM image of the inkjet printed GO thin film; (b) SEM image of the inkjet printed RGO thin film [208].

3.2.4 Final Packaging Steps

One important fabrication factor, which was explored in the framework of this work, is the impact of the contact between silver and graphene on system performance. Based on experimentation, we determined that the application of an additional 10 layers of silver on top of the graphene guarantees better connectivity between the graphene and silver traces. It also helps to de-embed any additional impedance which would offset the measured change of impedance unevenly among different samples of similar dimensions. We perform this step to reduce the variability between samples.

Optimization of the RGO thin films was performed in order to obtain the proper sensor area to ensure maximum sensitivity while obtaining the requisite intrinsic impedance to ensure the sensor's operation. To determine the optimum sensor area, three patterns of RGO material were produced from left to right, as shown in Figure 17 (b). It was expected that the larger surface area of the last pattern would yield the highest sensitivity. Based on previous efforts on thin film design, it was estimated that between 15-25 layers of the material would be necessary to achieve the desired resistance for the given dimensions of the RGO pads. To validate this assertion, samples of both 15 and 25 layer versions of the patterns were printed and reduced. The measured results confirm the assertion as shown in Table 6 below. These values represent the average resistance values for a given combination of RGO pad dimension and thickness (# layers). The resistance value did increase for increasing pattern area/dimension, and decrease for higher numbers of printed layers.

Table 6 Average intrinsic resistance values of RGO thin films

# LAYERS	PATTERN 1 1mm×3mm	PATTERN 2 2mm×3mm	PATTERN 3 3mm×3mm
17	501.9 Ω	1123.8 Ω	2014.8 Ω
27	248.2 Ω	488.0 Ω	818.8 Ω

3.2.5 Integration with WISP

After the validation of the DC performance of inkjet-printed RGO, we present the gas sensor prototype based on RGO DC performance and integrated with WISP platform. WISP is presented as an available off-the-shelf device that has been optimized for wireless sensing. The presented sensor prototype is a fully passive, battery-free, and programmable RFID tag that can be powered and read by off-the-shelf Generation 2 (EPC Gen2) UHF RFID readers [178]. It has an on-board microcontroller for sensing and computing functions and is a multi-functional platform. The block diagram of a WISP is shown in Figure 19, which includes power harvesting, sensor, signal processing, and modulation/demodulation capabilities. The WISP is solely powered by the RF energy generated by any commercial RFID Reader. This RF energy is rectified by a charge pump consisting of diodes and capacitors to charge the on-board capacitor. Whenever located within the interrogation zone of an RFID reader, the WISP based gas sensor is automatically activated and begins the transmission of the sensed information through the EPC Gen2 protocol.

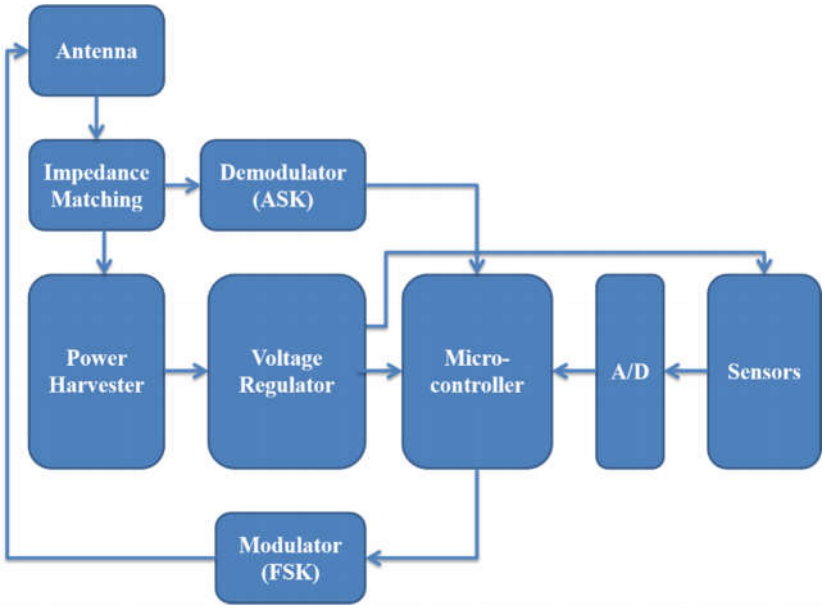

Figure 19 Block diagram of the WISP RFID wireless sensor platform.

EPC Gen2 is a standard that defines the physical and logic requirements for passive-backscattering RFID systems operating at 860-960 MHz, that are regarded as the most practical and cost effective RFID systems. A passive tag memory layout is composed of four main sections as defined in Gen2 protocols, there are: reserved, electronic product code, tag identification, and user memory banks. In Gen2, the reader issues commands to tags within the read range to access data found in the tags Gen2 packet. These commands can be:

- Select command: used to effectively select the tag to be communicated with;
- Inventory commands: include the query command followed by ACK (acknowledge) and NACK commands. The inventory command represents the handshake of the RFID passive communication.
- Access command: include the write, read, and kill commands responsible for accessing a tag in order to read from, write to, or make inaccessible.

The deposited graphene sensors shown in Figure 17 (b) are connected with the WISP RFID tag. As the conductivity of the RGO changes upon exposure to gas, the graphene sensor is used in a resistor divider configuration with a fixed resistor, which is placed across the WISP regulated 1.8 V and ground rails. When the WISP is interrogated by the reader, the voltage from the voltage divider circuit is read by the WISP's analog to digital converter (A/D), processed, and sent to the reader in the EPC Gen2 packet.

3.2.6 RGO-Based WISP Gas Sensor

Recently reported RGO-based inks have enabled the implementation of an inkjet-printed graphene NH_3 gas detection sensor that has a very rapid recovery time and high sensitivity [207, 208]. As demonstrated in [208], GO, which is the precursor to graphene, is inkjet printed onto a UV-ozone treated Kapton substrate with silver contact pads, as described in Section 3.2.2. Sintering GO using heat and laser can both be used for this process [20]. The printed GO is then inserted in post processing to reduce the GO to sheets of RGO, following the steps in Section 3.2.3. The deposited graphene sensors with printed silver electrodes are used to connect with the WISP RFID tag, as shown in Figure 20. As the conductivity of the RGO changes upon exposure to gas, the graphene sensor is used in a resistor divider configuration with a fixed resistor, which is placed across the WISPs regulated 1.8 V and ground rails. When the WISP is interrogated by the reader, the voltage from the voltage divider circuit is read by the WISP's analog to digital converter (ADC), processed, and sent to the reader in the EPCGen2 packet.

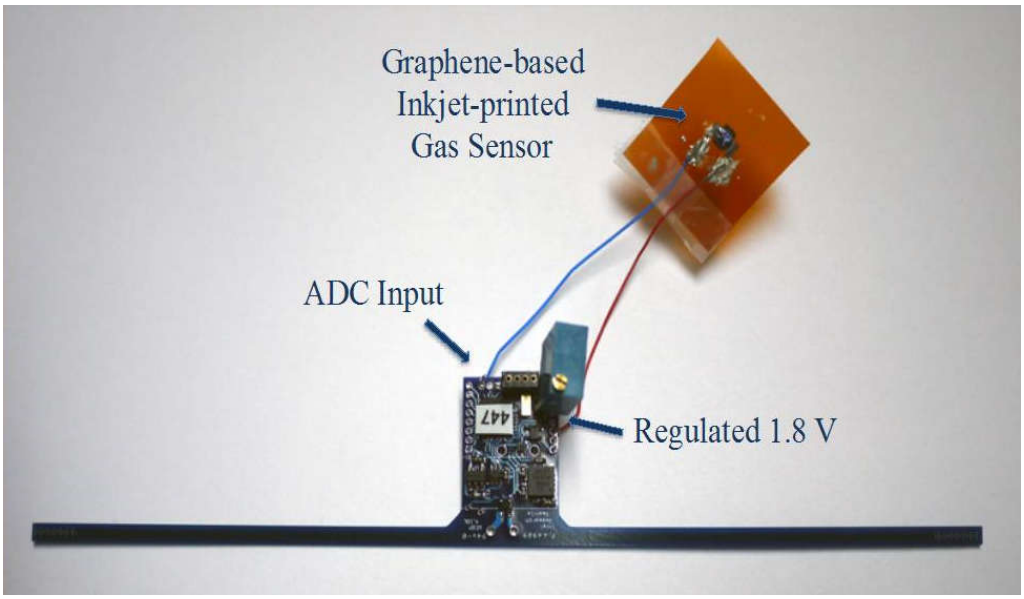

Figure 20 RGO-based WISP gas sensor

This RGO-based gas sensor was placed in an isolated gas chamber, as shown in Figure 21 (a), to expose the sensor to NH_3 and CO to characterize its sensitivity. The measurement setup is shown in Figure 21 (b). Figure 22 (a) and (b) show the extracted sensitivity, which is the change in DC resistance of the sensor over the initial (zero gas concertation) resistance. Resistance changes of up to 6% were realized with response times of less than five minutes when NH_3 was applied. Upon the removal of the gas at t = 15 minutes and application of air, the sensors recover 30% of the change caused by the gas within five minutes. This allows for reuse of the sensors, which is required for low cost and long-term end solutions. Figure 22 (b) shows the selectivity of the film between CO and NH_3 showing a noticeable difference in the characteristic response of the sensor to each gas. This can be used in data analysis to identify the type of gas present as well as the exposure amount.

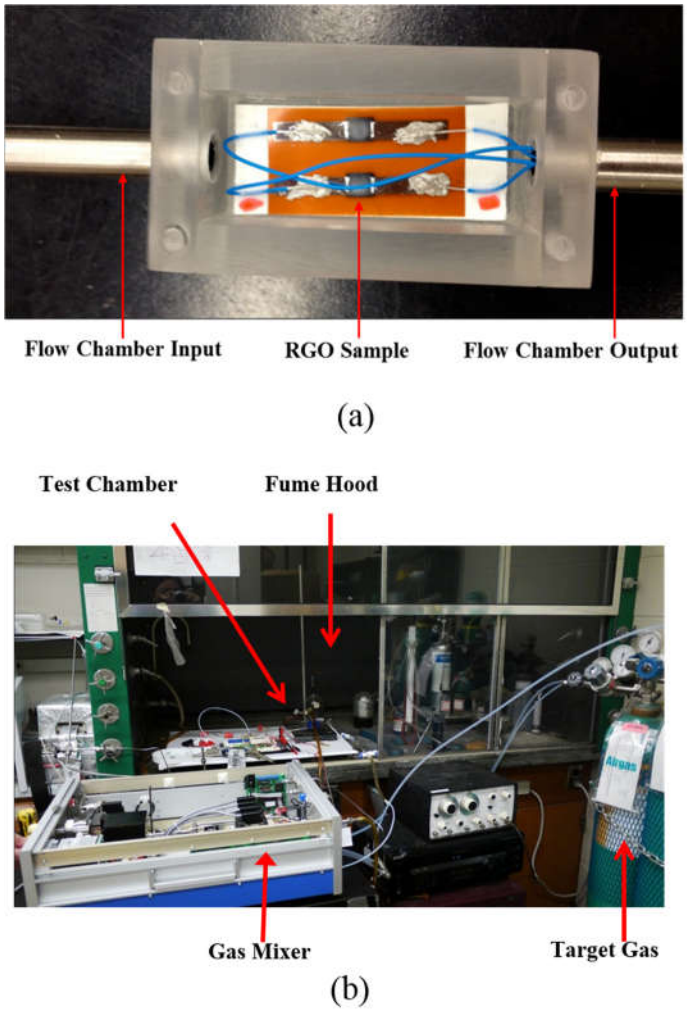

Figure 21 (a) RGO-based gas sensor in a gas chamber; (b) Measurement setup

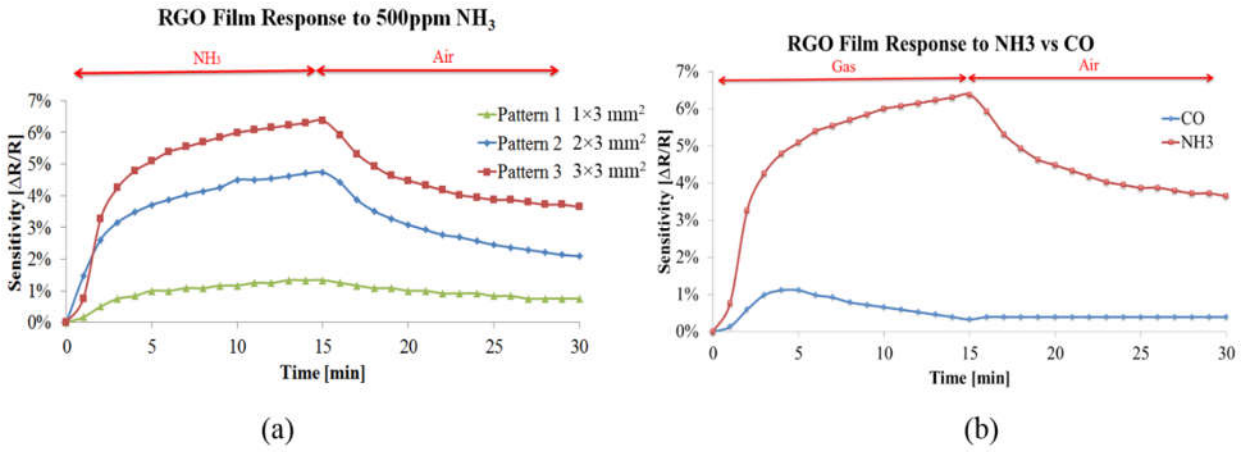

Figure 22 (a) Measured response of RGO thin films in presence of NH3; (b) Measured response of RGO thin films to NH3 and CO.

3.3 RGO-Based Passive UHF RFID Gas Sensor

Another RGO-based inkjet-printed prototype, that is integrated with a UHF RFID platform, thus allowing the simultaneous interrogation of multiple wireless sensors, is presented in this section. The RFID reader sends an interrogating signal to the RFID tag, which consists of an antenna and an IC chip. The IC responds to the reader by effectively varying the "sensor-enabled" antenna input impedance, thereby modulating the backscattered radiation levels. The modulation scheme often used in RFID applications is ASK. The IC impedance switches between the matched state and the mismatched state, altering levels of backscattered radiation to allow the transmission of the appropriate [209]. As illustrated in Figure 23, the RGO thin film is integrated with the printed antenna by direct-write methods, and acts as a tunable part of the antenna with an impedance value determined by the concentration of the target gas. The RFID reader monitors the backscattered power level. Once the power level changes, it shows that there is a variation of the RGO film impedance, therefore, the wireless sensor detects the existence and the concentration of the target gas.

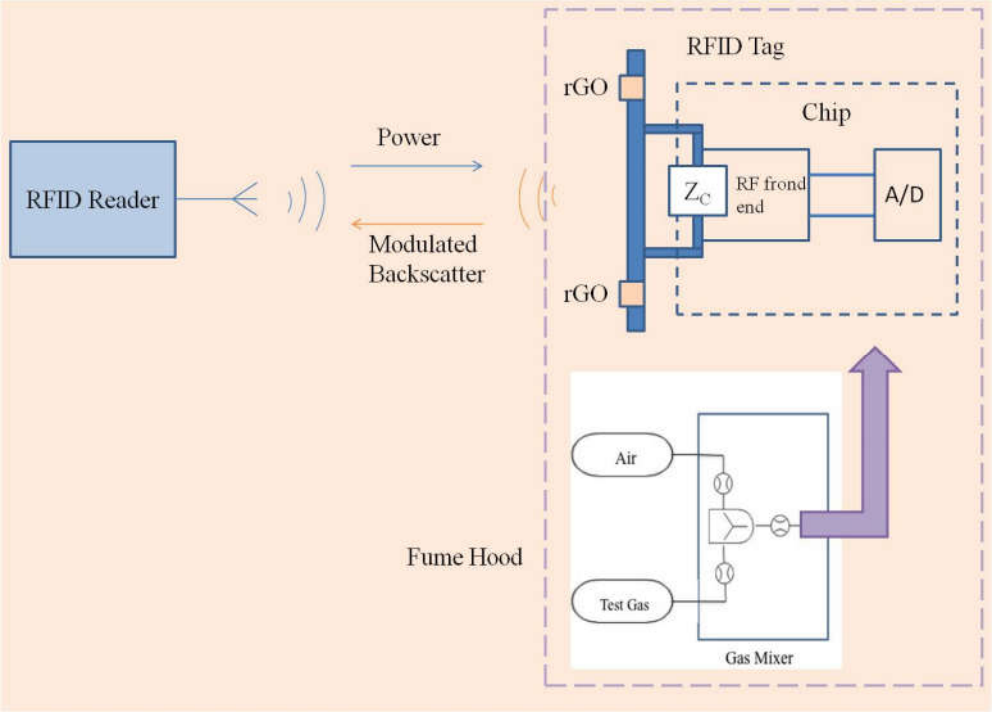

Figure 23 Conceptual diagram of the RFID-enabled wireless gas sensor module.

The power level of the received signal can be calculated using the Friis free-space equation as:

$$P_{tag} = P_t G_t G_r \left(\frac{\lambda}{4\pi d}\right)^2 \quad (8)$$

where P_t is the power transmitted from the reader antenna, G_t and G_r are the gains of the reader antenna and the antenna, respectively, and d is the distance between the reader and the tag.

The design goal for the tag antenna was to achieve an almost omnidirectional read pattern while maintaining a maximum read range. The maximum read range of a passive UHF RFID tag depends on the gain and the quality of impedance matching between the tag antenna and IC [210]. The read range can be optimized by selecting an IC with low-power consumption, maximizing the antenna gain, and arranging a complex-conjugate impedance match between the IC and tag antenna for maximal power transfer to the RFID IC [211]. The T-matching network is an effective

way to modify the input impedance of a dipole by introducing a centered short-circuit stub, as shown in Figure 24 [212] .

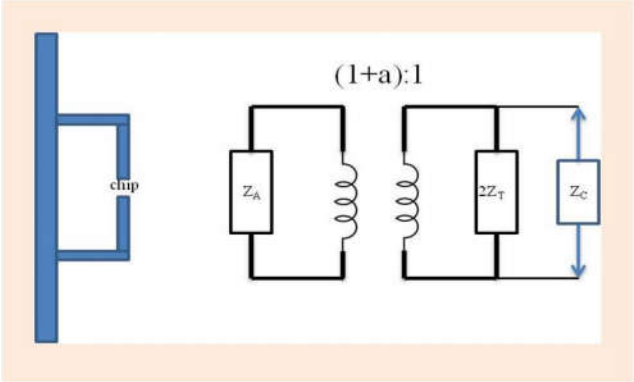

Figure 24 T-matching configuration for a dipole (left) and its equivalent circuit (right)

To demonstrate the printability of carbon-based nanoparticle inks, a preliminary prototype was developed and shown in Figure 25, which is made from RGO directly deposited onto Kodak photo paper. Graphene was chosen because of its special electronic and mechanical properties [195, 196]. Cabot's CCI-300 conductive silver nanoparticle ink was used to print the external circuitry - a dipole antenna, and the interconnect between the RGO thin film and the antenna.

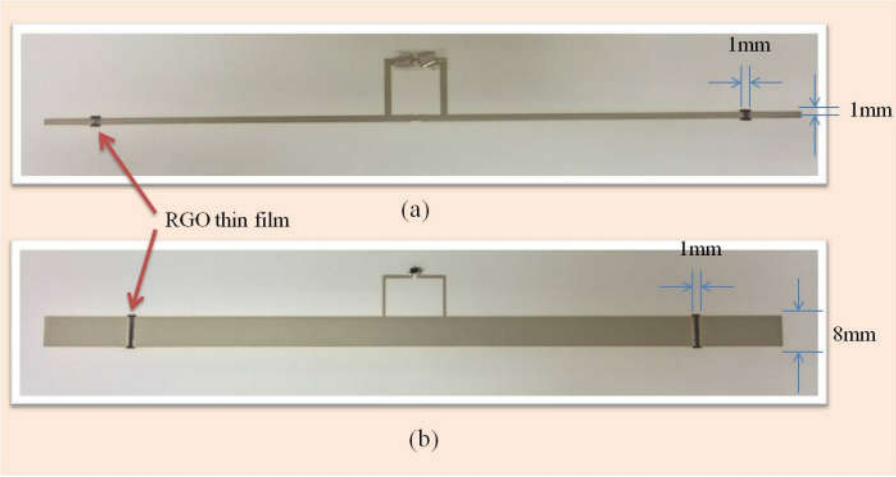

Figure 25 The antenna tags with RFIC printed on photo paper with different RGO sensing areas

This fabrication process, shown in Figure 26, includes:

1) Deposition of the GO ink on paper substrate;

2) Curing and reduction of the GO thin film;

3) Alignment of the RGO film and printing of the antenna;

4) Sintering of the printed silver Cabot ink;

5) Integration of a RFID IC chip on the tag.

In step 2, after printing and curing, each sample was reduced to obtain the desired graphene from the GO. SEM was utilized to observe the overall quality of the graphene thin films (i.e. presence of defects in the printed films, etc.), and to make adjustments in processing to further prints. The wrinkles on the surface of the samples shown in Figure 18 were observed here too, which are likely indicative of minor defects in the structure [213].

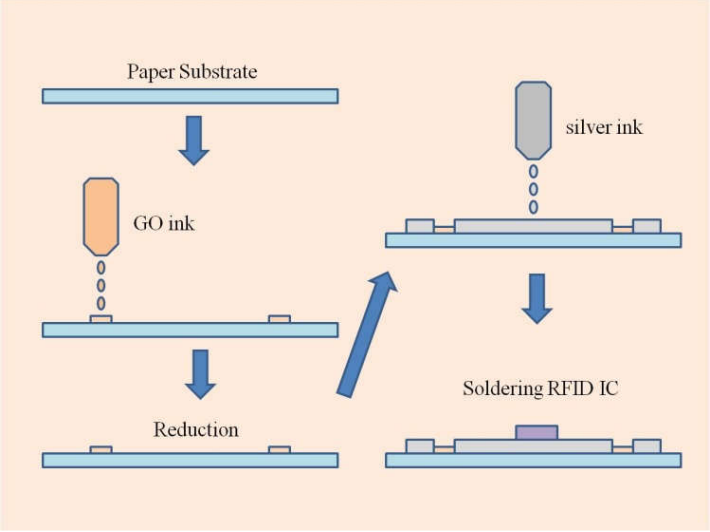

Figure 26 The fabrication process of the RFID-enabled gas sensor prototype.

The inkjet-printed tag prototypes were tested using a KIN-TEK FlexStream gas generator for the accurate control of the gas concentrations. The measurement setup was capable of producing reliable mixtures up to 50 ppm of nitrogen dioxide gas diluted in nitrogen gas. A Tagformance Lite RFID reader (Voyantic Inc. 2011) was adopted for measuring the minimum

required transmitted power to excite the RFID tag. The measurement setup is presented in Figure 27. At each frequency point, the reader varies the transmitting power down from 30 dBm until the power is not able to activate the RFID chip. After the reader sweeps throughout the entire frequency range from 800 MHz to 1 GHz, the minimum required transmitted power level versus frequency curve can be obtained. When the impedance of the antenna-based sensor varies due to the gas exposure, the antenna resonant frequency changes accordingly. Therefore, gas sensing can be achieved utilizing the relationship between the transmitted power to read the antenna-based sensor and the gas concentration.

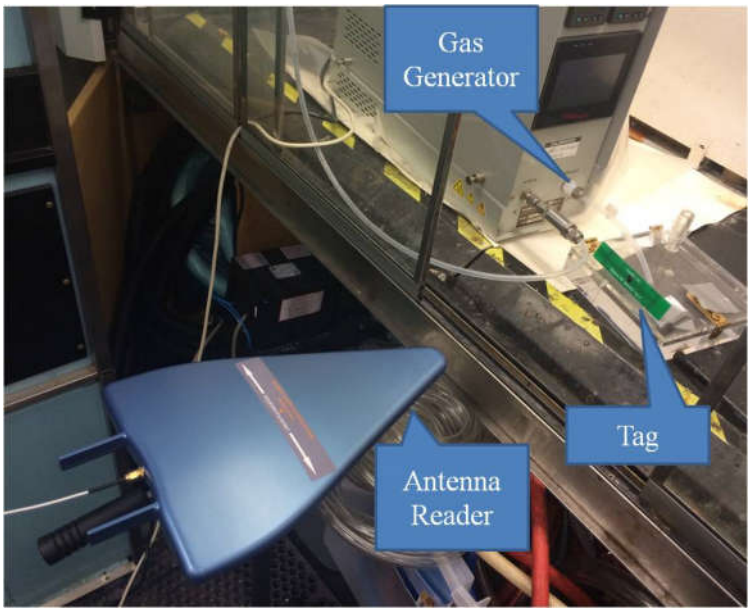

Figure 27 KIN-TEK FlexStream gas generator meausrment setup

The tags presented in Figure 25 were exposed to 20 ppm NH_3 as a proof-of-concept for the gas sensing test. After exposure to the target gas, the resulting mismatch of the impedance between the antenna and the IC chip caused the backscattered power level to be reduced compared to the original power level around 915MHz target frequency. A 600% difference in terms of the minimum interrogation power level was observed at the target frequency by the received antenna in less than 1 minute. This confirms the great potential of the presented approach to be the

foundation of the large-scale conformal RFID-enabled carbon-based smart skins for gas sensing applications.

3.4 Summary and outlook

Two graphene-enabled inkjet-printed wireless sensing topologies have been presented for gas sensing platforms that can be easily integrated with smart skins. These sensors exhibit the very important properties of zero/low-power operation and high sensitivity as well as a good selectivity. Cognitive printed smart skins relying on these approaches have the potential to greatly enhance the safety and longevity of large structures plus the quality of life in everyday environments, such as grocery store food aisles, or airport luggage safety check. In addition, by using industry-standard RFID platforms for sensing, it would be possible to leverage the low-cost, low-power benefits of the proposed platform along with the ease of integration with current and future rugged RFID systems.

CHAPTER 4
A NOVEL WIRELESS STRAIN SENSOR USING STRECHABLE CONDUCTORS

There is a pressing demand for deformable artificial skin with strain sensing capabilities in the areas of wearable computing, soft robotics, SHM, WBAN and SWS. Artificial skin with flexible sensors is usually called smart skin. Smart skin can be wrapped around generic objects in different applications. For strain sensing applications, changes in the object's dimensions will be reflected in changes to the dimensions of the flexible strain sensors. An important research topic is on methods for wirelessly detecting these dimensional changes. In the past, there have been several different methods for RF strain sensors, such as a split rings and metamaterial based strain sensor [114], a dipole antenna based strain sensor [116], and a rectangular microstrip patch antenna based strain sensor [112, 117, 119, 124].

In this chapter, two flexible wireless strain sensors are discussed. The main part of the presented novel wireless strain sensors is an antenna made of silver-filled electrically conductive adhesives (ECAs). The antenna handles both radiating and sensing functions and the whole flexible sensor device can wrap around the test object. Changes in the object's dimensions are reflected in a change in the dimensions of the antenna, resulting in a shift of the resonant frequency of the antenna. The strain on the object can be calculated based on the acquired resonant frequency of the antenna. First of all, a novel ECA material will be introduced. Afterwards, a 2D stretchable bow-tie antenna will be produced by stencil printing and a 3D stretchable dipole antenna will be fabricated by a 3D printer for 2D and 3D strain sensing applications.

4.1 Silver-filled Electrically Conductive Adhesives

ECAs feature numerous advantages compared with liquid metal alloys and thin rigid metal material with wave or arc-shaped structures, such as environmental friendliness, mild processing conditions, fewer processing steps, low stress on the substrates, fine pith interconnect capability and low temperature process environment (T<150°C). ECAs are conductive particles embedded in a polymeric resin. Here ECAs mainly refer to ICAs, which are with 1- 10 μm sized fillers and have uni-directional electrical conductivity. The conductive particles provide the composite with electrical conductivity through contact between the conductive particles. The polymeric resin provides the properties of flexibility and toughness. Silver flakes are the most popular conductive fillers, because of their intrinsic flexibility, high conductivity, simple process and the nature of silver conductive oxide. Several critical issues of ECAs are presented in this section.

4.1.1 Enhancement of Electrical Conductivity

High conductivity is one of the most critical requirements for the silver-filled ECAs to be used in stretchable antennae, because it will directly affect the conduction loss and thus the radiation efficiency. We take two approaches to enhance the conductivity of conventional ECAs.

As the first approach, a long-chain hydride-terminated polydimenthyl siloxane (H-PDMS) is used as the curing agent of the ECA. Commercial silver flakes are usually covered with a thin layer of lubricant, whose component is generally long chain fatty acid. The carboxylic group of the fatty acid can interact with the silver surface to form a silver carboxylate salt complex, while the hydrocarbon chain facilitates the dispersion of silver flakes and prevents oxidation [214]. However, these lubricants are insulating by nature, posing a significant energy barrier to electron conduction between neighboring silver flakes. Therefore, reducing agents were added to ECAs to chemically reduce the lubricant to nano/submicron-sized silver particles, and these in situ formed

nano/submicron-sized particles may then facilitate the sintering of the silver flakes during curing [215]. As a result, the high molecular weight of long-chain H-PDMS not only provides a high elasticity due to the low cross-linking density of the formed silicone matrix, but also enhances the electrical conductivity via the generation and sintering of silver nanoparticles [216].

In the second approach, we modified the filler particles through the iodination of the silver flakes. It was found that the nonstoichiometric Ag/AgI nanoislands sparsely formed on the silver flake surface by iodination treatment could activate the silver surface by exposing fresh silver from inside flakes to the surface. The exposure of fresh silver at the flake surface further facilitates the sintering between silver flakes during curing.

The combination of these two surface modification methods forms a strong electron conduction network and reaches an initial conductivity of 1.51×10^6 Sm^{-1} filled with 80 wt% silver flakes, which is comparable with conventional epoxy-based ECAs and in the same order of magnitude with many metals [217].

4.1.2 Maintaining High Conductivity during Stretching

The largest challenge for stretchable electronics, especially RF devices, is that the conductivity features a significant drop under mechanical strain. This is usually due to the piezo resistive effect, which has been extensively studied [218-220]. The conductivity after stretching is given by

$$\sigma_1 \approx \sigma_0 exp\left[\frac{4\pi\sqrt{2m\varphi}}{h}(s_0 - s_1)\right] \quad (9)$$

where σ_0 and σ_1 are the conductivity values before and after stretching, h is Plank's constant, φ is the height of the tunneling potential barrier, m is the mass of an electron, and s_0 and s_1 are the average interparticle distance between fillers before and after stretching, respectively. According

to this equation, there are two ways to maintain conductivity after mechanical deformation, either reduce the tunneling potential barrier φ, or minimize the interparticle distance s_1 during stretching.

The surface modification methods mentioned above remove the insulating lubricant off the silver flake surfaces and thus they reduce the tunneling potential barrier φ between the silver flakes, which not only benefits the initial conductivity, but also mitigates the conductivity change upon stretching. In order to minimize the interparticle distance s_1, the shape and morphology of the silver fillers used in ECA are carefully engineered. Silver flakes are stacked parallel to each other by applying a shear force during the printing processes [221]. As a result, even after stretching, the stacking allows silver flakes to keep the tunneling distance almost unaltered within a certain strain range, because the sliding between parallel flakes in the X-Y direction does not significantly alter the distance between these flakes, show in Figure 28 (a). The resistance can be kept almost constant for a certain range of tensile strain. In addition to the shape design, secondary textures due to the *in situ* formation of silver nanoparticles from the chemical reduction of the silver carboxylate complex (lubricant) are another important factor in reducing the interparticle distance. As illustrated in Figure 28 (b), these secondary textures could reduce the tunneling distance without changing the filler loading. This texture not only enhances the electrical conductivity of ECAs in the static state but also mitigates the interparticle separation in the stretched state.

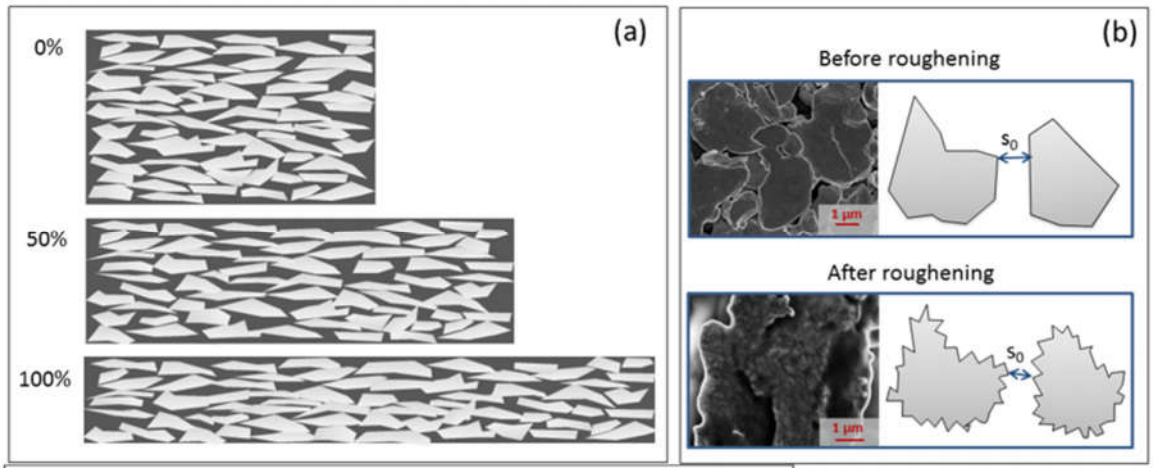

Figure 28 (a) Schematic illustration and SEM images of the silver flakes before and after stretching; (b) SEM images and schematic illustration showing the roughening process of the silver flakes by H-PDMS can decrease the interparticle distance between neighboring flakes [222].

To measure conductivity changes while stretching, a strip of ECA was printed on a silicone substrate and cut into a dumbbell shape. The specimen was then mounted on a tensile tester (Instron Microtester 5548). Real-time electrical resistance change was measured by a typical four-wire method with all wires "soldered" to the ECA strip with additional ECA. The applied strain is recorded by the tensile tester. The setup is shown in Figure 29.

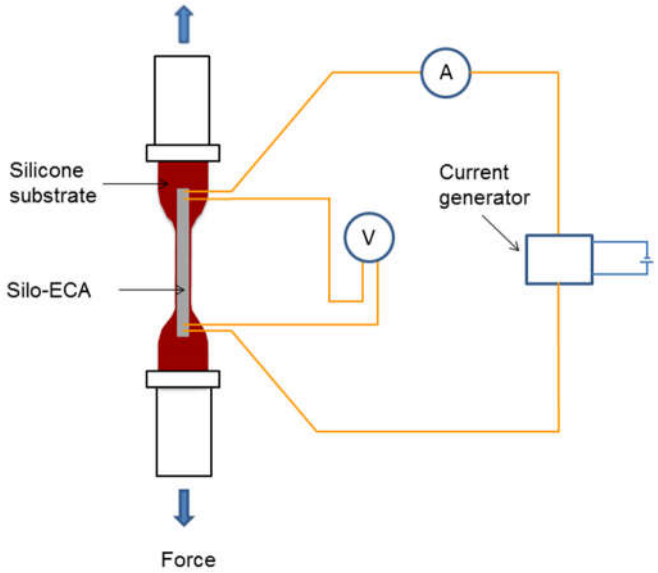

Figure 29 The illustration of the setup to measure conductivity change during stretching ECA

The conductivity of the ECA drops to 5.03×10^5 Sm $^{-1}$ after embedding in the substrate, yet it is still higher than previously reported stretchable conductors. Figure 30 (a) shows the conductivity change as a function of the applied tensile strain of the silo-ECA compared with previously reported stretchable conductors. A general trend emerges: the metal-filled conductive composites [146, 147, 223] have significantly higher conductivity than carbon-filled conductive composites [145, 224-227], while some CNT-based composites can maintain high conductivity at larger elongations due to their high aspect ratio [226]. The conductivity of the novel ECA introduced in this thesis features a conductivity that is two orders of magnitude higher than that of conventional silver/PDMS composites [146], and is comparable with gold nanoparticle/polyurethane composites [147]. More importantly, the reported in-house developed ECA features better elasticity than previously reported metal/polymer composites and can maintain a high conductivity at large deformations. For example, even at a strain of 240%, the conductivity is still as high as 1.11×10^5 Sm $^{-1}$, indicating that the external stress only leads to sliding between overlapping flakes and does not change the tunneling distance significantly. In addition, the conductivity change remains within 25% after 1000 cycles of stretching at 50% applied strain, as shown in Figure 30 (b).

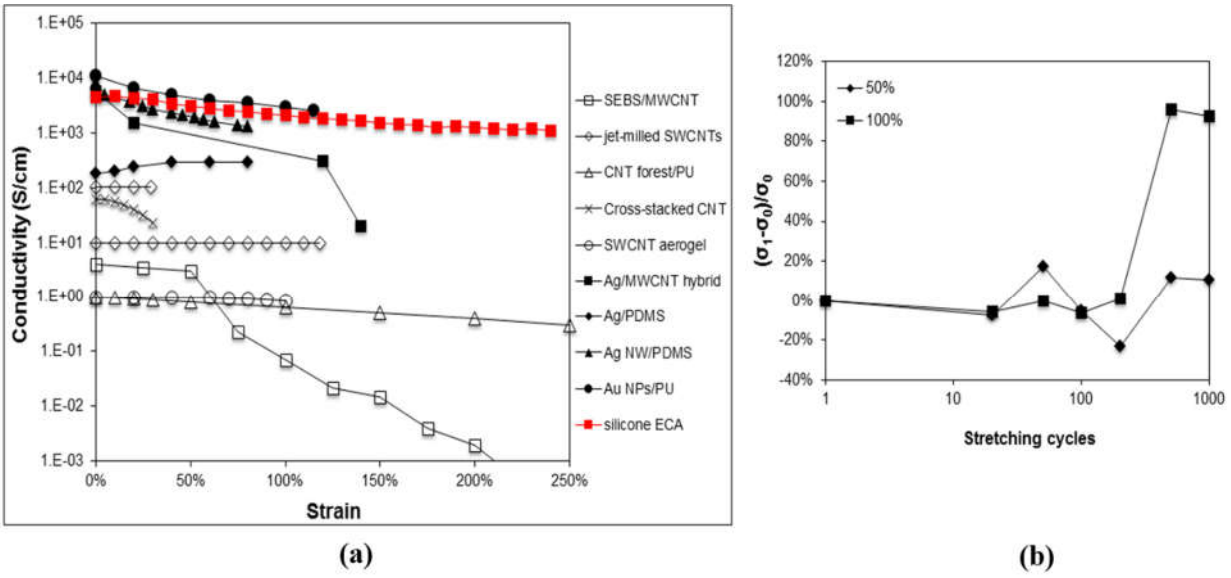

Figure 30 (a) Conductivity change of the in-house developed ECA as a function of tensile strain compared with the values from previous studies; (b) The conductivity of ECA after cycling at 50% strain and 100% strain features the same order of magnitude with many metals [222].

4.1.3 Synthesis of ECA

The silicone matrix for the silo-ECAs was prepared by mixing vinyl-modified PDMS (Wacker® V1K) and hydride-terminated PDMS (Gelest® H41) with a molar ratio of 1:1 and 50 ppm platinum(0)-1,3-divinyl-1,1,3,3-tetramethyldisiloxane complex (Sigma-Aldrich Co.) as a catalyst. The iodination treatment of silver flakes was performed by dispersing the flakes (Silflake® 144) in an ethanol solution of iodine (0.5μmol L^{-1}) for 1 hr. Then a simple filtration was performed to wash out remaining iodine, and the flakes were dried in a vacuum oven for 24 hours. In this silo-ECA formulation, 80 wt % treated silver flake and 20 wt % of silicone mixture were homogenized for 5 mins.

The commercial silver flakes are covered with a thin layer of lubricant, whose composition is a long-chain fatty acid. The existence of the long chain fatty acid is demonstrated by Raman spectrum and thermogravimetric analysis (TGA). In the Raman spectrum in Figure 31(a), the

presence of carboxylate groups on the surface of silver flakes was verified by the symmetric (vs(COO−)) stretching at 1395 cm^{-1} and asymmetric (vas(COO−)) stretching at 1590 cm^{-1} [228].The strong intensity of these peaks indicates that the surfactants are acids bonded to the surface as anions. The peak at 923 cm^{-1} is assigned to the C–COO− stretching [228].The peaks at 1094 and 1167 cm−1 are from the C-C backbones [229]. The peaks at 1288 and 1459 cm^{-1} are attributed to the twist and scissor of methylene groups [229]. The SERS peaks of C–H stretching of the lubricant on Ag are well-resolved in the region of 2800-2950 cm^{-1} [215]. In the TGA result in Figure 31(b), an obvious weight loss occurs at 207°C, which is attributed to the decomposition of the long-chain fatty acid lubricant [215]. All silver flakes were characterized as received.

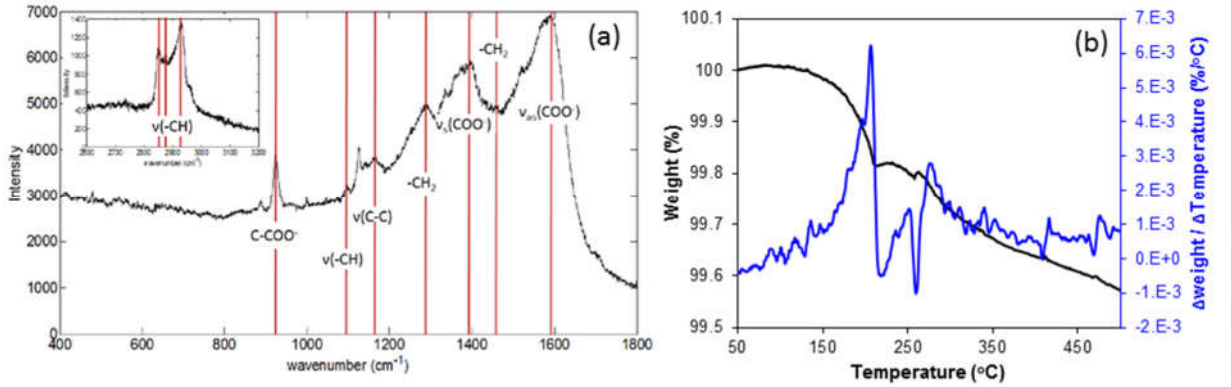

Figure 31 (a) Raman spectrum of the silver flakes; (b) TGA of silver flakes.

H-PDMS is able to chemically reduce the lubricant into silver nanoparticles during the curing process of Silo-ECA. To support this, silver stearate was reacted with H-PDMS at 160°C for different durations. A dark brown precipitation was observed immediately after the silver stearate and H-PDMS were mixed. The mixture was centrifuged at 5000 rpm for 15 minutes. The nanoparticles precipitatation were re-dispersed in toluene, and then characterized by UV-Visible spectroscopy, XRD and TEM. As shown in Figure 32(a), the peaks around 420-440nm in UV-Visible spectra are attributed to the surface plasmons from the generation of Ag nanoparticles

[230]. The nanoparticles were also characterized by XRD in Figure 32 (b). The peak at 38.3° and 44.3° resulted from (111) and (200) faces of silver, respectively. After mixing H-PDMS and silver stearate, the small and broad peak indicate an immediate formation of silver nanoparticles. After 20 minutes reaction, the peak becomes sharp, indicating the growth of crystal sizes with a longer reaction time. The nanoparticles formed after 20 minutes' reaction were also clearly observed by TEM, shown in Figure 32(c).

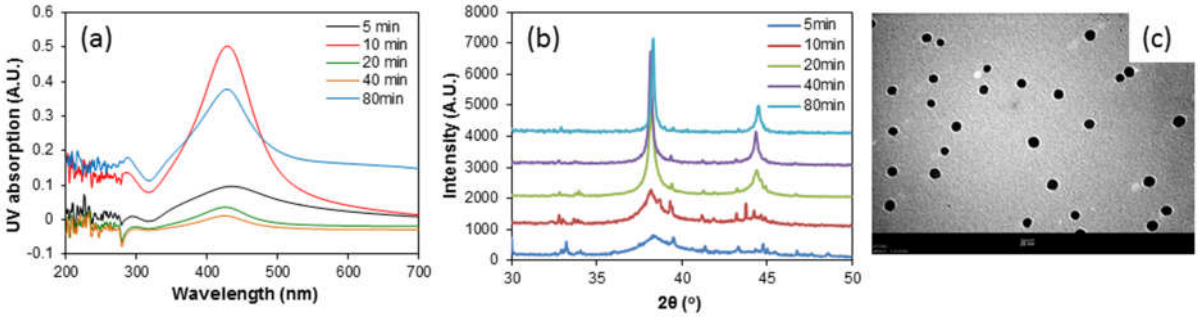

Figure 32 (a) UV-visible spectra and (b) XRD of the formed silver nanparticles after reacting silver stearate with H-PDMS for different durations. (c) TEM images of formed silver nanoparticles after 20 minute reaction.

4.1.4 Electrical Characterization of ECA

To measure the electrical conductivity of the in-house developed ECA, its paste was cast in a Teflon mold (22 mm × 7 mm × 0.5 mm). After curing at 160°C for 1 hour, the bulk resistance of the film was measured by the four-wire method with a Keithley 2000 multimeter. The thickness was measured with a profilometer (Heidenhain ND 281, Germany). Electrical conductivity σ was then calculated by

$$\sigma = \frac{l}{Rwt} \tag{10}$$

where R is the bulk resistance and l, w, and t are the length, width and thickness of the film, respectively. The results show excellent conductivity under strain and are presented in the red line in Figure 30 (a).

High conductivity and elasticity, as well as easy fabrication, make the in-house made ECA a promising building block for stretchable RF devices for wirelessly strain sensors. For proof-of-concept demonstration purposes, one 2D bow-tie antenna and one 3D dipole antenna were designed using the Ansoft high frequency structural simulator (HFSS) Version 14.0. Stencil printing and 3D printing technologies were used for the fabrication process.

4.2 Stretchable 2D Bow-tie Antenna

A 2D bow-tie antenna made of silo-ECSs is presented here. The substrate characterization, the design of the antenna, the fabrication steps and the measure results are discussed in order.

4.2.1 Silicone Substrate Characterization

The silicone substrate, Elastosil® M 4642, was selected in this study. To do the tensile test of the silicone substrate, a piece silicone substrate in a dumbbell shape was mounted on a tensile tester (Instron Microtester 5548), as shown in Figure 33(a). The applied strain is recorded by the tensile tester. The tensile test results are shown in Figure 33(b). The silicone substrate (Elastosil® M 4642) has an elongation at break of 787%. The circle patterns and the line patterns formed by soft-lithography on silicone substrate are presented in Figure 33(c) and (d) to prove that it is suitable for patterning by soft-lithography. The dielectric constant and the dissipation factor of the silicone substrate from 10MHz to 1GHz are measured by an RF impedance analyzer (Agilent E4991A). The results are in Figure 33(e) and (f). A low dielectric constant of 3 and dissipation factor <0.01 are shown.

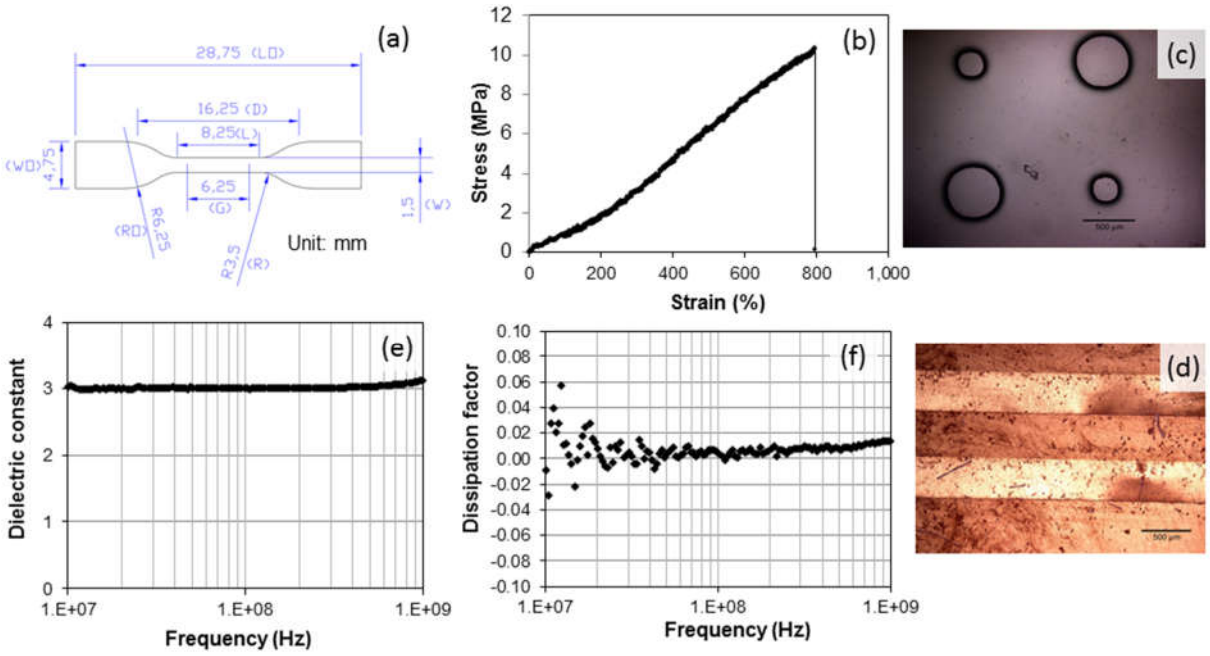

Figure 33 (a) The dumbbell shape for the tensile test of silicone substrate on Elastosil® M 4642. (b) The tensile test result of the silicone substrate. (c) The circle patterns and (d) the line patterns formed by soft-lithography on silicone substrate. (e) The dielectric constant and (f) dissipation factor of the silicone substrate from 10MHz to 1GHz.

4.2.2 Design of the Bow-tie Antenna

As a proof-of-concept stretchable prototype, a quarter-wavelength bow-tie antenna on silicone substrate was simulated in HFSS. The dimension of the quarter-wavelength bow-tie antenna is shown in Figure 34 (a). The silo-ECA conductors can be rationally designed to achieve 1) a high conductivity at both static state and stretching state for a high radiation efficiency; 2) a proper viscosity to enable stencil printing or soft-lithography for high-resolution and large scale fabrication; and 3) cross-linking with the silicone substrate to eliminate delamination and leaking issues.

The dimension changes of the fabricated quarter-wavelength antenna during stretching was simulated using COMSOL multiphysics®. A rectangular substrate (35mm×30mm×0.7mm) was

stretched in the simulation, with the assumption that the silicone substrate has a Poisson's ratio of 0.49 [231].

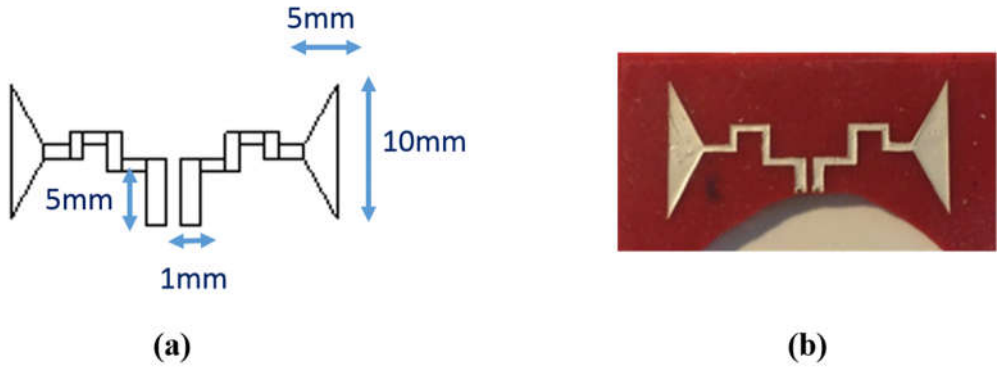

Figure 34 (a) The dimension of the bow-tie antenna; (b) the prototype of the bow-tie antenna.

Figure 35 (a) shows the simulated return loss of the ECA based bow-tie antenna without strain. Then the dimension change results from COMSOL were taken into HFSS. Up to 100% strain was added, the center frequency results are presented in Figure 35 (b).

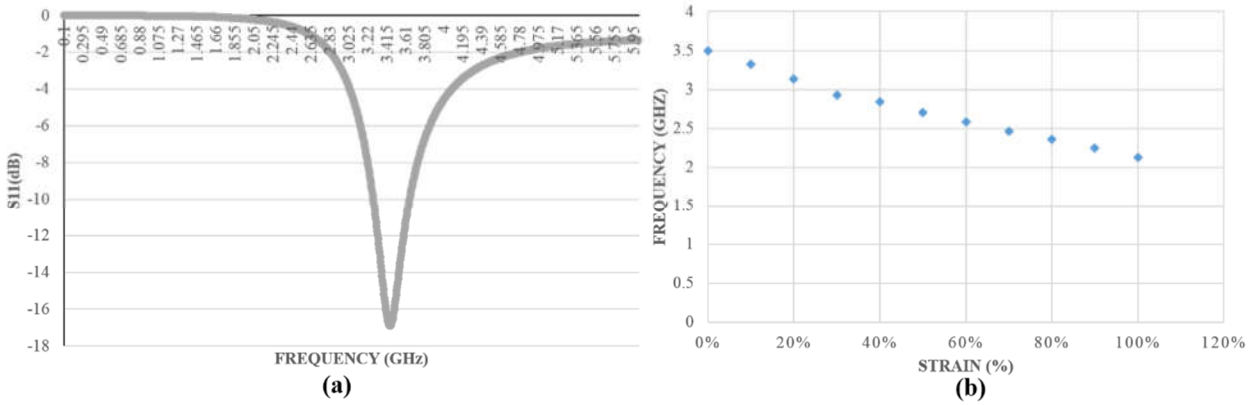

Figure 35 (a) ECA-based antenna return loss without strain; (b) ECA-based antenna center frequencies under different strains.

4.2.3 Fabrication of the antenna Prototype

Another advantage of the hereby-presented silo-ECA is the printability of the material in fine patterns, which is critical for the fabrication of stretchable antennas. Figure 36 (a) and Figure 36 (b) illustrate the two processes to fabricate the antenna pattern. In the stencil printing process, ECA is stencil-printed on a PTFE board and is partially cured. Then the ECA pattern is covered by silicone. After curing the ECA and silicone, the bonded silicone substrate and ECA are both peeled off from the PTFE board and form the stretchable antenna. It should be noted that during the curing process, cross-linking occurs at the interface between ECA and silicone substrate, eliminating the delamination issues. In the soft-lithography process, a master mold is fabricated by patterning a silicon wafer via photolithography. Then the silicon wafer is treated with 1H,1H,2H,2H-perfluorododecyltrichlorosilane to make it hydrophobic and to facilitate the peeling of the silicone substrate from the silicon wafer. A silicone prepolymer is poured onto the master mold and is cured to form an elastomeric mold. After peeling off the silicone elastomeric mold, the silo-ECA is dispensed into the cavity of the silicone substrate to form the conductive pattern. Figure 36 c-f show the printed lines and circles created by the two methods. Patterns on the scale of hundreds of microns can be accurately replicated through both methods, though the soft-lithography process can duplicate shapes with clearer definition and more uniform thickness.

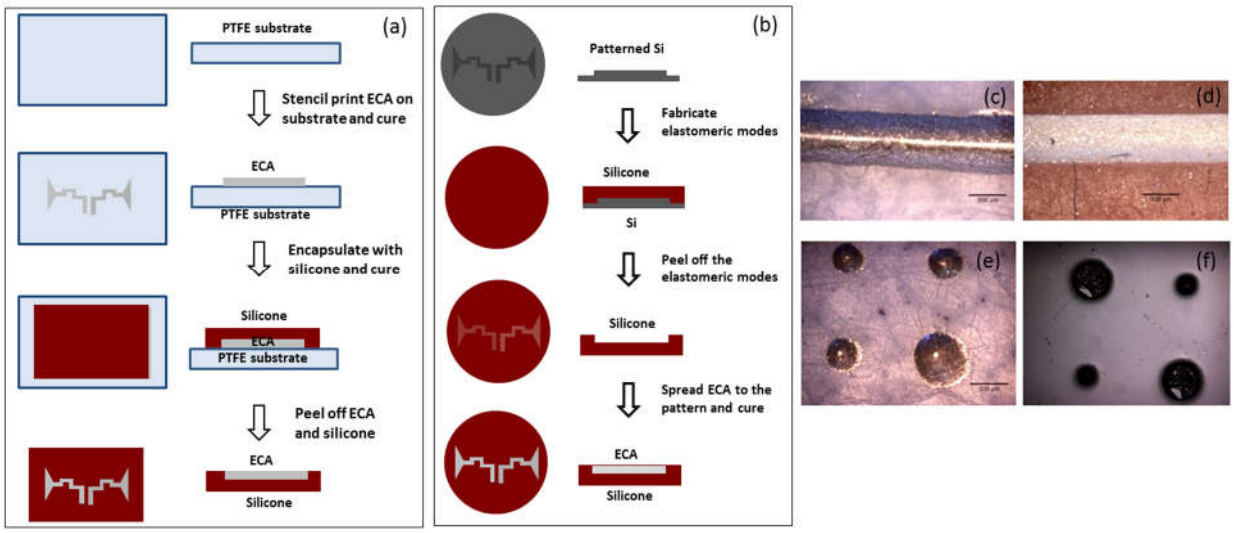

Figure 36. (a) Stencil printing process to fabricate a stretchable antenna. (b) Soft-lithography process to fabricate a stretchable antenna. Lines printed by (c) stencil printing and (d) soft-lithography. Circles printed by (e) stencil printing and (f) soft-lithography.

4.2.4 Measurement results of 2D antenna based strain sensor

High conductivity and elasticity, as well as facile fabrication, make the in-house-made silo-ECA a promising building block for stretchable RF devices. For demonstration purposes, one quarter-wavelength bow-tie antenna as designed in the Section 4.2.2 is fabricated through the soft-lithography process, as shown in Figure 37 (b). It is clear that the fabricated antenna samples have a high fidelity to the original design.

The reflected electromagnetic (EM) power of this bow-tie antenna was measured by a R&S®ZVA8 vector network analyzer (VNA) and compared with the simulated data. If the antenna radiates efficiently at a certain frequency, the majority of incident EM power is radiated into space with little reflected power. The measured resonance frequency lies in 3.50GHz at the range of 50MHz-4GHz, very close to the simulated value of 3.45 GHz. The S_{11} of the real antenna is -17.7dB, also slightly lower than the simulated value of -16.9dB, which indicates that the antenna is better matched with 50Ω input with all the loss. The bandwidth of the actual antenna is larger

than that of the simulated data, resulting in a lower Q factor. This lowered Q factor should result from the conduction loss of the ECA material.

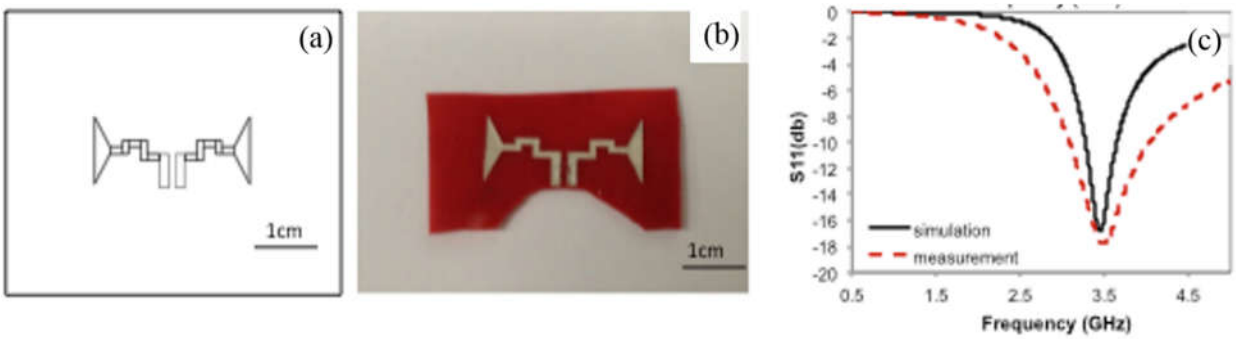

Figure 37. (a) The design of bow-tie antenna; (b) Bow-tie antenna prototype fabricated by soft-lithography process; (c) The measured and simulated reflected EM power as a function of frequency.

The bowtie antenna has also been tested on the tensile tester(Instron Microtester 5548) for the strain test. The setup is illustrated in the Figure 38.

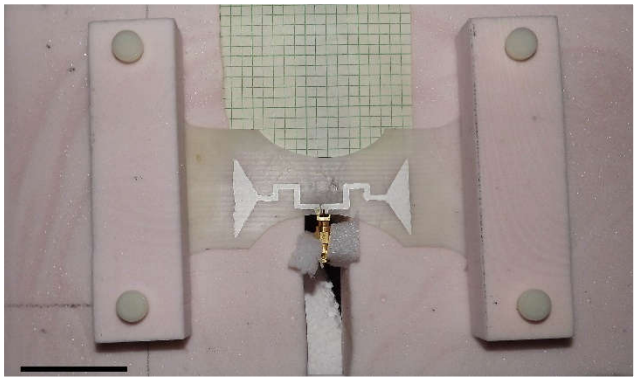

Figure 38 The setup of the bow-tie antenna on the tensile tester

Figure 39 demonstrates the performance of the quarter-wavelength antenna under different tensile strains. The dimension change of the antenna is simulated by finite element analysis and then fed to the HFSS to predict the reflected power of the deformed antenna. In order to determine the actual antenna performance under strain, the prepared quarter-wavelength antenna is mounted

on the tensile tester and its reflected power is measured by the VNA during stretching. As shown in Figure 39 (a), the resonance frequency decreases monotonically from 3.45 to 2.42GHz as it is stretched up to 60% strain, demonstrating the tunability of the fabricated antenna over a wide range of frequencies by simple mechanical modulation. The consistent agreement between measurement and simulation suggests the frequency tuning can be predicted theoretically. Figure 39 (b) shows that the reflected power of the antenna is kept below -15dB when the antenna is stretched by up to 60%, indicating that the high-quality radiation efficiency is maintained during stretching. After retracting, the resonance frequency returns to 3.45 GHz. It should be noted that the antenna could be stretched to a strain larger than 60%, but the connections with the SMA connector become weak and may cause antenna mismatching.

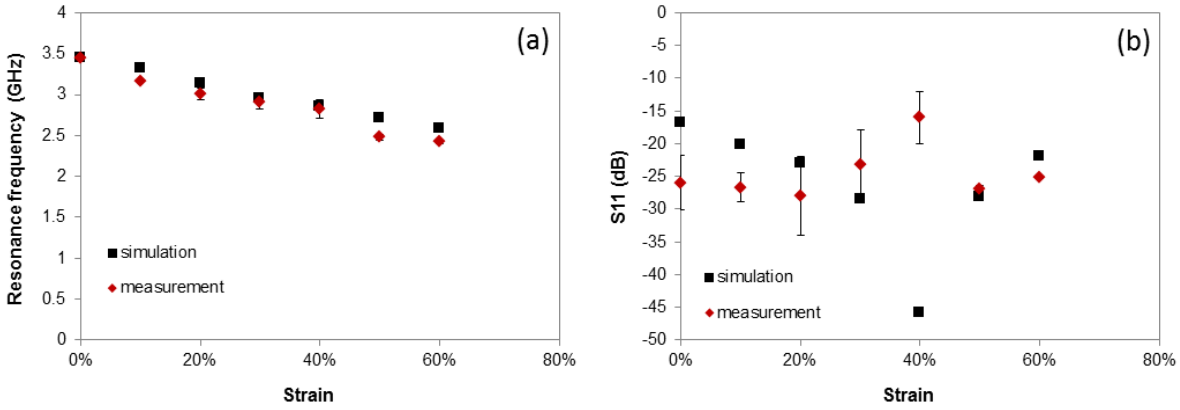

Figure 39. (a) The simulated and measured resonance frequency of the quarter-wavelength antenna as a function of tensile strain; (b) The simulated and measured reflected power of the quarter-wavelength antenna as a function of tensile strain.

In conclusion, we have developed silo-ECA materials that have a conductivity of 1.51×10^4S/cm and can maintain conductivity above 1.11×10^3S/cm, even at a large stain of 240%. By using the stretchable silo-ECAs as a conductor pattern and pure silicone elastomers as a base substrate, stretchable antennae can be fabricated by stencil printing or soft-lithography. The resulting antenna's resonance frequency is tunable over a wide range by mechanical modulation.

The strain sensitivity is around 1.71 MHz/με. This fabrication method is low-cost, can support large-scale production, has high reliability over a wide temperature range, and eliminates the concerns of leaking or delamination between conductor and substrate experienced in previously reported micro-fluidic antennae.

4.3 Stretchable 3D Dipole Antenna

A 3D diple antenna made of ECAs is presented in this section. The substrate RF characterization, the design of the 3D antenna, the printing prototype process and the measurement results are discussed in order.

4.3.1 3D Printing NinjaFlex and NinjaFlex RF Characterization

Due to the flexibility and low cost of NinjaFlex, NinjaFlex (color: snow white) was selected for the strain sensor substrate in this study. First, we will discussed the printability of NinjaFlex on the 3D printer. Then the RF characterization of NinjaFlex will be presented.

4.3.1.a 3D Printing NinjaFlex

Most commercial low-cost 3D printers today are using fused deposition modeling (FDM), of which the patent was first filed back in 1989 by S. Scott Crump [184]. This technology feeds a plastic filament into a heated extruder and then precisely lays down the material [183]. A variety of adjustable options of this technique affect the printing quality. Important properties include layer height, amount of top and bottom solid layers, amount of perimeter walls, solid/infill patterns, and infill densities.

A layer height of 100 microns is considered standard and is achievable for most 3D printers in the market today, such as the Stratasys Dimension 1200es and the Printrbot Simple Metal [232, 233]. The amount of both top and bottom layers both affects the mechanical strength of those sides; if there are not enough layers, the top layer may become porous. An increase in the amount of

perimeter walls increases the strength of the print, but one wall suffices to create a non-porous surface. Various benchmarking 3D printable infill patterns have been tested. During testing, a Hilbert curve pattern is preferable for solid layers to create a non-porous bottom and top layer. As many printers by default print rectilinear, the rectilinear pattern was chosen for fabrication repeatability among different printer models [233]. The density can be easily varied arbitrarily, and the material is typically characterized for densities of 40%, 70%, and 100%, as shown in Figure 40, which can lead to varying mechanical properties.

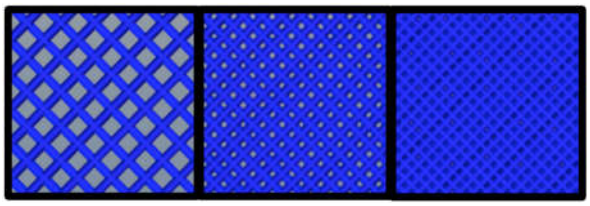

Figure 40 Variety of infill Rectlinear patterns available to print in slic3r. Left to Right: 40%, 70%,100%.

The proof-of-concept 3D-printed 3D antenna presented in this paper was fabricated on a 100% infill density cube shell for operation up to 3GHz. All samples tested were made on the Hyrel System 30 3D printer [234], as shown in Figure 41. This hardware uses a modified version of the Repetier controller software called Repetrel, which still uses the common slicing CAD software slic3r [235, 236].

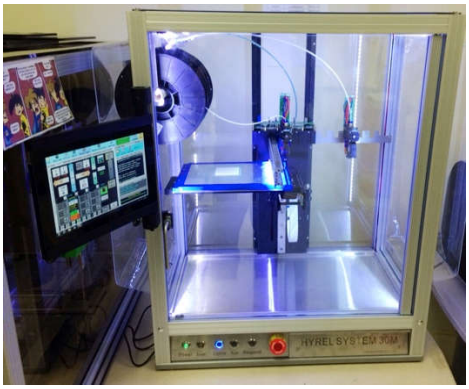

Figure 41 Hyrel System 30 3D printer

4.3.1.b NinjaFlex RF characterization

The most important electrical characteristics of any new material are the dielectric permittivity and the loss tangent. Due to the lack of information of NinjaFlex's properties in wireless/RF frequencies, a microstrip-fed ring resonator was chosen for the material characterization up to 3GHz [178].

The design of the ring-resonator was aided by the ANSYS HFSS. Two microstrip feeding lines were adopted to excite the ring and to collect the transmitted power. These feeding lines were separated by the resonator through 0.8 mm gaps. The line width is set to achieve a characteristic impedance as close as possible to 50 Ohms by assuming a dielectric permittivity close to 3 and a substrate thickness of 1.27 mm. The gap was set intentionally large in order to more accurately get the loaded and unloaded quality factors of the resonator in case the transmitted power was very low and noisy measurements were expected. Moreover, this distance was also chosen to relax the constraints due to the process variations.

The design of the central part of this component, the ring, concerns mainly two dimensions: the radius and the width of the strip. The first one was set to achieve a resonant frequency as close as possible to 2.4 GHz. Starting from this point, the width of the ring strip had to be chosen in order to avoid higher modes [237] and to take into account the constraints of the manufacturing technique. As the ratio of the width and the summation of inner and outer radius had to be lower than 0.05, the chosen width was the maximum one that satisfies this relationship. The final design of the resonator is shown in Figure 42.

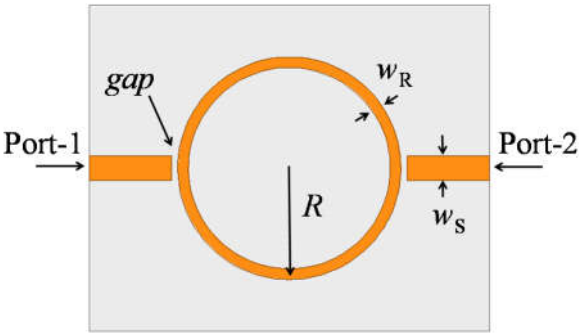

Figure 42 Design of the ring resonator for the characterization of NinjaFlex's properties up to 3GHz. The distance between Port-1 and Port-2 is 48.9 mm while the overall width of the substrate is 40 mm. w_S=3 mm *gap*=0.8 mm, R=13 mm w_R=1.3 mm

The ring structure was manufactured on three different substrates made of NinjaFlex of 40%, 70% and 100% densities (infill). As the material had never before been adopted for any electronics application, a proper manufacturing technique was chosen. Since chemical etching involves acids, the risk in damaging NinjaFlex was very high using the traditional etching-based metallization fabrication approaches, thus making additively manufacturing approaches a very attractive alternative. Inkjet printing is a possibility for characterization. Nevertheless, a potential issue that could reduce the quality of printed conductors was the high porosity that 3D printed materials commonly exhibit. Thus, the metallization option initially utilized was the employment of a high precision milling machine, widely adopted for in-lab PCB realization. A 0.025 mm thick copper foil was stacked on the top of the substrate through a thin layer of epoxy glue. The Gorilla Glue epoxy solidified allowing the milling machine to mill with additional precision [238]. The electromagnetic characterization hereby proposed exploits not only the dielectric substrate but also considers the thin film of glue that is required to manufacture copper clad NinjaFlex. The bottom is fully grounded through its complete coverage with copper. The measurement setup involved an R&S®ZVA8 vector network analyzer (VNA). The input and output feeding lines were connected

to the VNA thanks to standard SMA-to-microstrip connectors fastened to the circuit with conductive epoxy glue. The ring resonator under test is shown in Figure 43.

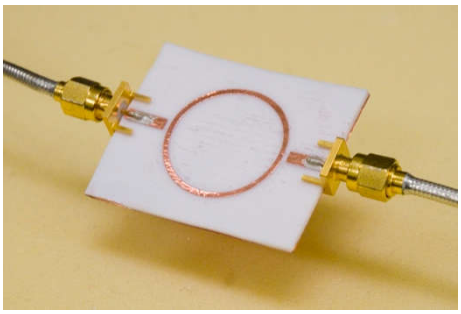

Figure 43 The ring resonator realized on the 3D printed NinjaFlex substrate.

Figure 44 below shows the frequency peaks for the samples with the three different densities (infill percentages). As expected, the higher infill densities lower the resonant frequency. This phenomenon is due to the high percentage of air in the substrate for low infill sample that lowers the effective permittivity. Starting from these measurements the dielectric permittivity can be retrieved for each sample [178].

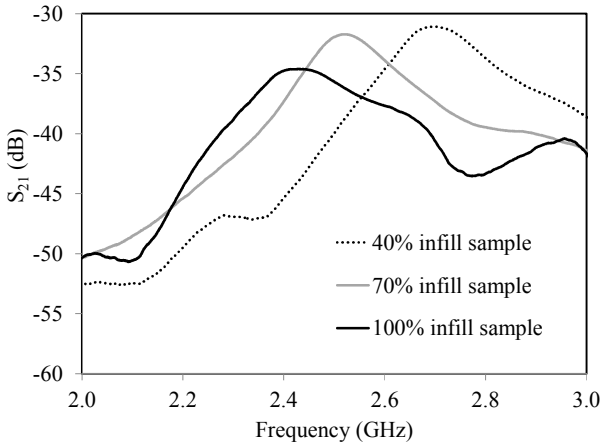

Figure 44 Measurements of the transmission parameter of the three different ring resonators. The frequency shift due to different infill percentages can be noticed.

Figure 45 below shows the value of ε_r versus the infill percentage as well as the calculated loss tangent for the same substrates at 2.4GHz. The results show high losses compared to standard microwave substrates and as expected. The higher value of loss tangent (0.06 @2.4 GHz) and the dielectric permittivity of 2.98 @ 2.4GHz are related to the sample with 100% of infill.

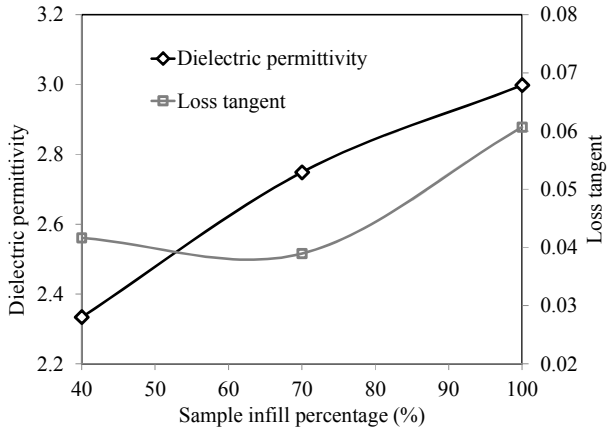

Figure 45 Dielectric permittivity and loss tangent versus the infill percentage of the 3D-printed NinjaFlex samples around 2.4 GHz.

4.3.2 Design of 3D Antenna

The geometry of the proposed 3D dipole antenna is depicted in HFSS in Figure 46. The substrate is a 30mm×30mm×30mm 3D-printed hollow cube made of 100% infill NinjaFlex (relative permittivity 2.98 and loss tangent 0.06 @ 2.4 GHz) [239]. The dipole antenna with two perpendicular arms was realized with ECA by 3D printing as well. As shown in Figure 46 (a), the dipole was placed on the top surface of the cube and bent towards two other surfaces on the side. The feed port of the dipole was located in the center of the top surface. The two arms extended to the edge of the top surface, then bent along two other vertical surfaces. This 3D structure makes it simple to quantitatively analyze the antenna topology change caused by strain.

The structure was a cube with a hollow, which is a rotated 45° smaller cube. The reason for this structure design was to ensure the best quantity of 3D-printed NinjaFlex and simplify the

folded and stretchable antenna sections to be used as a train sensor. The tested strain directions are shown in Figure 46 b. The simulated return loss results are in the Figure 46 c. The black line shows that the center frequency is at 2.4GHz without any external strain. The two different lengths of 0.6mm and 1mm were added on the antenna section of the front side of the cube to emulate the dimension variations under different external strains. The featuring resonant frequency shifts given by the red and blue lines, respectively.

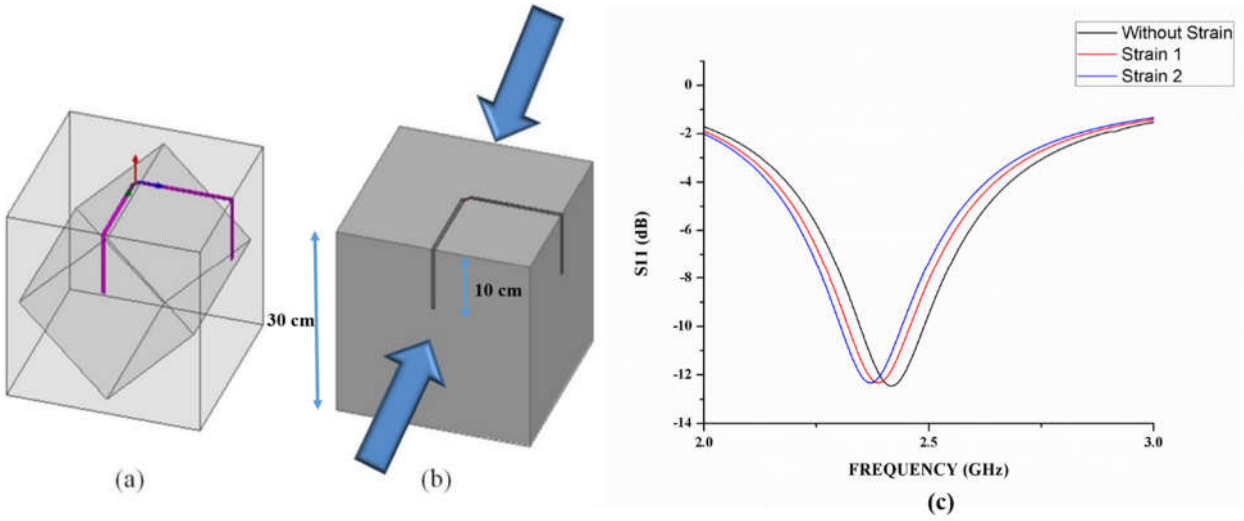

Figure 46 (a) 3D antenna on a 3D-printed hollow cube; (b) tested directions of applied strain on the front and the back surfaces of the cube; (c) The return loss of the dipole antenna with and without strains.

4.3.3 3D Printing Antenna Prototype

The "strain sensing" cube with the antenna traces in the three of its faces was first 3D printed by the Hyrel System 30 3D printer using NinjaFlex (snow white) filament. Then the antenna traces were filled by the ECAs based on the design in HFSS. Between the two antennas perpendicularly placed branches on the top surface, an impedance matching balun was added to allow for the low-loss connection of the SMA connector that was utilized for the insertion loss tests for different strain levels, as shown in Figure 47.

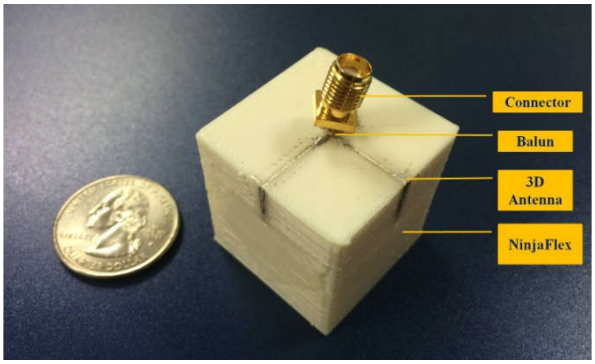

Figure 47 The ready-to-test 3D printed strain sensor prototype

4.3.4 Measurement Results of 3D antenna based strain sensor

The strain experiments involved the application of different strain levels on the front and the back sides of the cube (Figure 47) and the subsequent recoding of the strain-included shift of the center frequency of the antenna. There were two different levels of strain applied on the cube during the experiment. The measurement and the simulation results are presented in the solid lines and the dashed lines, respectively, in Figure 48. 30MHz and 50MHz of the center frequency shifts were observed for the two strain levels strain1 and strain2 leading to respective elongations of 0.6mm and 1mm in the front side antenna sections, in both simulations and experiments although there were some slight differences in the absolute values. So the sensitivity of the strain sensor is around 0.5 MHz/με.

Due to the cubic 3D structure and the direction of the applied strain, the most significant length change of the antenna is the part of the antenna on the front side of the cube. After applying strain on it, this part of the antenna was stretched by the underlying 3D printed NinjaFlex material causing a decrease of the resonant frequency.

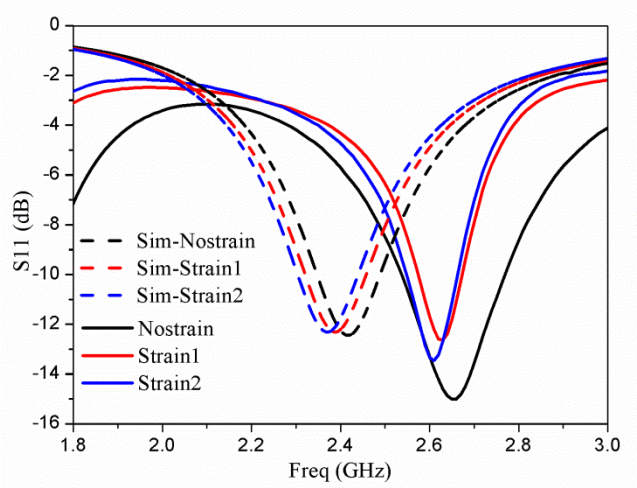

Figure 48 The S_{11} parameter measurement and simulation results of the 3D-printed strain sensor prototype under two levels of strain

We noticed that the center frequency of the antenna has a 200MHz shift between the simulations and the measurements. It might be caused by the process of filling ECAs into traces process, potentially introducing air bubbles. Also the RF characterization of NinjaFlex was using the copper foil instead of printed ECAs. This can bring the measurement error as well. In the future, it is planned to 3D print both ECAs and NinjaFlex at the same time by two extruders on the Hyrel System for the NinjaFlex RF characterization and the fabrication of the prototype.

The first ever 3D printed flexible RF strain sensor system was presented in this section. The common 3D printing material – NinjaFlex - was RF characterized and a 3D antenna was designed and fabricated by NinjaFlex and stretchable ECAs as well. It brings a huge potential for future 3D printed RF applications, such as wearable RF circuits and 3D flexible sensors.

4.4 Conclusion

In-house-produced ECA has been applied on a flexible 2D strain sensor and a flexible 3D strain sensor. This chapter shows the bright future of flexible electronics in strain sensor applications, which can bring a revolution in SHM, soft robotic, wearable electronics, etc.

CHAPTER 5
A NOVEL 3D-PRINTED WEARABLE HAND GESTURE SENSOR

Human-computer interaction (HRI) keeps moving towards the natural and intuitive user interfaces. Human beings have a good manipulating ability with their hands and thus interfaces like keyboard, mouse and touch screen are popular ways to interact with computers [35]. Hand gestures, including movements and positioning of hands, are an appealing way to interact with such a system as they are already nature parts of how human being communicate [240-242]. Hand gestures can be classified into two categories: static gestures (the user assumes a certain pose or configuration) and dynamic gestures (with prestrike, stroke, and poststroke phases). In sign language, some gesture have both static and dynamic elements. The basic goal of hand gesture sensor/recognition is to have an automated system that can identify the specific hand gestures and also use these gestures to communicate and control the devices or virtual environment. In generally, hand gesture sensor/recognition applications fall into four areas:

- Interactive displays/tabletops/whiteboards [20, 34, 243, 244]
- Robot motion control [31, 33, 245]
- Sign language recognition [24, 27, 242, 246, 247]
- Virtual reality training/game [248, 249]

5.1 Different Technologies for Hand Gesture Sensor

In Section 1.1, common approaches for hand gesture sensors have been discussed. There mainly are vision-based hand gesture sensors or wearable Hand Data Glove (HDG). A vision-based gesture sensor/recognition system is usually limited by the threshold of the depth/range estimation, influenced by the environment color and light and requires effective methods for

capturing and processing images. And most importantly, there cannot be objects between the cameras and the hands. Wearable HDG is another popular technology for hand gesture sensor/recognition, which can address these above limitations. Table 7 lists various HDGs during the past decade. Especially, following the flexible/stretchable conductor developments, there are more comfortable HDGs reported in the past five years. But all of these HDGs need batteries or wired with energy source to record and communicate the real-time hand gestures. However, wireless depth sensors are expensive or not appropriate for use Flex-sensor-based smart gloves are bulky, with rigid components [15], or with an internal/external battery [43], or not real-time applications [40]. Therefore, a novel approach is desirable.

This thesis proposed a comfortable HDG technology for hand gesture sensor/recognition system using passive chipless RFID, which is easy to wear and without the battery burden. The chipless RFID technology has been discussed in Secession 2.3.2. a spiral resonator topology was chosen for chipless RFID tags of the hand gesture sensor.

Table 7 Hand Data Gloves Based on Different Technologies

HDG	Sensor	Rigid/Flexible	Wireless	Real time	Passive
[35] 	Bi-Flex Bend	Rigid	Yes (Bluetooth)	Yes	No
[37] 	Tri-axis accelerometers	Rigid	Yes (Bluetooth)	Yes	No

Table 7 Hand Data Gloves Based on Different Technologies (cont'd)

[43] 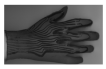	Strain sensor based on piezoresistance	Flexible	No	No	No
[42] 	Strain sensor based on conductive carbon grease ink	Flexible	No	Yes	No
[129] 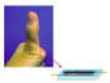	Strain sensor based on silver nanowire stretchable conductor	Flexible	No	Yes	No
[250] 	Strain sensor based on Si nano-membrane gauges	Flexible	No	Yes	No

5.2 ECA Based Wireless Hand Gesture Sensor Concept

In this thesis, a static design of the first 3D-printed wearable hand gesture sensor has been investigated. Among all the gesture recognition, finger counting is an important expression during static gesture [17, 18, 22, 251]. In our preliminary proof-of-concept sign of the hand gesture sensor, a strain sensor is placed on the four joints of the hand, as presented in Figure 49 (a). The sensor is made from four cascaded spiral resonators, with each resonator having a slightly different resonant frequency. All the resonators are then coupled with a microstrip transmission line that is terminated on both ends with receiving and transmitting antennas. A reader sends out a multi-frequency interrogation signal and the four resonators of the hand gesture sensor node create a

unique spectral signature for numerous individual hand gestures, as shown in Figure 49 (b). The transmission and receive signals are cross-polarized in order to achieve isolation between them.

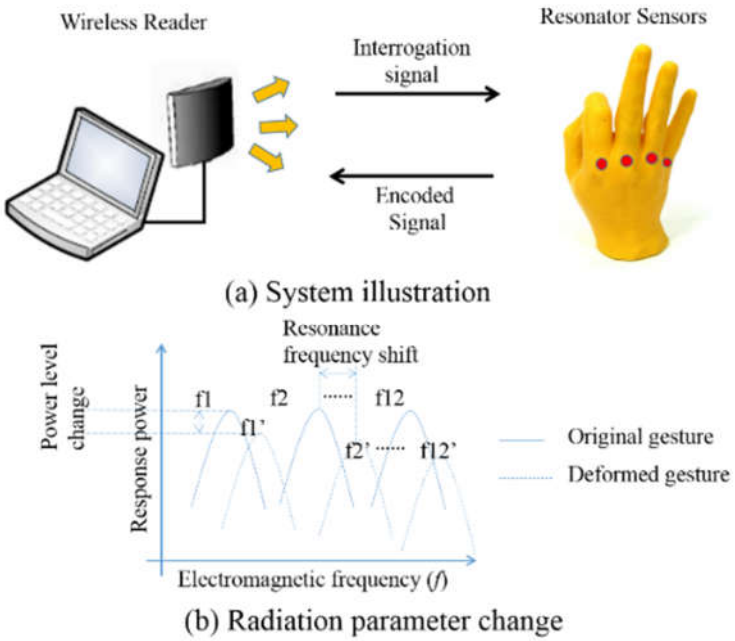

Figure 49 The proposed chipless RFID based wearable hand gesture sensor system

The presented chipless hand gesture sensor encodes the data regarding the gesture directly on the frequency spectrum itself. The varying spatial topology of the relative positions of the four resonators produced in a given gesture causes the resonators to resonate at particular frequencies and to create narrow, high Q factor stopbands. The hand gesture sensor retransmits the received interrogation signal and the resulting backscatter radiation contains information characterizing the gesture encoded in both magnitude and phase.

The design process started with the initial goal of obtaining the ability to encode the various positions of the four fingers as presented in Figure 50 (a). The layout for the hand gesture sensor is presented in Figure 50 (b) – here the Tag Rx/Tx antennas are located on the backside of the hand. The four resonators are placed on the largest joint of each finger, also known as the

metacarpophalangeal (MCP) joint. Each resonator is placed on a 5mm×5mm area to accurately represent the available space above each MCP joint. Due to the required narrow cavity resonant bandwidth and the size constraints, the compact rectangular spiral resonator topology is chosen here [252].

(a) The coding of each hand gesture for 4-resonator circuit

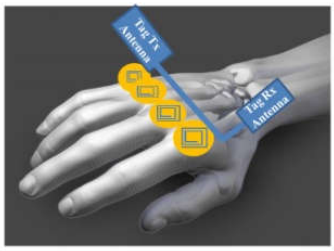

(b) Layout of 4 resonators with Tag Tx/Rx antennas

Figure 50 RFID hand-gesture sensor tag

The proposed hand gesture sensor is built on silicone rubber. A ground plane of ECA is placed beneath the silicone to isolate the hand gesture sensor from the human body. The stencil printing process is used for this prototype for its low cost and 3D printing will be applied for the future work.

Due to the hand joints' limited size, a 4-bit chipless RFID based hand gesture sensor was designed with around 270 MHz separation between each other in the frequency range of 1.5-3GHz for proof-of-concept, as shown in Figure 51. The four resonators introduce a gesture-specific variable attenuation and phase ripple to the transmitted interrogation signal at the designed resonant frequency, which can be detected at the reader side. Based on the resonators of silo-ECA under 50% strain and a total bending of 90^{o}, the simulation results of each gesture using the

Computer Simulation Technology (CST) STUDIO SUITE® 2014 are shown in Figure 52, which presents the respective attenuation and phase ripple. The Q factor values of the 4 resonators fabricated with silo-ECA are in the range of 50-70.

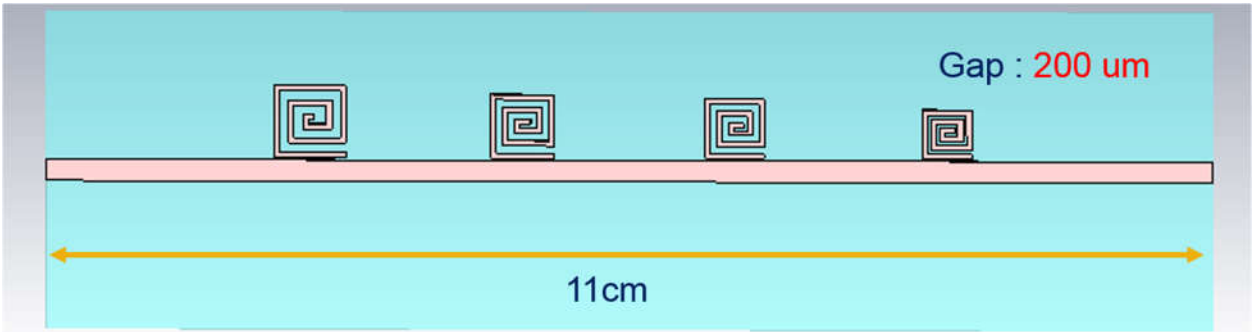

Figure 51 The design of the chipless RFID tag

Table 8 Four resonators' parameters

f_0 [GHz]	BW [MHz]	Q
1.872	30	62.4
2.169	39	55.6
2.361	30	78.7
2.682	54	49.7

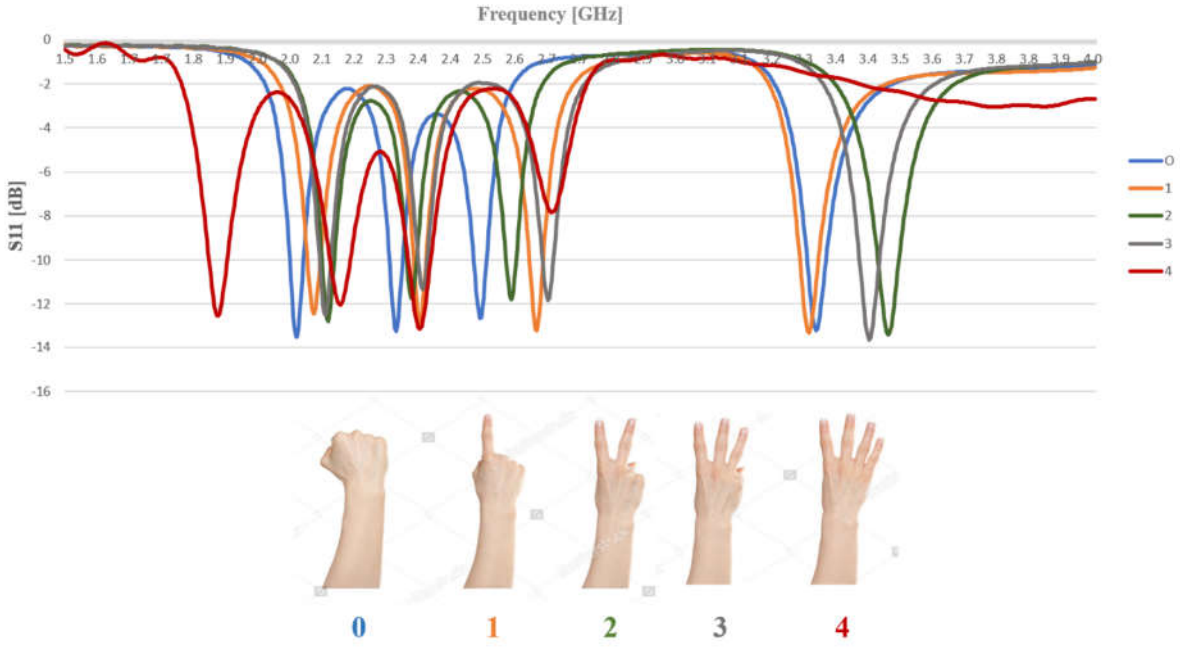

Figure 52 Simulated insertion loss for each gesture

5.3 Cross-polarized RFID Antenna

The operating frequency bandwidth of the RFID tag antenna determines the number of bits that can be used or encoded into the tag. The wireless hand-gesture RFID-based sensing tag requires preferably an omni-directional or wide-beamwidth wideband antenna. The chosen microstrip-fed UWB trapezoidal antenna has a simple structure and a large bandwidth. The microstrip line is designed around a 50 ohm impedance at 2.3 Ghz. The trapezoidal antenna is matched to the microstrip line, which then transfers the power through the multi-resonator system. As the RFID antennas will be located on the back side of the hand, there is only very small need for the flexibility of these antennas compared to the resonators at the joints. A benchmarking RFID antenna was printed on photo paper ($\mathcal{E}r$ =3.1, $tan\delta$ =0.05) using silver nano-particles with inkjet printing technology [253]. The preliminary tag antenna prototype that can be easily integrated in a wearable glove or uniform and can be coupled inductively with the resonators is presented in Figure 53.

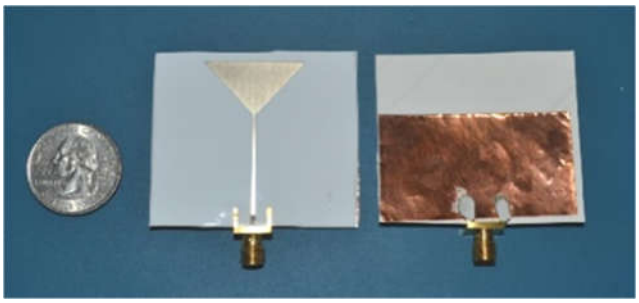

Figure 53 Inkjet printed RFID antenna prototype on paper: top and bottom sides

The hand sensor tag includes two UWB antennas: one is for receiving the interrogation signal, the other is for transmitting the signal passing through the resonant structures back to the reader antenna. In order to minimize the cross-coupling of these two antennas, the reader and tag

antennas are cross-polarized, which introduces further restrictions on the sensor tag's positioning and orientation.

The measured vs simulated return loss of the inkjet printed trapezoidal antenna is presented in Figure 54 below. This antenna can cover the 2-3 GHz band for the 4 resonators of the hand sensor. The realized gain is 2.52 dBi.

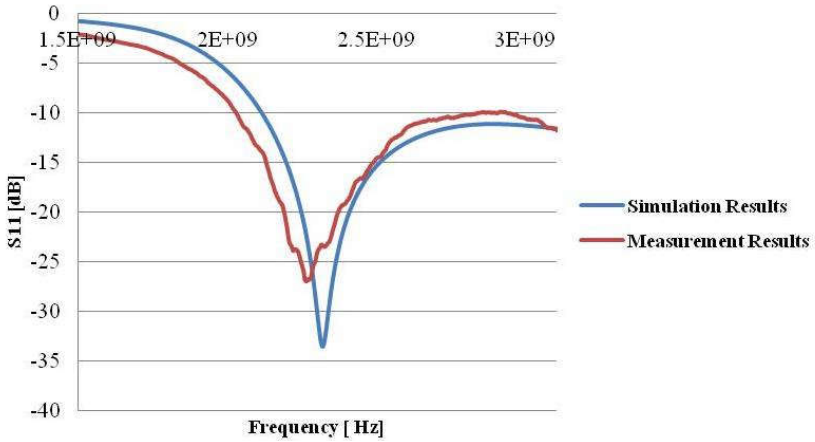

Figure 54 Simulated and measured return loss of tag antenna

5.4 Reader Tx/Rx Antenna Design

The reading range highly depends on the radiation pattern and on the gain of the interrogating reader antenna. The LPDA is one of the preferred candidates for the implementation of an effective reader antenna interrogating the hand gesture sensor due to its inherent good isolation between two cross-polarized antennas, which are 90 degrees to each other, directive radiation pattern, and very high bandwidth. A custom designed LPDA reader antenna on RT/duroid 5880 ($\mathcal{E}r$ =2.2, $tan\delta$ =0.0009) is proposed for this hand gesture sensor system, due to the requirement of high gain and reliability, as shown in Figure 55.

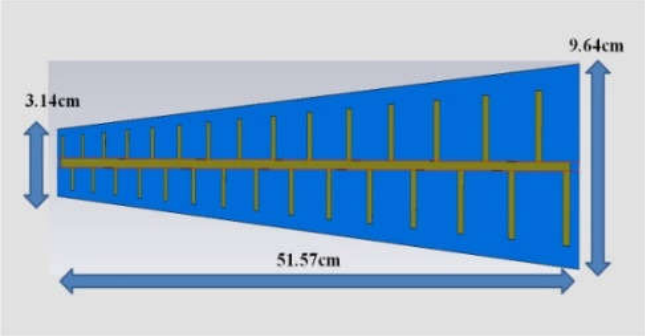

Figure 55 The top view of the proposed LPDA reader antenna

5.5 3D-printed Wearable Hand-gesture Sensor Prototype

A benchmarking proof-of-concept 4-resonator circuit was fabricated by 3D printing silo-ECA on silicone, as shown in Figure 56. A copper sheet at the bottom of the silicone acts as the ground plane, which will be replaced with ECA in the future. The ECA conductivity remains almost invariant under a 50% strain. Nevertheless, the current ECA can not guarantee the ECA uniformity using the proposed stencil printing method, due to the resonators' 100 um thickness and the 200 um gap between the transmission line and the resonators. It would be necessary to use SmartPumpTM from nScypt Inc., as introduced in Section 2.6.2, in order to fit for the circuit design without impairing the mechanical and electrical properties of the composite.

Figure 56 3D printed hand gesture chipless RFID tag

5.6 The Hand-gesture Sensor Tag Measurement

Test results for two specific gestures are presented in Figure 57 below. The first gesture has all four fingers out, whereas the second gesture has the pinky at 90 degrees. The resonant frequency for the resonator on the pinky finger was shifted by 136 MHz in response to the bending action. However, other frequencies were also shifted by up to 70 MHz. It is believed that the copper sheet at the bottom of the silicone substrate negatively affected the isolation of each finger's action. We plan to use ECA instead of a copper sheet to make the tag more flexible in the next prototype to prevent this issue. We have recorded the gesture signatures into our data bank for later machine learning exercises.

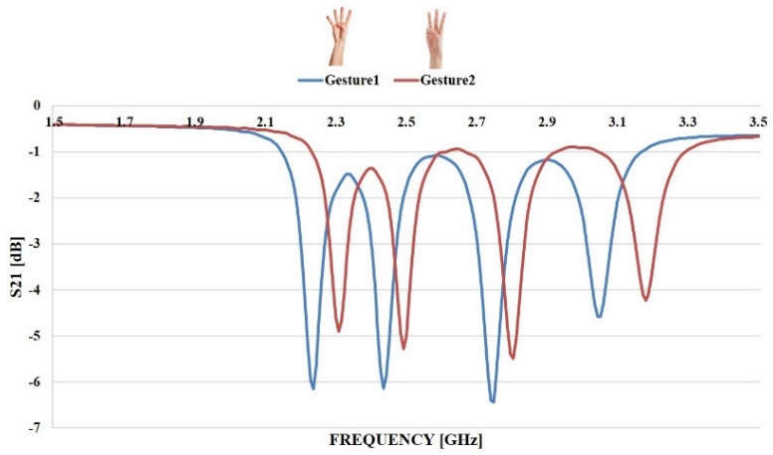

Figure 57 Hand-gesture sensor's insertion loss measurements for two gestures

5.7 Conclusion

This chapter has presented the concept of a novel chipless RFID-based stretchable hand-gesture sensor system, which can be realized using silo-ECAs. 3D printing technology has been applied in the prototype fabrication, which shows the 3D printer having a promising future in flexible electronics.

CHAPTER 6
CONCLUSION AND FUTURE WORK

In Chapter 3, a first ever inkjet printed graphene based wireless gas sensor was introduced. It has fast response, high sensitivity, even selectivity to hazardous gases.

In Chapter 4, a common 3D printing material – NinjaFlex was first time RF characterized up to 10 GHz. A 3D antenna based strain sensor system was designed and fabricated by fulling 3D printing NinjaFlex and ECAs.

In Chapter 5, a chipless-RFID-based stretchable hand gesture sensor was first time 3D printed by a commercial 3D printer. It's a promising pursue for more accurate technique to wirelessly detect hand gesture in robust environments.

The current work status has been outlined. There are still steps remained in order for this proposed research to be completed.

- Gas Sensor

The inkjet printed graphene based gas sensor can be tested with more types of gases to verify the selectivity for the gas bank and keep working on sensitivity enhancements.

- Strain Sensor

The conductivity of the in-house-produced ECAs can be improved by changing the recipe of the ECAs. The 2D antenna based strain sensor can be printed by 3D printer. For the 3D antenna based strain sensor can be printed by ECAs and NinjaFlex at the same time in the near future.

- Hand Gesture Sensor

The Tx/Rx antennas need to be designed and integrated with the resonators sensor tag. The sensing system needs to be completed with a RFID reader. A smart glove with the sensor tag on the top can be fully 3D printed in the near future.

AUTHOR'S PATENTS AND PUBLICATIONS

Pending Patents

1. Battery-Less, Bio-Compatible and Conformal Carbon-Nano-Material-Based Wireless Sensing and Alert System for Biomedical Applications 2012/07/14
2. Fabrication of Graphene Nanostructures via Inkjet Printing Methods 2012/04/30

Book Chapters

1. "Integrating Tiny RFID and NFC Based Sensors with the Internet," Vasileios Lakafosis, Rushi Vyas, Chiara Mariotti, Taoran Le and Manos M. Tentzeris, contribution for "Green RFID Systems" (Editor Luca Roselli) , Ch. 6., Cambridge University Press, pages 152-175, 2014. ISBN-13: 978-1107030404.
2. "Materials for substrates," Sangkil Kim, Ben Cook, Taoran Le, Anya Traille and Manos M. Tentzeris, contribution for "Green RFID Systems" (Editor Luca Roselli) , Ch. 7., Cambridge University Press, pages 176-194, 2014. ISBN-13: 978-1107030404.
3. Power Issues in Biomedical Telemetry," Manos M. Tentzeris, Rushi Vyas, Wei Wei, Yoshihiro Kawahara, Li Yang, Stavros Georgakopoulos, Vasileios Lakafosis, Sangkil Kim, Hoseon Lee, Taoran Le, Sagar Mukala, Anya Traille, Konstantina S Nikita, contribution for 'Handbook of Biomedical Telemetry', Publisher John Wiley & Sons, Inc, pages 108-130, 2014.
4. Advanced Material-Based Sensing Structures," Manos M. Tentzeris, Sangkil Kim, Vasileios Lakafosis, Hoseon Lee, Taoran Le, Rushi Vyas, Sagar Mukala, Anya Traille,

Konstantina S Nikita, chapter contribution for 'Handbook of Biomedical Telemetry', Publisher John Wiley & Sons, Inc., pages 633-689, 2014.

Journals

1. Qi Liu, **Taoran Le**, Sailing He, and Manos M. Tentzeris. "Button-shaped radio-frequency identification tag combining three-dimensional and inkjet printing technologies." IET Microwaves, Antennas & Propagation 10, no. 7, pp. 737-741, 2016.
2. Moscato Stefano, Ryan Bahr, **Taoran Le**, Marco Pasian, Maurizio Bozzi, Luca Perregrini, and Manos M. Tentzeris. "Infill Dependent 3D-Printed Material Based on NinjaFlex Filament for Antenna Applications", IEEE Antennas and Wireless Propagation Letters. 08 January 2016, Issue 99.
3. **Taoran Le**, Ziyin Lin, C. P. Wong, and M. M. Tentzeris. "Smart Skins: Could they be the ultimate sensing tool?" IEEE Nanotechnology Magazine, Vol.9, No.2, pp.4-10, June 2015.
4. Hester, Jimmy G., Sangkil Kim, Jo Bito, **Taoran Le**, John Kimionis, Daniel Revier, Christy Saintsing et al. "Additively manufactured nanotechnology and origami-enabled flexible microwave electronics." Proceedings of the IEEE103, no. 4 (2015): 583-606.
5. Moscato Stefano, Ryan Bahr, **Taoran Le**, Marco Pasian, Maurizio Bozzi, Luca Perregrini, and Manos M. Tentzeris. "Additive manufacturing of 3D substrate integrated waveguide components." Electronics Letters 51, no. 18 (2015): 1426-1428.
6. Zhuo Li, **Taoran Le**, Zhenkun Wu, Yagang Yao, Liyi Li, Manos Tentzeris, Kyoung-Sik Moon, and C. P. Wong. "Rational Design of a Printable, Highly Conductive Silicone-based Electrically Conductive Adhesive for Stretchable Radio-Frequency Antennas." Advanced Functional Materials 25, no. 3 (2015): 464-470.

7. Kim, Sangkil, **Taolan Le**, Manos M. Tentzeris, Amal Harrabi, Ana Collado, and Apostolos Georgiadis. "An RFID-enabled inkjet-printed soil moisture sensor on paper for "smart" agricultural applications." In SENSORS, 2014 IEEE, pp. 1507-1510. IEEE, 2014.
8. Cook, Benjamin S., Raul Vyas, Sangkil Kim, Trang Thai, **Taoran Le**, Anya Traille, Herve Aubert, and Manos M. Tentzeris. "RFID-based sensors for zero-power autonomous wireless sensor networks." Sensors Journal, IEEE14, no. 8 (2014): 2419-2431.
9. **Taoran Le**, Ziyin Lin, Rushi Vyas, Vasileios Lakafosis, Li Yang, Anya Traille, Manos M. Tentzeris, and Ching-ping Wong. "Inkjet printing of radio frequency electronics: design methodologies and application of novel nanotechnologies." Journal of Electronic Packaging 135, no. 1 (2013): 011007.
10. Li, Zhuo, Rongwei Zhang, Kyoung-Sik Moon, Yan Liu, Kristen Hansen, **Taoran Le**, and C. P. Wong. "Highly Conductive, Flexible, Polyurethane-Based Adhesives for Flexible and Printed Electronics." Advanced Functional Materials 23, no. 11 (2013): 1459-1465.
11. Kim, Sangkil, Benjamin Cook, **Taoran Le**, James Cooper, Hoseon Lee, Vasileios Lakafosis, Raul Vyas et al. "Inkjet-printed antennas, sensors and circuits on paper substrate." Microwaves, Antennas & Propagation, IET 7, no. 10 (2013): 858-868. **(**2015 Premium Award for Best Paper in IET Microwaves, Antennas, & Propagation)
12. Cook, Benjamin S., Yunnan Fang, Sangkil Kim, **Taoran Le**, W. Brandon Goodwin, Kenneth H. Sandhage, and Manos M. Tentzeris. "Inkjet catalyst printing and electroless copper deposition for low-cost patterned microwave passive devices on paper." Electronic Materials Letters 9, no. 5 (2013): 669-676.

13. Cook, Benjamin S., **Taoran Le**, S.Palacios, Anya Traille and Manos M.Tentzeris, ``Only Skin Deep: Inkjet-printed Zero-Power Sensors for Large-Scale RFID-Integrated Smart Skins", IEEE Microwave Magazine, Vol.14, No.3, pp.103-114, May 2013.
14. Lin, Ziyin, Taoran Le, Xiaojuan Song, Yagang Yao, Zhuo Li, Kyoung-sik Moon, Manos M. Tentzeris, and Ching-ping Wong. "Preparation of Water-Based Carbon Nanotube Inks and Application in the Inkjet Printing of Carbon Nanotube Gas Sensors." Journal of Electronic Packaging 135, no. 1 (2013): 011001.
15. Yi, Xiaohua, Chunhee Cho, Yang Wang, **Taoran Le**, Manos M. Tentzeris, and Roberto T. Leon. "Inkjet-printed silver patch antenna for wireless strain sensing." Hydro-Environmental Analysis: Freshwater Environments (2013): 297.
16. Tentzeris, Manos M, Rushi Vyas, Vasileios Lakafosis, **Taoran Le**, Amin Rida, and Sangkil Kim. "Conformal 2 D/3 D Wireless Modules Utilizing Inkjet Printing and Nanotechnology." Microwave Journal 55, no. 2 (2012): 20-40.
17. Fang, Yunnan, Jimmy Hester, Chia-Chi Tuan, Philip Brooke, **Taoran Le**, C. P. Wong, Manos M. Tentzeris, and Kenneth H. Sandhage. "A Novel, Facile, Layer-by-Layer Substrate Surface Modification for the Fabrication of All-Inkjet-Printed Flexible Electronic Devices on Kapton." *Journal of Materials Chemistry C* (2016).

Conferences

1. **Taoran Le**, Chia-Chi Tuan, Ryan A. Bahr, C. P. Wong, and M. M. Tentzeris. “A Novel Approach to Integrating 3D/4D Printing and Stretchable Conductive adhesive Technologies for High Frequency Packaging Applications” Accepted to IEEE ECTC 2016

2. **Taoran Le**, Bo Song, Qi Liu, Ryan A. Bahr, Stefano Moscato, Ching-Ping Wong, and Manos Tentzeris, " A novel strain sensor based on 3D printing technology and 3D antenna design", In Electronic Components and Technology Conference (ECTC), 2015 IEEE 65rd, May 2015.
3. **Taoran Le**, Ryan A. Bahr, Manos M. Tentzeris, Bo Song, and Ching-ping Wong. "A novel chipless RFID-based stretchable and wearable hand gesture sensor." In Microwave Conference (EuMC), 2015 European, pp. 371-374. IEEE, 2015.
4. Moscato, Stefano, Marco Pasian, Maurizio Bozzi, Luca Perregrini, Ryan Bahr, **Taoran Le**, and Manos M. Tentzeris. "Exploiting 3D printed substrate for microfluidic SIW sensor." In Microwave Conference (EuMC), 2015 European, pp. 28-31. IEEE, 2015. Best Paper Award Finalist.
5. Bahr, Ryan, **Taoran Le**, Manos M. Tentzeris, Stefano Moscato, Marco Pasian, Maurizio Bozzi, and Luca Perregrini. "RF characterization of 3D printed flexible materials-NinjaFlex Filaments." In Microwave Conference (EuMC), 2015 European, pp. 742-745. IEEE, 2015.
6. **Taoran Le**, Ziyin Lin, C. P. Wong, and M. M. Tentzeris. "Enhanced-Performance Wireless Conformal "Smart Skins" Utilizing Inkjet-Printed Carbon-Nanostructures." In Electronic Components and Technology Conference (ECTC), 2014 IEEE 64rd.
7. **Taoran Le**, Vasileios Lakafosis, Manos M. Tentzeris, Ziyin Lin, Yunnan Fang, Kenneth H. Sandhage, and Ching-ping Wong. "Novel techniques for performance enhancement of inkjet-printed graphene-based thin films for wireless sensing platforms." In Microwave Conference (EuMC), 2013 European, pp. 17-20. IEEE, 2013.

8. **Taoran Le**, Ziyin Lin, C. P. Wong, and M. M. Tentzeris. "Novel enhancement techniques for ultra-high-performance conformal wireless sensors and" smart skins" utilizing inkjet-printed graphene." In Electronic Components and Technology Conference (ECTC), 2013 IEEE 63rd, pp. 1640-1643. IEEE, 2013.
9. Cho, C., Yi, X., Wang, Y., **Le, T.**, Tentzeris, M.M. and Leon, R.T. (2013). "Inkjet-printed RFID antenna sensor for strain monitoring," Proceeding of the 11th International Conference on Structural Safety & Reliability (ICOSSAR), New York, NY, USA, June 16-20, 2013.
10. De Paolis, Rosa, **Taoran Le**, Fabio Coccetti, Giuseppina Monti, Luciano Tarricone, Manos M. Tentzeris, and Robert Plana. "A novel circuit model of nanotechnology-enabled inkjet-printed gas sensors using multi-wall carbon nanotubes." In Microwave Symposium Digest (IMS), 2013 IEEE MTT-S International, pp. 1-4. IEEE, 2013.
11. **Taoran Le**, Vasileios Lakafosis, Sangkil Kim, Byron Cook, Manos M. Tentzeris, Ziyin Lin, and Ching-ping Wong. "A novel graphene-based inkjet-printed WISP-enabled wireless gas sensor." In Microwave Conference (EuMC), 2012 42nd European, pp. 412-415. IEEE, 2012. Listed among Best Conference Papers.
12. **Taoran Le**, Vasileios Lakafosis, Trang Thai, Ziyin Lin, and Manos Tentzeris. "Inkjet printing of graphene thin films for wireless sensing applications." InElectromagnetics in Advanced Applications (ICEAA), 2012 International Conference on, pp. 954-957. IEEE, 2012.
13. **Taoran Le**, Trang Thai, Vasileios Lakafosis, Manos Tentzeris, Ziyin Lin, Yunnan Fang, Kenneth Sandhage, and Chingping Wong. "Graphene enhanced wireless sensors." In Sensors, 2012 IEEE, pp. 1-4. IEEE, 2012.

14. **Taoran Le**, Vasileios Lakafosis, Ziyin Lin, C. P. Wong, M. M.Tentzeris. "Inkjet-printed graphene-based wireless gas sensor modules," Electronic Components and Technology Conference (ECTC), 2012 IEEE 62nd, pp.1003-1008, May 29 2012-June 1 2012.
15. Lakafosis, Vasileios, Xiaohua Yi, **Taoran Le**, Edward Gebara, Yang Wang, and Manos M. Tentzeris. "Wireless sensing with smart skins." In Sensors, 2011 IEEE, pp. 623-626. IEEE, 2011.

REFERENCES

[1] H. Sundmaeker, P. Guillemin, P. Friess, and S. Woelffl, "Vision and challenges for realising the Internet of Things," *Cluster of European Research Projects on the Internet of Things, European Commision,* 2010.

[2] R. H. Reuss, G. B. Raupp, and B. E. Gnade, "Special issue on advanced flexible electronics for sensing applications [Scanning the Issue]," *Proceedings of the IEEE,* vol. 103, pp. 491-496, 2015.

[3] P. Moseley, "Solid state gas sensors," *Measurement Science and technology,* vol. 8, pp. 223-237, 1997.

[4] S. Capone, A. Forleo, L. Francioso, R. Rella, P. Siciliano, J. Spadavecchia*, et al.*, "Solid state gas sensors: state of the art and future activities," *Journal of Optoelectronics and Advanced Materials,* vol. 5, pp. 1335-1348, 2003.

[5] Y. Shimizu and M. Egashira, "Basic aspects and challenges of semiconductor gas sensors," *Mrs Bulletin,* vol. 24, pp. 18-24, 1999.

[6] G. Martinelli, M. C. Carotta, E. Traversa, and G. Ghiotti, "Thick-film gas sensors based on nano-sized semiconducting oxide powders," *MRS Bulletin,* vol. 24, pp. 30-36, 1999.

[7] D. E. Williams, "Semiconducting oxides as gas-sensitive resistors," *Sensors and Actuators B: Chemical,* vol. 57, pp. 1-16, 1999.

[8] D. Marculescu, R. Marculescu, N. H. Zamora, P. S. Marbell, P. K. Khosla, S. Park*, et al.*, "Electronic textiles: A platform for pervasive computing," *Proceedings of the IEEE,* vol. 91, pp. 1995-2018, 2003.

[9] N. Lu and D.-H. Kim, "Flexible and stretchable electronics paving the way for soft robotics," *Soft Robotics,* vol. 1, pp. 53-62, 2014.

[10] J. P. Lynch and K. J. Loh, "A summary review of wireless sensors and sensor networks for structural health monitoring," *Shock and Vibration Digest,* vol. 38, pp. 91-130, 2006.

[11] Y.-L. Park, B.-R. Chen, and R. J. Wood, "Design and fabrication of soft artificial skin using embedded microchannels and liquid conductors," *Sensors Journal, IEEE,* vol. 12, pp. 2711-2718, 2012.

[12] A. Deivasigamani, A. Daliri, C. H. Wang, and S. John, "A review of passive wireless sensors for structural health monitoring," *Modern Applied Science,* vol. 7, p. p57, 2013.

[13] M. Chan, D. Estve, J.-Y. Fourniols, C. Escriba, and E. Campo, "Smart wearable systems: Current status and future challenges," *Artificial intelligence in medicine,* vol. 56, pp. 137-156, 2012.

[14] D. Curone, G. Dudnik, G. Loriga, J. Luprano, G. Magenes, R. Paradiso*, et al.*, "Smart garments for safety improvement of emergency/disaster operators," in *Engineering in Medicine and Biology Society, 2007. EMBS 2007. 29th Annual International Conference of the IEEE*, 2007, pp. 3962-3965.

[15] D. Curone, E. L. Secco, A. Tognetti, G. Loriga, G. Dudnik, M. Risatti*, et al.*, "Smart garments for emergency operators: the ProeTEX project," *Information Technology in Biomedicine, IEEE Transactions on,* vol. 14, pp. 694-701, 2010.

[16] K. Abe, H. Saito, and S. Ozawa, "Virtual 3-D interface system via hand motion recognition from two cameras," *Systems, Man and Cybernetics, Part A: Systems and Humans, IEEE Transactions on,* vol. 32, pp. 536-540, 2002.

[17] Z. Ren, J. Yuan, and Z. Zhang, "Robust hand gesture recognition based on finger-earth mover's distance with a commodity depth camera," in *Proceedings of the 19th ACM international conference on Multimedia*, 2011, pp. 1093-1096.

[18] Z. Ren, J. Yuan, J. Meng, and Z. Zhang, "Robust part-based hand gesture recognition using kinect sensor," *Multimedia, IEEE Transactions on,* vol. 15, pp. 1110-1120, 2013.

[19] K. K. Biswas and S. K. Basu, "Gesture recognition using microsoft kinect," in *Automation, Robotics and Applications (ICARA), 2011 5th International Conference on*, 2011, pp. 100-103.

[20] M. Avancini, "Using Kinect to emulate an interactive whiteboard," *Unpublished Dissertation,* 2012.

[21] C. Chan and S. S. Mirfakhraei, "Hand Gesture Recognition using Kinect," ed: Boston, 2013.

[22] H. Du and T. To, "Hand gesture recognition using Kinect," *Boston University,* 2011.

[23] K. Lai, J. Konrad, and P. Ishwar, "A gesture-driven computer interface using Kinect," in *Image Analysis and Interpretation (SSIAI), 2012 IEEE Southwest Symposium on*, 2012, pp. 185-188.

[24] Y. Li, "Hand gesture recognition using Kinect," in *Software Engineering and Service Science (ICSESS), 2012 IEEE 3rd International Conference on*, 2012, pp. 196-199.

[25] J. L. Raheja, A. Chaudhary, and K. Singal, "Tracking of fingertips and centers of palm using kinect," in *Computational intelligence, modelling and simulation (CIMSiM), 2011 third international conference on*, 2011, pp. 248-252.

[26] Z. Ren, J. Meng, J. Yuan, and Z. Zhang, "Robust hand gesture recognition with kinect sensor," in *Proceedings of the 19th ACM international conference on Multimedia*, 2011, pp. 759-760.
[27] Z. Zafrulla, H. Brashear, T. Starner, H. Hamilton, and P. Presti, "American sign language recognition with the kinect," in *Proceedings of the 13th international conference on multimodal interfaces*, 2011, pp. 279-286.
[28] J. Suarez and R. R. Murphy, "Hand gesture recognition with depth images: A review," in *RO-MAN, 2012 IEEE*, 2012, pp. 411-417.
[29] P. Breuer, C. Eckes, and S. Mller, "Hand gesture recognition with a novel IR time-of-flight range camera–a pilot study," in *Computer Vision/Computer Graphics Collaboration Techniques*, ed: Springer, 2007, pp. 247-260.
[30] M. Van den Bergh and L. Van Gool, "Combining RGB and ToF cameras for real-time 3D hand gesture interaction," in *Applications of Computer Vision (WACV), 2011 IEEE Workshop on*, 2011, pp. 66-72.
[31] D. Droeschel, J. Stckler, and S. Behnke, "Learning to interpret pointing gestures with a time-of-flight camera," in *Proceedings of the 6th international conference on Human-robot interaction*, 2011, pp. 481-488.
[32] T. I. Cerlinca and S. G. Pentiuc, "Robust 3D hand detection for gestures recognition," in *Intelligent Distributed Computing V*, ed: Springer, 2011, pp. 259-264.
[33] K. R. Konda, A. Knigs, H. Schulz, and D. Schulz, "Real time interaction with mobile robots using hand gestures," in *Proceedings of the seventh annual ACM/IEEE international conference on Human-Robot Interaction*, 2012, pp. 177-178.
[34] N. Jojic, B. Brumitt, B. Meyers, S. Harris, and T. Huang, "Detection and estimation of pointing gestures in dense disparity maps," in *Automatic Face and Gesture Recognition, 2000. Proceedings. Fourth IEEE International Conference on*, 2000, pp. 468-475.
[35] P. Kumar, J. Verma, and S. Prasad, "Hand data glove: a wearable real-time device for human-computer interaction," *International Journal of Advanced Science and Technology,* vol. 43, 2012.
[36] T. D. Bui and L. T. Nguyen, "Recognizing postures in Vietnamese sign language with MEMS accelerometers," *Sensors Journal, IEEE,* vol. 7, pp. 707-712, 2007.
[37] J.-H. Kim, N. D. Thang, and T.-S. Kim, "3-d hand motion tracking and gesture recognition using a data glove," in *Industrial Electronics, 2009. ISIE 2009. IEEE International Symposium on*, 2009, pp. 1013-1018.
[38] I. S. Inc, "Flex Sensor Construction Article Page 1," 2016.
[39] T. G. Zimmerman, J. Lanier, C. Blanchard, S. Bryson, and Y. Harvill, "A hand gesture interface device," in *ACM SIGCHI Bulletin*, 1987, pp. 189-192.
[40] D. Akshay and K. U. Rao, "Low cost smart glove for remote control by the physically challenged," in *Global Humanitarian Technology Conference: South Asia Satellite (GHTC-SAS), 2013 IEEE*, 2013, pp. 36-39.
[41] K. N. Tarchanidis and J. N. Lygouras, "Data glove with a force sensor," *Instrumentation and Measurement, IEEE Transactions on,* vol. 52, pp. 984-989, 2003.
[42] J. T. Muth, D. M. Vogt, R. L. Truby, Y. i. Meng, D. B. Kolesky, R. J. Wood*, et al.*, "Embedded 3D printing of strain sensors within highly stretchable elastomers," *Advanced Materials,* vol. 26, pp. 6307-6312, 2014.
[43] F. Lorussi, E. P. Scilingo, M. Tesconi, A. Tognetti, and D. D. Rossi, "Strain sensing fabric for hand posture and gesture monitoring," *Information Technology in Biomedicine, IEEE Transactions on,* vol. 9, pp. 372-381, 2005.
[44] R. Das. (2006). *Chipless RFID - The End Game*. Available: http://www.idtechex.com/research/articles/chipless_rfid_the_end_game_00000435.asp
[45] S. Greengard, *The Internet of Things*: MIT Press, 2015.
[46] @TripwireInc, "How to (Begin) Harnessing the Internet of Things | The State of Security," ed: @TripwireInc, 2014.
[47] J. Fraden, *Handbook of modern sensors: physics, designs, and applications*: Springer Science & Business Media, 2004.
[48] A. Rida, L. Yang, and M. Tentzeris, *RFID-Enabled sensor design and applications*: Artech House, 2010.
[49] K. Kalantar-zadeh and B. Fry, *Nanotechnology-enabled sensors*: Springer Science & Business Media, 2007.
[50] J. Kong, N. R. Franklin, C. Zhou, M. G. Chapline, S. Peng, K. Cho*, et al.*, "Nanotube molecular wires as chemical sensors," *Science,* vol. 287, pp. 622-625, 2000.
[51] P. Qi, O. Vermesh, M. Grecu, A. Javey, Q. Wang, H. Dai*, et al.*, "Toward large arrays of multiplex functionalized carbon nanotube sensors for highly sensitive and selective molecular detection," *Nano letters,* vol. 3, pp. 347-351, 2003.
[52] F. Schedin, A. K. Geim, S. V. Morozov, E. W. Hill, P. Blake, M. I. Katsnelson*, et al.*, "Detection of individual gas molecules adsorbed on graphene," *Nature Materials,* vol. 6, pp. 652-655, 2007-07-29 2007.

[53] B. R. Goldsmith, J. G. Coroneus, V. R. Khalap, A. A. Kane, G. A. Weiss, and P. G. Collins, "Conductance-controlled point functionalization of single-walled carbon nanotubes," *Science,* vol. 315, pp. 77-81, 2007.
[54] J. T. Robinson, F. K. Perkins, E. S. Snow, Z. Wei, and P. E. Sheehan, "Reduced graphene oxide molecular sensors," *Nano letters,* vol. 8, pp. 3137-3140, 2008.
[55] D. Jariwala, V. K. Sangwan, L. J. Lauhon, T. J. Marks, and M. C. Hersam, "Carbon nanomaterials for electronics, optoelectronics, photovoltaics, and sensing," *Chemical Society Reviews,* vol. 42, pp. 2824-2860, 2013.
[56] W. Wu, X. Wen, and Z. L. Wang, "Taxel-addressable matrix of vertical-nanowire piezotronic transistors for active and adaptive tactile imaging," *Science,* vol. 340, pp. 952-957, 2013.
[57] X. Wang, C. Drew, S.-H. Lee, K. J. Senecal, J. Kumar, and L. A. Samuelson, "Electrospinning technology: a novel approach to sensor application," *Journal of Macromolecular Science, Part A,* vol. 39, pp. 1251-1258, 2002.
[58] Z.-M. Huang, Y.-Z. Zhang, M. Kotaki, and S. Ramakrishna, "A review on polymer nanofibers by electrospinning and their applications in nanocomposites," *Composites science and technology,* vol. 63, pp. 2223-2253, 2003.
[59] S. Kwoun, R. Lec, B. Han, and F. Ko, "Polymer nanofiber thin films for biosensor applications," in *Bioengineering Conference, 2001. Proceedings of the IEEE 27th Annual Northeast*, 2001, pp. 9-10.
[60] E. G. Straser, A. S. Kiremidjian, and T. H. Meng, "Modular, wireless damage monitoring system for structures," ed: Google Patents, 2001.
[61] J. P. Lynch, "Decentralization of wireless monitoring and control technologies for smart civil structures," Stanford University, 2002.
[62] Y. Wang, J. P. Lynch, and K. H. Law, "Wireless structural sensors using reliable communication protocols for data acquisition and interrogation," *Ann Arbor,* vol. 1001, p. 48109, 2005.
[63] S. Meninger, J. O. Mur-Miranda, R. Amirtharajah, A. P. Chandrakasan, and J. H. Lang, "Vibration-to-electric energy conversion," *Very Large Scale Integration (VLSI) Systems, IEEE Transactions on,* vol. 9, pp. 64-76, 2001.
[64] N. G. Elvin, A. A. Elvin, and M. Spector, "A self-powered mechanical strain energy sensor," *Smart Materials and Structures,* vol. 10, p. 293, 2001.
[65] D. L. Churchill, M. J. Hamel, C. P. Townsend, and S. W. Arms, "Strain energy harvesting for wireless sensor networks," in *Smart Structures and Materials*, 2003, pp. 319-327.
[66] H.-C. Chung, T. Enomoto, M. Shinozuka, P. Chou, C. Park, I. Yokoi*, et al.*, "Real-time visualization of structural response with wireless MEMS sensors," in *Proceedings of 13th World Conference on Earthquake Engineering*, 2004, pp. 1-10.
[67] L. Tan and N. Wang, "Future internet: The internet of things," in *Advanced Computer Theory and Engineering (ICACTE), 2010 3rd International Conference on*, 2010, pp. V5-376-V5-380.
[68] D. M. Dobkin, *The RF in RFID: UHF RFID in Practice*: Newnes, 2012.
[69] J.-P. Curty, N. Joehl, C. Dehollain, and M. J. Declercq, "Remotely powered addressable UHF RFID integrated system," *Solid-State Circuits, IEEE Journal of,* vol. 40, pp. 2193-2202, 2005.
[70] J. Virtanen, L. Ukkonen, T. Bjrninen, A. Z. Elsherbeni, and L. Sydanheimo, "Inkjet-printed humidity sensor for passive UHF RFID systems," *Instrumentation and Measurement, IEEE Transactions on,* vol. 60, pp. 2768-2777, 2011.
[71] T. T. Thai, L. Yang, G. R. DeJean, and M. M. Tentzeris, "Nanotechnology enables wireless gas sensing," *IEEE Microwave Magazine,* vol. 12, pp. 84-95, 2011.
[72] P. V. Nikitin and K. S. Rao, "Theory and measurement of backscattering from RFID tags," *Antennas and Propagation Magazine, IEEE,* vol. 48, pp. 212-218, 2006.
[73] S. Shrestha, M. Balachandran, M. Agarwal, V. V. Phoha, and K. Varahramyan, "A chipless RFID sensor system for cyber centric monitoring applications," *Microwave Theory and Techniques, IEEE Transactions on,* vol. 57, pp. 1303-1309, 2009.
[74] P. M. Senadeera, N. S. Dogan, Z. Xie, H. S. Savci, I. A. Kateeb, and M. Ketel, "Recent trends in RFID transponders," in *IEEE SoutheastCon 2013: Moving America into the Future*, 2013.
[75] (2015). *Chipless RFID—The End Game*. Available: http://www.idtechex.com/research/articles/chipless_rfid_the_end_game_00000435.asp
[76] S. Preradovic, I. Balbin, N. C. Karmakar, and G. F. Swiegers, "Multiresonator-based chipless RFID system for low-cost item tracking," *Microwave Theory and Techniques, IEEE Transactions on,* vol. 57, pp. 1411-1419, 2009.

[77] S. Preradovic and N. C. Karmakar, *Multiresonator-based Chipless RFID: Barcode of the Future*: Springer Science & Business Media, 2012.
[78] S. Tedjini, E. Perret, V. Deepu, and M. Bernier, "Chipless tags, the next RFID frontier," in *The Internet of Things*, ed: Springer, 2010, pp. 239-249.
[79] U. Kaiser and W. Steinhagen, "A low-power transponder IC for high-performance identification systems," *Solid-State Circuits, IEEE Journal of,* vol. 30, pp. 306-310, 1995.
[80] B. Shao, Q. Chen, Y. Amin, R. Liu, and L.-R. Zheng, "Chipless RFID tags fabricated by fully printing of metallic inks," *annals of telecommunications-annales des tlcommunications,* vol. 68, pp. 401-413, 2013.
[81] S. Preradovic and N. C. Karmakar, "Chipless RFID: bar code of the future," *IEEE Microwave Magazine,* vol. 7, pp. 87-97, 2010.
[82] R. R. Fletcher, "Low-cost electromagnetic tagging: design and implementation," Citeseer, 2002.
[83] V. Subramanian, J. M. Frchet, P. C. Chang, D. C. Huang, J. B. Lee, S. E. Molesa*, et al.*, "Progress toward development of all-printed RFID tags: materials, processes, and devices," *Proceedings of the IEEE,* vol. 93, pp. 1330-1338, 2005.
[84] C. S. Hartmann, "A global SAW ID tag with large data capacity," in *Ultrasonics Symposium, 2002. Proceedings. 2002 IEEE*, 2002, pp. 65-69.
[85] A. Chamarti and K. Varahramyan, "Transmission delay line based ID generation circuit for RFID applications," *Microwave and Wireless Components Letters, IEEE,* vol. 16, pp. 588-590, 2006.
[86] L. Zhang, S. Rodriguez, H. Tenhunen, and L.-R. Zheng, "An innovative fully printable RFID technology based on high speed time-domain reflections," in *High Density Microsystem Design and Packaging and Component Failure Analysis, 2006. HDP'06. Conference on*, 2006, pp. 166-170.
[87] C. Mandel, M. Schler, M. Maasch, and R. Jakoby, "A novel passive phase modulator based on LH delay lines for chipless microwave RFID applications," in *Wireless Sensing, Local Positioning, and RFID, 2009. IMWS 2009. IEEE MTT-S International Microwave Workshop on*, 2009, pp. 1-4.
[88] R. Nair, E. Perret, and S. Tedjini, "Temporal multi-frequency encoding technique for chipless RFID applications," in *Microwave Symposium Digest (MTT), 2012 IEEE MTT-S International*, 2012, pp. 1-3.
[89] L. Zheng, S. Rodriguez, L. Zhang, B. Shao, and L.-R. Zheng, "Design and implementation of a fully reconfigurable chipless RFID tag using Inkjet printing technology," in *2008 IEEE International Symposium on Circuits and Systems, ISCAS 2008; Seattle, WA; 18 May 2008 through 21 May 2008*, 2008, pp. 1524-1527.
[90] A. Vena, E. Perret, and S. Tedjni, "A depolarizing chipless RFID tag for robust detection and its FCC compliant UWB reading system," *Microwave Theory and Techniques, IEEE Transactions on,* vol. 61, pp. 2982-2994, 2013.
[91] N. Lim, J. Kim, S. Lee, N. Kim, and G. Cho, "Screen printed resonant tags for electronic article surveillance tags," *Advanced Packaging, IEEE Transactions on,* vol. 32, pp. 72-76, 2009.
[92] I. Jalaly and I. Robertson, "Capacitively-tuned split microstrip resonators for RFID barcodes," in *Microwave Conference, 2005 European*, 2005, p. 4 pp.
[93] H.-S. Jang, W.-G. Lim, K.-S. Oh, S.-M. Moon, and J.-W. Yu, "Design of low-cost chipless system using printable chipless tag with electromagnetic code," *Microwave and Wireless Components Letters, IEEE,* vol. 20, pp. 640-642, 2010.
[94] A. Vena, E. Perret, and S. Tedjini, "Chipless RFID tag using hybrid coding technique," *Microwave Theory and Techniques, IEEE Transactions on,* vol. 59, pp. 3356-3364, 2011.
[95] J. McVay, A. Hoorfar, and N. Engheta, "Space-filling curve RFID tags," in *Radio and Wireless Symposium, 2006 IEEE*, 2006, pp. 199-202.
[96] J. McVay, A. Hoorfar, and N. Engheta, "Theory and experiments on Peano and Hilbert curve RFID tags," in *Defense and Security Symposium*, 2006, pp. 624808-624808-10.
[97] M. Manteghi, "A novel approach to improve noise reduction in the matrix pencil algorithm for chipless rfid tag detection," in *Antennas and Propagation Society International Symposium (APSURSI), 2010 IEEE*, 2010, pp. 1-4.
[98] A. T. Blischak and M. Manteghi, "Embedded singularity chipless RFID tags," *Antennas and Propagation, IEEE Transactions on,* vol. 59, pp. 3961-3968, 2011.
[99] I. Balbin and N. C. Karmakar, "Phase-encoded chipless RFID transponder for large-scale low-cost applications," *Microwave and Wireless Components Letters, IEEE,* vol. 19, pp. 509-511, 2009.
[100] M. A. Islam and N. C. Karmakar, "A novel compact printable dual-polarized chipless RFID system," *Microwave Theory and Techniques, IEEE Transactions on,* vol. 60, pp. 2142-2151, 2012.

[101] I. Balbin and N. Karmakar, "Novel chipless RFID tag for conveyor belt tracking using multi-resonant dipole antenna," in *Microwave Conference, 2009. EuMC 2009. European*, 2009, pp. 1109-1112.
[102] J. Vemagiri, A. Chamarti, M. Agarwal, and K. Varahramyan, "Transmission line delay based radio frequency identification (RFID) tag," *Microwave and optical technology letters,* vol. 49, pp. 1900-1904, 2007.
[103] M. Schler, C. Mandel, M. Maasch, A. Giere, and R. Jakoby, "Phase modulation scheme for chipless RFID- and wireless sensor tags," in *Microwave Conference, 2009. APMC 2009. Asia Pacific*, 2009, pp. 229-232.
[104] D. Dardari, R. D. Errico, C. Roblin, A. Sibille, and M. Z. Win, "Ultrawide bandwidth RFID: The next generation?," *Proceedings of the IEEE,* vol. 98, pp. 1570-1582, 2010.
[105] FCC. (2016). Available: https://apps.fcc.gov/edocs_public/attachmatch/FCC-02-48A1.pdf
[106] S. Hrm, W. G. Arthur, C. S. Hartmann, R. G. Maev, and V. P. Plessky, "Inline SAW RFID tag using time position and phase encoding," *Ultrasonics, Ferroelectrics, and Frequency Control, IEEE Transactions on,* vol. 55, pp. 1840-1846, 2008.
[107] V. P. Plessky and L. M. Reindl, "Review on SAW RFID tags," *Ultrasonics, Ferroelectrics, and Frequency Control, IEEE Transactions on,* vol. 57, pp. 654-668, 2010.
[108] K. Finkenzeller, "Fundamental Operating Principles," *RFID Handbook: Fundamentals and Applications in Contactless Smart Cards, Radio Frequency Identification and near-Field Communication, Third Edition,* pp. 29-59, 2003.
[109] J. Kirschner, "Surface Acoustic Wave Sensors (SAWS)," *Micromechanical Systems,* 2010.
[110] M. Balachandran, S. Shrestha, M. Agarwal, Y. Lvov, and K. Varahramyan, "SnO2 capacitive sensor integrated with microstrip patch antenna for passive wireless detection of ethylene gas," *Electronics Letters,* vol. 44, pp. 464-466, 2008.
[111] V. Deepu, A. Vena, E. Perret, and S. Tedjini, "New RF identification technology for secure applications," in *RFID-Technology and Applications (RFID-TA), 2010 IEEE International Conference on*, 2010, pp. 159-163.
[112] V. Lakafosis, X. Yi, T. Le, E. Gebara, Y. Wang, and M. M. Tentzeris, "Wireless sensing with smart skins," in *Sensors, 2011 IEEE*, 2011, pp. 623-626.
[113] X. Yi, C. Cho, Y. Wang, T. Le, M. M. Tentzeris, and R. T. Leon, "Inkjet-printed silver patch antenna for wireless strain sensing," *Hydro-Environmental Analysis: Freshwater Environments,* p. 297, 2013.
[114] R. Melik, E. Unal, N. K. Perkgoz, C. Puttlitz, and H. V. Demir, "Flexible metamaterials for wireless strain sensing," *Applied Physics Letters,* vol. 95, p. 181105, 2009.
[115] R. Melik, E. Unal, N. K. Perkgoz, C. Puttlitz, and H. V. Demir, "Metamaterial based telemetric strain sensing in different materials," *Optics express,* vol. 18, pp. 5000-5007, 2010.
[116] R. Matsuzaki, M. Melnykowycz, and A. Todoroki, "Antenna/sensor multifunctional composites for the wireless detection of damage," *Composites Science and Technology,* vol. 69, pp. 2507-2513, 2009.
[117] U. Tata, H. Huang, R. Carter, and J. Chiao, "Exploiting a patch antenna for strain measurements," *Measurement Science and Technology,* vol. 20, p. 015201, 2008.
[118] S. Deshmukh and H. Huang, "Wireless interrogation of passive antenna sensors," *Measurement Science and Technology,* vol. 21, p. 035201, 2010.
[119] A. Daliri, A. Galehdar, S. John, C. H. Wang, W. S. Rowe, and K. Ghorbani, "Wireless strain measurement using circular microstrip patch antennas," *Sensors and Actuators A: Physical,* vol. 184, pp. 86-92, 2012.
[120] S. Chopra, A. Pham, J. Gaillard, and A. Rao, "Development of RF carbon nanotube resonant circuit sensors for gas remote sensing applications," in *Microwave Symposium Digest, 2002 IEEE MTT-S International*, 2002, pp. 639-642.
[121] J. Chuang, D. Thomson, and G. Bridges, "Embeddable wireless strain sensor based on resonant RF cavities," *Review of Scientific Instruments,* vol. 76, p. 094703, 2005.
[122] T. Yamada, Y. Hayamizu, Y. Yamamoto, Y. Yomogida, A. Izadi-Najafabadi, D. N. Futaba*, et al.*, "A stretchable carbon nanotube strain sensor for human-motion detection," *Nature nanotechnology,* vol. 6, pp. 296-301, 2011.
[123] N. Lu, C. Lu, S. Yang, and J. Rogers, "Highly Sensitive Skin Mountable Strain Gauges Based Entirely on Elastomers," *Advanced Functional Materials,* vol. 22, pp. 4044-4050, 2012.
[124] U. Tata, H. Cao, V. Landge, C. M. Nguyen, Y.-S. Seo, and J.-C. Chiao, "Wireless strain sensor based on amorphous carbon for human-motion detection," in *Biomedical Wireless Technologies, Networks, and Sensing Systems (BioWireleSS), 2013 IEEE Topical Conference on*, 2013, pp. 31-33.
[125] A. Gluhak, S. Krco, M. Nati, D. Pfisterer, N. Mitton, and T. Razafindralambo, "A survey on facilities for experimental internet of things research," *IEEE Communications Magazine,* vol. 49, pp. 58-67, 2011.
[126] J. A. Rogers and Y. Huang, "A curvy, stretchy future for electronics," *Proceedings of the National Academy of Sciences,* vol. 106, pp. 10875-10876, 2009.

[127] F. Garnier, R. Hajlaoui, A. Yassar, and P. Srivastava, "All-polymer field-effect transistor realized by printing techniques," *Science,* vol. 265, pp. 1684-1686, 1994.
[128] W. S. Wong, M. L. Chabinyc, T.-N. Ng, and A. Salleo, "Materials and Novel Patterning Methods for Flexible Electronics," in *Flexible Electronics*, ed: Springer, 2009, pp. 143-181.
[129] S. Yao and Y. Zhu, "Wearable multifunctional sensors using printed stretchable conductors made of silver nanowires," *Nanoscale,* vol. 6, pp. 2345-2352, 2014.
[130] A. Levi, M. Piovanelli, S. Furlan, B. Mazzolai, and L. Beccai, "Soft, transparent, electronic skin for distributed and multiple pressure sensing," *Sensors,* vol. 13, pp. 6578-6604, 2013.
[131] R. V. Martinez, J. L. Branch, C. R. Fish, L. Jin, R. F. Shepherd, R. Nunes*, et al.*, "Robotic tentacles with three dimensional mobility based on flexible elastomers," *Advanced Materials,* vol. 25, pp. 205-212, 2013.
[132] S.-I. Park, Y. Xiong, R.-H. Kim, P. Elvikis, M. Meitl, D.-H. Kim*, et al.*, "Printed assemblies of inorganic light-emitting diodes for deformable and semitransparent displays," *science,* vol. 325, pp. 977-981, 2009.
[133] Z. Suo, E. Ma, H. Gleskova, and S. Wagner, "Mechanics of rollable and foldable film-on-foil electronics," *Applied Physics Letters,* vol. 74, pp. 1177-1179, 1999.
[134] S. W. Hwang, X. Huang, J. H. Seo, J. K. Song, S. Kim, S. Hage Ali*, et al.*, "Materials for bioresorbable radio frequency electronics," *Advanced Materials,* vol. 25, pp. 3526-3531, 2013.
[135] S. Xu, Y. Zhang, L. Jia, K. E. Mathewson, K.-I. Jang, J. Kim*, et al.*, "Soft microfluidic assemblies of sensors, circuits, and radios for the skin," *Science,* vol. 344, pp. 70-74, 2014.
[136] Y. Sun and J. A. Rogers, "Inorganic semiconductors for flexible electronics," *ADVANCED MATERIALS-DEERFIELD BEACH THEN WEINHEIM-,* vol. 19, p. 1897, 2007.
[137] A. Verma, B. Weng, R. Shepherd, C. Fumeaux, V.-T. Truong, G. G. Wallace*, et al.*, "6 GHz microstrip patch antennas with PEDOT and polypyrrole conducting polymers," in *Electromagnetics in Advanced Applications (ICEAA), 2010 International Conference on*, 2010, pp. 329-332.
[138] T. Kaufmann, A. Verma, V.-T. Truong, B. Weng, R. Shepherd, and C. Fumeaux, "Efficiency of a compact elliptical planar ultra-wideband antenna based on conductive polymers," *International Journal of Antennas and Propagation,* vol. 2012, 2012.
[139] J. Agar, J. Durden, D. Staiculescu, R. Zhang, E. Gebara, and C. Wong, "Electrically conductive silicone nano-composites for stretchable RF devices," in *Microwave Symposium Digest (MTT), 2011 IEEE MTT-S International*, 2011, pp. 1-4.
[140] M. Kubo, X. Li, C. Kim, M. Hashimoto, B. J. Wiley, D. Ham*, et al.*, "Stretchable microfluidic radiofrequency antennas," *Advanced Materials,* vol. 22, pp. 2749-2752, 2010.
[141] J. H. So, J. Thelen, A. Qusba, G. J. Hayes, G. Lazzi, and M. D. Dickey, "Reversibly deformable and mechanically tunable fluidic antennas," *Advanced Functional Materials,* vol. 19, pp. 3632-3637, 2009.
[142] S. Cheng, Z. Wu, P. Hallbjrner, K. Hjort, and A. Rydberg, "Foldable and stretchable liquid metal planar inverted cone antenna," *Antennas and Propagation, IEEE Transactions on,* vol. 57, pp. 3765-3771, 2009.
[143] D. J. Lipomi, M. Vosgueritchian, B. C. Tee, S. L. Hellstrom, J. A. Lee, C. H. Fox*, et al.*, "Skin-like pressure and strain sensors based on transparent elastic films of carbon nanotubes," *Nature nanotechnology,* vol. 6, pp. 788-792, 2011.
[144] L. Hu, W. Yuan, P. Brochu, G. Gruner, and Q. Pei, "Highly stretchable, conductive, and transparent nanotube thin films," *Applied Physics Letters,* vol. 94, p. 161108, 2009.
[145] T. Sekitani, Y. Noguchi, K. Hata, T. Fukushima, T. Aida, and T. Someya, "A rubberlike stretchable active matrix using elastic conductors," *Science,* vol. 321, pp. 1468-1472, 2008.
[146] X. Niu, S. Peng, L. Liu, W. Wen, and P. Sheng, "Characterizing and patterning of PDMS-based conducting composites," *ADVANCED MATERIALS-DEERFIELD BEACH THEN WEINHEIM-,* vol. 19, p. 2682, 2007.
[147] Y. Kim, J. Zhu, B. Yeom, M. Di Prima, X. Su, J.-G. Kim*, et al.*, "Stretchable nanoparticle conductors with self-organized conductive pathways," *Nature,* vol. 500, pp. 59-63, 2013.
[148] Y. Li, K.-s. Moon, and C. Wong, "Electronics without lead," *Science,* vol. 308, pp. 1419-1420, 2005.
[149] Y. Li and C. Wong, "Recent advances of conductive adhesives as a lead-free alternative in electronic packaging: materials, processing, reliability and applications," *Materials Science and Engineering: R: Reports,* vol. 51, pp. 1-35, 2006.
[150] H. Dong, Y. Li, M. J. Yim, K. S. Moon, and C. Wong, "Investigation of electrical contact resistance for nonconductive film functionalized with -conjugated self-assembled molecules," *Applied physics letters,* vol. 90, p. 092102, 2007.
[151] C. Murray, R. Rudman, M. Sabade, and A. Pocius, "Conductive adhesives for electronic assemblies," *MRS bulletin,* vol. 28, pp. 449-454, 2003.

[152] J. Liu, Z. Lai, H. Kristianse, and C. Khoo, "Overview of conductive adhesive joining technology in electronics packaging applications," in *Adhesive Joining and Coating Technology in Electronics Manufacturing, 1998. Proceedings of 3rd international Conference on*, 1998, pp. 1-18.
[153] J. Liu, "Recent advances in conductive adhesives for direct chip attach applications," *Microsystem technologies,* vol. 5, pp. 72-80, 1998.
[154] J. Liu, A. Tolvgrd, J. Malmodin, and Z. Lai, "A reliable and environmentally friendly packaging technology-flip-chip joining using anisotropically conductive adhesive," *Components and Packaging Technologies, IEEE Transactions on,* vol. 22, pp. 186-190, 1999.
[155] J. Liu, "ACA bonding technology for low cost electronics packaging applications-current status and remaining challenges," *Soldering & surface mount technology,* vol. 13, pp. 39-57, 2001.
[156] H. Yu, S. Mhaisalkar, and E. Wong, "Cure shrinkage measurement of nonconductive adhesives by means of a thermomechanical analyzer," *Journal of electronic materials,* vol. 34, pp. 1177-1182, 2005.
[157] H. Yu, S. Mhaisalkar, and E. Wong, "Effect of temperature on the cure shrinkage measurement of non-conductive adhesives for flip chip interconnects," *Journal of materials research,* vol. 20, pp. 1324-1329, 2005.
[158] F. Ferrando, J.-F. Zeberli, P. Clot, and J.-M. Chenuz, "Industrial approach of a flip-chip method using the stud-bumps with a non-conductive paste," in *Adhesive Joining and Coating Technology in Electronics Manufacturing, 2000. Proceedings. 4th International Conference on*, 2000, pp. 205-211.
[159] A. Aharony and D. Stauffer, *Introduction to percolation theory*: Taylor & Francis, 2003.
[160] D. Stauffer and A. Aharony, *Introduction to percolation theory*: CRC press, 1994.
[161] M. A. Gaynes, R. H. Lewis, R. F. Saraf, and J. M. Roldan, "Evaluation of contact resistance for isotropic electrically conductive adhesives," *Components, Packaging, and Manufacturing Technology, Part B: Advanced Packaging, IEEE Transactions on,* vol. 18, pp. 299-304, 1995.
[162] R. Saraf, J. Roldan, C. Sambucetti, M. Gaynes, and R. Lewis, "High performance isotropic polymer/metal composite for interconnect applications," in *Electronic Manufacturing Technology Symposium, 1995, Proceedings of 1995 Japan International, 18th IEEE/CPMT International*, 1995, pp. 425-428.
[163] D. Klosterman, L. Li, and J. E. Morris, "Materials characterization, conduction development, and curing effects on reliability of isotropically conductive adhesives," *Components, Packaging, and Manufacturing Technology, Part A, IEEE Transactions on,* vol. 21, pp. 23-31, 1998.
[164] K. Gilleo, "Assembly with conductive adhesives," *Soldering & Surface Mount Technology,* vol. 7, pp. 12-17, 1995.
[165] J. Liu, "Reliability of surface-mounted anisotropically conductive adhesive joints," *Circuit World,* vol. 19, pp. 4-15, 1993.
[166] B. Y. Ahn, E. B. Duoss, M. J. Motala, X. Guo, S.-I. Park, Y. Xiong*, et al.*, "Omnidirectional printing of flexible, stretchable, and spanning silver microelectrodes," *Science,* vol. 323, pp. 1590-1593, 2009.
[167] S. I. Park, J. H. Ahn, X. Feng, S. Wang, Y. Huang, and J. A. Rogers, "Theoretical and experimental studies of bending of inorganic electronic materials on plastic substrates," *Advanced Functional Materials,* vol. 18, pp. 2673-2684, 2008.
[168] G. H. Gelinck, H. E. A. Huitema, E. van Veenendaal, E. Cantatore, L. Schrijnemakers, J. B. van der Putten*, et al.*, "Flexible active-matrix displays and shift registers based on solution-processed organic transistors," *Nature materials,* vol. 3, pp. 106-110, 2004.
[169] J. A. Rogers, Z. Bao, K. Baldwin, A. Dodabalapur, B. Crone, V. Raju*, et al.*, "Paper-like electronic displays: Large-area rubber-stamped plastic sheets of electronics and microencapsulated electrophoretic inks," *Proceedings of the National Academy of Sciences,* vol. 98, pp. 4835-4840, 2001.
[170] L. Hu, H. Wu, and Y. Cui, "Printed energy storage devices by integration of electrodes and separators into single sheets of paper," *Applied Physics Letters,* vol. 96, p. 183502, 2010.
[171] L. Hu, H. Wu, F. La Mantia, Y. Yang, and Y. Cui, "Thin, flexible secondary Li-ion paper batteries," *Acs Nano,* vol. 4, pp. 5843-5848, 2010.
[172] B. E. Kahn, "Patterning Processes for Flexible Electronics," *Proceedings of the IEEE,* vol. 103, pp. 497-517, 2015.
[173] B. S. Cook, T.-V. Le, S. Palacios, A. Traille, and M. M. Tentzeris, "Only skin deep: Inkjet-printed zero-power sensors for large-scale RFID-integrated smart skins," *Microwave Magazine, IEEE,* vol. 14, pp. 103-114, 2013.
[174] D. B. Chrisey, "The power of direct writing," *Science,* vol. 289, pp. 879-881, 2000.

[175] (2015). *Dimatix Materials Printer DMP-2831 | Deposition Products | Industrial Inkjet Printheads | Fujifilm USA*. Available: http://www.fujifilmusa.com/products/industrial_inkjet_printheads/deposition-products/dmp-2800/
[176] J. G. Hester, S. Kim, J. Bito, T. Le, J. Kimionis, D. Revier*, et al.*, "Additively Manufactured Nanotechnology and Origami-Enabled Flexible Microwave Electronics," *Proceedings of the IEEE,* vol. 103, pp. 583-606, 2015.
[177] "Piezoelectric Print Heads Vs. Thermal Print Heads - Alder Technology," 2014-02-26 2014.
[178] L. Yang, A. Rida, R. Vyas, and M. M. Tentzeris, "RFID tag and RF structures on a paper substrate using inkjet-printing technology," *Microwave Theory and Techniques, IEEE Transactions on,* vol. 55, pp. 2894-2901, 2007.
[179] B. S. Cook, J. R. Cooper, and M. M. Tentzeris, "Multi-layer RF capacitors on flexible substrates utilizing inkjet printed dielectric polymers," *Microwave and Wireless Components Letters, IEEE,* vol. 23, pp. 353-355, 2013.
[180] B. S. Cook, C. Mariotti, J. R. Cooper, D. Revier, B. Tehrani, L. Aluigi*, et al.*, "Inkjet-printed, vertically-integrated, high-performance inductors and transformers on flexible LCP substrate," in *Microwave Symposium (IMS), 2014 IEEE MTT-S International*, 2014, pp. 1-4.
[181] M. L. Allen, M. Aronniemi, T. Mattila, A. Alastalo, K. Ojanper, M. Suhonen*, et al.*, "Electrical sintering of nanoparticle structures," *Nanotechnology,* vol. 19, p. 175201, 2008.
[182] P. Laakso, S. Ruotsalainen, E. Halonen, M. Mntysalo, and A. Kemppainen, "Sintering of printed nanoparticle structures using laser treatment," in *Proceedings of ICALEO*, 2009, pp. 1360-1366.
[183] M. Frauenfelder, *Make: Ultimate guide to 3D printing 2014*: Maker Media, Inc., 2013.
[184] S. S. Crump, "Apparatus and method for creating three-dimensional objects," ed: Google Patents, 1992.
[185] B. Li, P. A. Clark, and K. Church, "Robust direct-write dispensing tool and solutions for micro/meso-scale manufacturing and packaging," in *ASME 2007 International Manufacturing Science And Engineering Conference*, 2007, pp. 715-721.
[186] U. Robles, P. Deffenbaugh, H. Tsang, and R. Rumpf, "3D Printed Impedance Elements by Micro-Dispensing," 2013.
[187] nscrypt. (2016). *nScrypt | 3D conformal dispensing systems & laser micro printing*. Available: http://nscrypt.com/
[188] P. Deffenbaugh, "3D printed electromagnetic transmission and electronic structures fabricated on a single platform using advanced process integration techniques," Ph. D. dissertation, Elect. & Comput. Eng., UTEP, El Paso, TX, 2014.
[189] (2015). *Recreus 3D printing materials. Elastic & flexible filament Filaflex - Recreus.com*. Available: http://recreus.com/en/
[190] @MakerShed, "Make: magazine, Volume 42 - the Ultimate Guide to 3D Printing 2015," 2015.
[191] @3ders. (2014). *Quack-Quack the duck gets his 3D printed leg brace and the chance to walk again*. Available: http://www.3ders.org/articles/20140813-quack-quack-the-duck-gets-his-3d-printed-leg-brace-and-the-chance-to-walk-again.html
[192] p. Jack Krecek, Fenner Drives & Harris Kenny, communications manager, Aleph Objects. (2014). *3D Technology Kicks at the World Cup*. Available: http://www.pddnet.com/news/2014/06/3d-technology-kicks-world-cup
[193] J. Hu and M.-F. Yu, "Meniscus-confined three-dimensional electrodeposition for direct writing of wire bonds," *Science,* vol. 329, pp. 313-316, 2010.
[194] J. J. Adams, E. B. Duoss, T. F. Malkowski, M. J. Motala, B. Y. Ahn, R. G. Nuzzo*, et al.*, "Conformal Printing of Electrically Small Antennas on Three Dimensional Surfaces," *Advanced Materials,* vol. 23, pp. 1335-1340, 2011.
[195] A. K. Geim and K. S. Novoselov, "The rise of graphene," *Nature materials,* vol. 6, pp. 183-191, 2007.
[196] D. Li and R. B. Kaner, "Graphene-based materials," *Nat Nanotechnol,* vol. 3, p. 101, 2008.
[197] A. A. Balandin, S. Ghosh, W. Bao, I. Calizo, D. Teweldebrhan, F. Miao*, et al.*, "Superior thermal conductivity of single-layer graphene," *Nano letters,* vol. 8, pp. 902-907, 2008.
[198] Available: https://wisp.wikispaces.com/
[199] Z. Lin, Y. Yao, Z. Li, Y. Liu, Z. Li, and C.-P. Wong, "Solvent-assisted thermal reduction of graphite oxide," *The Journal of Physical Chemistry C,* vol. 114, pp. 14819-14825, 2010.
[200] Z. Li, Y. Yao, Z. Lin, K.-S. Moon, W. Lin, and C. Wong, "Ultrafast, dry microwave synthesis of graphene sheets," *Journal of Materials Chemistry,* vol. 20, pp. 4781-4783, 2010.

[201] W. S. Hummers Jr and R. E. Offeman, "Preparation of graphitic oxide," *Journal of the American Chemical Society,* vol. 80, pp. 1339-1339, 1958.
[202] B. S. Cook and A. Shamim, "Inkjet printing of novel wideband and high gain antennas on low-cost paper substrate," *IEEE Transactions on Antennas and Propagation,* vol. 60, pp. 4148-4156, 2012.
[203] L. Yang, A. Rida, and M. M. Tentzeris, "Design and development of radio frequency identification (RFID) and RFID-enabled sensors on flexible low cost substrates," *Synthesis Lectures on RF/Microwaves,* vol. 1, pp. 1-89, 2009.
[204] J. Vaillancourt, H. Zhang, P. Vasinajindakaw, H. Xia, X. Lu, X. Han*, et al.*, "All ink-jet-printed carbon nanotube thin-film transistor on a polyimide substrate with an ultrahigh operating frequency of over 5 GHz," *Applied Physics Letters,* vol. 93, p. 243301, 2008.
[205] R. Vyas, V. Lakafosis, H. Lee, G. Shaker, L. Yang, G. Orecchini*, et al.*, "Inkjet printed, self powered, wireless sensors for environmental, gas, and authentication-based sensing," *Sensors Journal, IEEE,* vol. 11, pp. 3139-3152, 2011.
[206] (2016). *Kapton HN Polyimide Film, Datasheet*. Available: http://www.dupont.com/content/dam/dupont/products-and-services/membranes-and-films/polyimde-films/documents/DEC-Kapton-HN-datasheet.pdf
[207] L. T. Le, M. H. Ervin, H. Qiu, B. E. Fuchs, and W. Y. Lee, "Graphene supercapacitor electrodes fabricated by inkjet printing and thermal reduction of graphene oxide," *Electrochemistry Communications,* vol. 13, pp. 355-358, 2011.
[208] T. Le, V. Lakafosis, Z. Lin, C. Wong, and M. Tentzeris, "Inkjet-printed graphene-based wireless gas sensor modules," in *2012 IEEE 62nd Electronic Components and Technology Conference*, 2012, pp. 1003-1008.
[209] P. V. Nikitin and K. Rao, "Performance limitations of passive UHF RFID systems," in *IEEE Antennas and Propagation Society International Symposium*, 2006.
[210] K. S. Rao, P. V. Nikitin, and S. F. Lam, "Antenna design for UHF RFID tags: A review and a practical application," *IEEE Transactions on antennas and propagation,* vol. 53, pp. 3870-3876, 2005.
[211] K. Kurokawa, "Power waves and the scattering matrix," *IEEE transactions on microwave theory and techniques,* vol. 13, pp. 194-202, 1965.
[212] C. A. Balanis, *Antenna theory: analysis and design*: John Wiley & Sons, 2016.
[213] O. C. Compton and S. T. Nguyen, "Graphene Oxide, Highly Reduced Graphene Oxide, and Graphene: Versatile Building Blocks for Carbon Based Materials," *small,* vol. 6, pp. 711-723, 2010.
[214] D. Lu, Q. K. Tong, and C. Wong, "A study of lubricants on silver flakes for microelectronics conductive adhesives," *Components and Packaging Technologies, IEEE Transactions on,* vol. 22, pp. 365-371, 1999.
[215] R. Zhang, K.-s. Moon, W. Lin, J. C. Agar, and C.-P. Wong, "A simple, low-cost approach to prepare flexible highly conductive polymer composites by in situ reduction of silver carboxylate for flexible electronic applications," *Composites Science and Technology,* vol. 71, pp. 528-534, 2011.
[216] Z. Li, K. Hansen, Y. Yao, Y. Ma, K.-s. Moon, and C. Wong, "The conduction development mechanism of silicone-based electrically conductive adhesives," *Journal of Materials Chemistry C,* vol. 1, pp. 4368-4374, 2013.
[217] R. Zhang, W. Lin, K.-s. Moon, and C. Wong, "Fast preparation of printable highly conductive polymer nanocomposites by thermal decomposition of silver carboxylate and sintering of silver nanoparticles," *ACS applied materials & interfaces,* vol. 2, pp. 2637-2645, 2010.
[218] J. Kost, A. Foux, and M. Narkis, "Quantitative model relating electrical resistance, strain, and time for carbon black loaded silicone rubber," *Polymer Engineering & Science,* vol. 34, pp. 1628-1634, 1994.
[219] X. W. Zhang, Y. Pan, Q. Zheng, and X. S. Yi, "Time dependence of piezoresistance for the conductor filled polymer composites," *Journal of Polymer Science part B: polymer physics,* vol. 38, pp. 2739-2749, 2000.
[220] M. H. Wichmann, S. T. Buschhorn, J. Gehrmann, and K. Schulte, "Piezoresistive response of epoxy composites with carbon nanoparticles under tensile load," *Physical Review B,* vol. 80, p. 245437, 2009.
[221] C. Yang, H. Gu, W. Lin, M. M. Yuen, C. P. Wong, M. Xiong*, et al.*, "Silver nanowires: from scalable synthesis to recyclable foldable electronics," *Advanced Materials,* vol. 23, pp. 3052-3056, 2011.
[222] Z. Li, T. Le, Z. Wu, Y. Yao, L. Li, M. Tentzeris*, et al.*, "Rational Design of a Printable, Highly Conductive Silicone based Electrically Conductive Adhesive for Stretchable Radio Frequency Antennas," *Advanced Functional Materials,* vol. 25, pp. 464-470, 2015.
[223] K.-Y. Chun, Y. Oh, J. Rho, J.-H. Ahn, Y.-J. Kim, H. R. Choi*, et al.*, "Highly conductive, printable and stretchable composite films of carbon nanotubes and silver," *Nature nanotechnology,* vol. 5, pp. 853-857, 2010.

[224] T. Sekitani, H. Nakajima, H. Maeda, T. Fukushima, T. Aida, K. Hata*, et al.*, "Stretchable active-matrix organic light-emitting diode display using printable elastic conductors," *Nature materials,* vol. 8, pp. 494-499, 2009.
[225] Y. Li and H. Shimizu, "Toward a stretchable, elastic, and electrically conductive nanocomposite: morphology and properties of poly [styrene-b-(ethylene-co-butylene)-b-styrene]/multiwalled carbon nanotube composites fabricated by high-shear processing," *Macromolecules,* vol. 42, pp. 2587-2593, 2009.
[226] M. K. Shin, J. Oh, M. Lima, M. E. Kozlov, S. J. Kim, and R. H. Baughman, "Elastomeric conductive composites based on carbon nanotube forests," *Advanced Materials,* vol. 22, pp. 2663-2667, 2010.
[227] K. H. Kim, M. Vural, and M. F. Islam, "Single Walled Carbon Nanotube Aerogel Based Elastic Conductors," *Advanced Materials,* vol. 23, pp. 2865-2869, 2011.
[228] M. Moskovits and J. Suh, "Surface selection rules for surface-enhanced Raman spectroscopy: calculations and application to the surface-enhanced Raman spectrum of phthalazine on silver," *The Journal of Physical Chemistry,* vol. 88, pp. 5526-5530, 1984.
[229] S. Yamamoto, K. Fujiwara, and H. Watarai, "Surface-enhanced Raman scattering from oleate-stabilized silver colloids at a liquid/liquid interface," *Analytical sciences,* vol. 20, pp. 1347-1352, 2004.
[230] W. Wang, X. Chen, and S. Efrima, "Silver nanoparticles capped by long-chain unsaturated carboxylates," *The Journal of Physical Chemistry B,* vol. 103, pp. 7238-7246, 1999.
[231] L. Johansson, J. Enlund, S. Johansson, I. Katardjiev, and V. Yantchev, "Surface acoustic wave induced particle manipulation in a PDMS channel—principle concepts for continuous flow applications," *Biomedical Microdevices,* vol. 14, pp. 279-289, 2012/04/01 2012.
[232] (2016). *Assembled Printrbot Simple | Printrbot*. Available: https://printrbot.com/shop/assembled-simple-metal/
[233] (2016). *Dimension 1200es 3D Modeling Printers| Stratasys*. Available: http://www.stratasys.com/3d-printers/design-series/dimension-1200es
[234] (2016). *Hyrel 3D*. Available: http://www.hyrel3d.com/
[235] @Repetier. (2016). - *Repetier Software*. Available: https://www.repetier.com/
[236] (2016). *Slic3r - G-code generator for 3D printers*. Available: http://slic3r.org/
[237] L.-F. Chen, C. Ong, C. Neo, V. Varadan, and V. K. Varadan, *Microwave electronics: measurement and materials characterization*: John Wiley & Sons, 2004.
[238] "| Gorilla Glue," 2016.
[239] T. Le, B. Song, Q. Liu, R. A. Bahr, S. Moscato, C.-P. Wong*, et al.*, "A novel strain sensor based on 3D printing technology and 3D antenna design," in *Electronic Components and Technology Conference (ECTC), 2015 IEEE 65th*, 2015, pp. 981-986.
[240] E. Benoit, T. Allevard, T. Ukegawa, and H. Sawada, "Fuzzy sensor for gesture recognition based on motion and shape recognition of hand," in *Virtual Environments, Human-Computer Interfaces and Measurement Systems, 2003. VECIMS'03. 2003 IEEE International Symposium on*, 2003, pp. 63-67.
[241] S. Mitra and T. Acharya, "Gesture recognition: A survey," *Systems, Man, and Cybernetics, Part C: Applications and Reviews, IEEE Transactions on,* vol. 37, pp. 311-324, 2007.
[242] J. P. Wachs, M. Klsch, H. Stern, and Y. Edan, "Vision-based hand-gesture applications," *Communications of the ACM,* vol. 54, pp. 60-71, 2011.
[243] C. Bellmore, R. Ptucha, and A. Savakis, "Interactive display using depth and RGB sensors for face and gesture control," in *Image Processing Workshop (WNYIPW), 2011 IEEE Western New York*, 2011, pp. 1-4.
[244] B. Yoo, J.-J. Han, C. Choi, K. Yi, S. Suh, D. Park*, et al.*, "3D user interface combining gaze and hand gestures for large-scale display," in *CHI'10 Extended Abstracts on Human Factors in Computing Systems*, 2010, pp. 3709-3714.
[245] M. Van den Bergh, D. Carton, R. De Nijs, N. Mitsou, C. Landsiedel, K. Kuehnlenz*, et al.*, "Real-time 3D hand gesture interaction with a robot for understanding directions from humans," in *RO-MAN, 2011 IEEE*, 2011, pp. 357-362.
[246] C. Keskin, F. K ra, Y. E. Kara, and L. Akarun, "Real time hand pose estimation using depth sensors," in *Consumer Depth Cameras for Computer Vision*, ed: Springer, 2013, pp. 119-137.
[247] K. Fujimura and X. Liu, "Sign recognition using depth image streams," in *Automatic Face and Gesture Recognition, 2006. FGR 2006. 7th International Conference on*, 2006, pp. 381-386.
[248] C.-C. P. Chu, T. H. Dani, and R. Gadh, "Multi-sensory user interface for a virtual-reality-based computeraided design system," *Computer-Aided Design,* vol. 29, pp. 709-725, 1997.
[249] D. Xu, "A neural network approach for hand gesture recognition in virtual reality driving training system of SPG," in *Pattern Recognition, 2006. ICPR 2006. 18th International Conference on*, 2006, pp. 519-522.

[250] M. Ying, A. P. Bonifas, N. Lu, Y. Su, R. Li, H. Cheng, *et al.*, "Silicon nanomembranes for fingertip electronics," *Nanotechnology,* vol. 23, p. 344004, 2012.
[251] X. Liu and K. Fujimura, "Hand gesture recognition using depth data," in *Automatic Face and Gesture Recognition, 2004. Proceedings. Sixth IEEE International Conference on*, 2004, pp. 529-534.
[252] J. Joubert, "Spiral microstrip resonators for narrow-stopband filters," *IEE Proceedings-Microwaves, Antennas and Propagation,* vol. 150, pp. 493-496, 2003.
[253] S. Kim, Y. Kawahara, A. Georgiadis, A. Collado, and M. M. Tentzeris, "Low-cost inkjet-printed fully passive RFID tags for calibration-free capacitive/haptic sensor applications," *IEEE Sensors Journal,* vol. 15, pp. 3135-3145, 2015.

VITA

Taoran Le was born in Wuhu, China. Taoran LE received her B.Sc. degree in Applied Physics from Hefei University of Technology in China. She received M.S. degrees in Electronic Engineering from Politecnico di Torino in Italy and Communication Systems Engineering from the Institut Polytechnique de Grenoble in France. In August 2012, she joined the Ph.D. program in Electrical Engineering at Georgia Institute of Technology, while as a Graduate Research Assistant in the ATHENA group. Taoran has hold a research position in Mitsubishi Electric Research Laboratories (Cambridge, MA). Her research interests include application of novel nano-materials in high performance sensing platforms, flexible electronics, wireless sensor applications, inkjet printing/3D printing technology, graphene based electronics, "smart skin" applications and RF packaging.

Taoran has two pending patents, has been a co-author of four book chapters and has co-authored published 16 peer-reviewed journal papers and 15 papers in conference proceedings of international symposia. She assisted to write a proposal to DTRA and was a co-PI of a proposal to USGS. She is a recipient of the BMW Summer School 2015 and of the French American Scientific Exchange Seminar: Chemical Analysis at the Nanoscale in 2014. She has also been awarded Erasmus Scholarship in CSE-Grenoble program (2010-2011) and Politecnico di Torino scholarship (2009-2011) during her master degree studies in Europe.